UiT The Arctic University of Norway

Uptake of Polystyrene Nanoplastic and its Impacts on the Proteome of Salmonid Cells

60 credits

Oda Heim

Master's thesis in Marine Biotechnology (BIO-3901)

May 2023

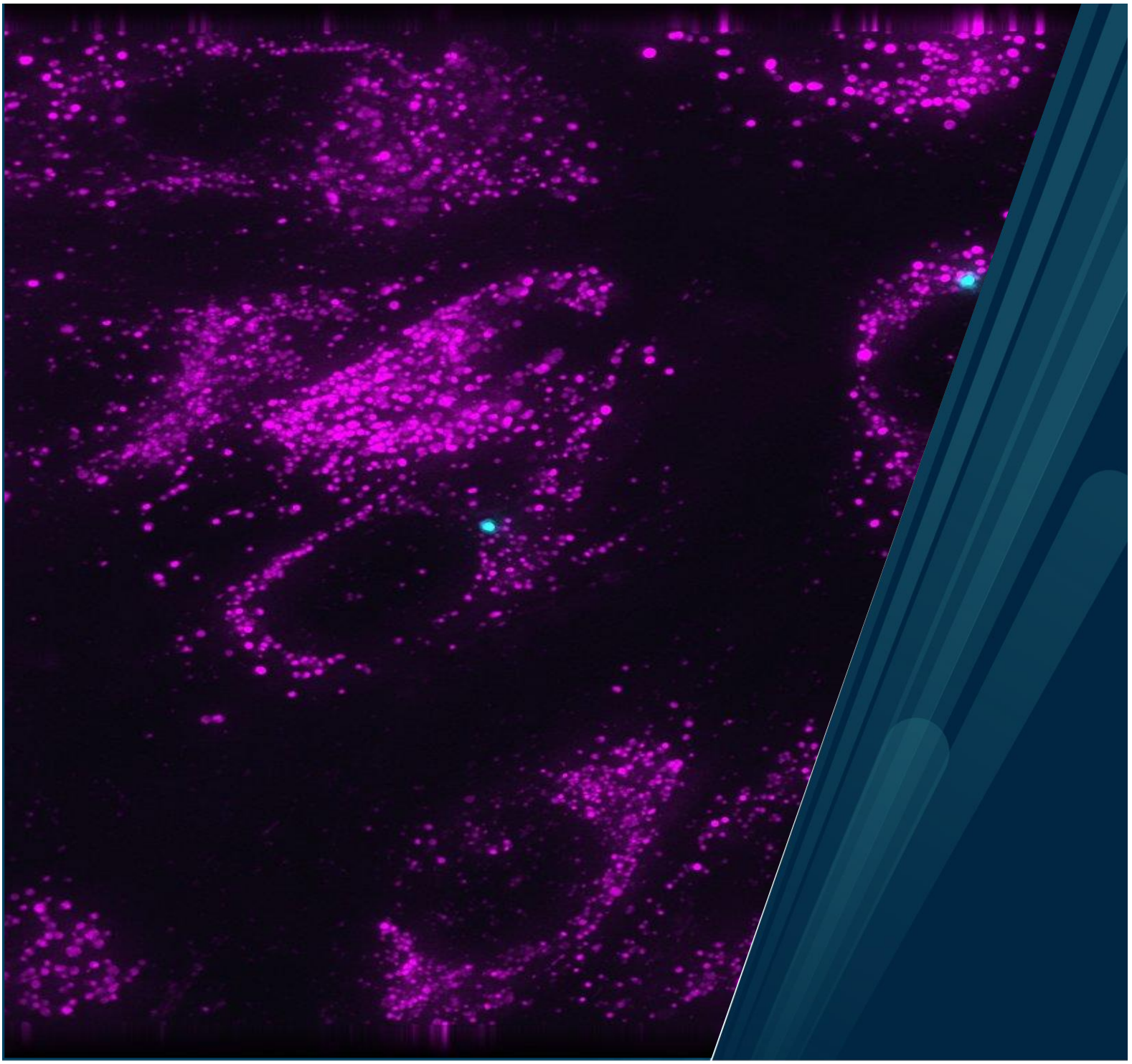

Abstract

Micro- and nanoplastic particles, produced from the breakdown of larger plastic debris, represent a whole new field of hazardous pollution with the potential to cause great damage on a range of marine species. This escalating concern of plastic pollution in marine environments and its consequential impacts on marine species, has emphasized the urgency for an in-depth understanding of the uptake and resultant impacts of plastic particles at both cellular and tissue levels, in aquaculture species such as Atlantic salmon (*Salmo salar L.*). To date, there is limited information regarding the uptake and subsequent effects of nanoplastics in salmon species, especially at cellular level. This study aimed to provide insight on the uptake of polystyrene nanoplastics (PS-NPs) and the potential responses that are activated in salmonids cells by the ingestion of these external stressors. The immortalized cell lines Atlantic Salmon Kidney cells and Salmon Head Kidney cells (ASK-1 and SHK-1), as well as Chinook Salmon (*Oncorhynchus tshawytscha*) Embryonic cells (CHSE-214) were exposed to nanoplastic (NP) particles embedded with fluorescent dye. The presence of the NPs within the cells was confirmed through fluorescent microscopy and DeltaVision™ deconvolution imaging, as well as a fluorescence-based flow cytometry, demonstrating their internalization by the cells. A comprehensive proteomic analysis utilizing liquid chromatography-mass spectrometry (LC-MS), revealed a diverse set of differentially expressed proteins. These proteins play crucial roles in essential cellular biological functions, including oxidative stress, apoptosis, endocytosis and immune responses, suggesting a perturbation of these biological processes by NPs in the salmonid cells. The findings from this study provided new information on the uptake and potential impact of polystyrene nanoplastic exposure on the proteomes of ASK-1, SHK-1 and CHSE-214 cells. These results will contribute to our understanding of the effects of nanoplastic exposure on fish health, and broadly provide valuable insights into the implications of nanoplastic pollution in the aquatic ecosystems.

Foreword

The current master's thesis concludes my Master of Marine Biotechnology at the Arctic University of Tromsø (UiT), and Faculty of Biosciences, Fisheries and Economics (BFE). The project is a collaboration between the university and the Norwegian Research Centre (NORCE) within the division for Gene technology, Environment and Society. This project is also a part of the ongoing project collaboration between UiT and NORCE: "Nano- and microplastics: Do they impact fish health and welfare?", which is also referred to as "NanoFish", where two of my supervisors, Roy A. Dalmo and Arinze S. Okoli are members. The project is based specifically on work package 3: Proteomic studies of Atlantic salmon cells exposed to NPs and MPs. The members of the NanoFish project, has been a great help all throughout my project and the researchers have been very supportive when challenges have risen.

I am grateful for the invaluable support and contributions that have made my master's thesis possible. I would like to express my gratitude to my supervisors, Arinze S. Okoli, Roy A. Dalmo, and Klara Stensvåg, for their exceptional guidance, expertise, and support throughout this project. Special thanks to Arinze Okoli for his hands-on guidance and insightful advice. I extend my appreciation to Deanna L. Wolfson for her outstanding assistance with imaging and processing, which greatly enhanced the quality of my research. I am also thankful to Dhivya B. Thiyagarajan for her invaluable discussions and assistance concerning cells and plastic particles. I would like to thank the NanoFish group for granting me the opportunity to be a part of this fascinating and cutting-edge project.

I would also like to thank my fellow master students at NORCE, Jocelyn Hernandez Palerud and Memunat Agbaje-Abdulrauf, for their great company, advice, and assistance, as well as to the employees at the NORCE Tromsø offices for their valuable teachings, particularly in the laboratory. To my family and friends, I am incredibly grateful for their unwavering support and understanding throughout this journey, and for letting me obsess in my project over the past year.

Tromsø, 30.05.2023

Oda Heim

Abbreviations

2D	Two-dimensional
3D	Three-dimensional
ASK-1	Atlantic Salmon Kidney cell line
BCA	Bicinchoninic Acid Assay
BSA	Bovine Serum Albumin
cDNA	Complementary DNA
CHSE-214	Chinook Salmon Embryonic cell line
CMG	CellMask™ Green
Cy5	Cyanine-5
DAPI	Diamidino-2-phenylindole
DNA	Deoxyribonucleic acid
DPX	Disposable pipette extraction
DTT	1,4-dithiothreitol
DV	DeltaVision™
Ef-1α	Elongation factor 1α
ER	Endoplasmic Reticulum
FACS	Fluorescence-Activated Cell Sorting
FBS	Fetal Bovine Serum
HK	Head Kidney
HSP	Heat Shock Protein
IAA	Iodoacetamide
KEGG	Kyoto Encyclopaedia of Genes and Genomes
LC-MS	Liquid Chromatography Mass Spectrometry
LTDR	LysoTracker Deep Red
MP	Microplastic
MS	Mass Spectrometry
NORCE	Norwegian Research Centre
NP	Nanoplastic
PBS	Phosphate Buffered Saline
PCA	Principal component analysis

PCR	Polymerase chain reaction
PD	Proteome Discoverer™
PRiME	Proteomics and Metabolomics Core Facility
qPCR	Quantitative-Polymerase chain reaction
RNA	Ribonucleic acid
ROS	Reactive Oxygen Species
sCMOS	Scientific Complementary Metal–Oxide–Semiconductor
SDC	Sodium Deoxycholate
SHK-1	Salmon Head Kidney Cell line
UiT	The Arctic University of Norway

Table of Contents

List of Tables

List of Figures

1 Introduction

1.1 Salmon aquaculture

The Norwegian aquaculture industry has experienced significant growth and expansion over the past few decades, especially considering the inception of the initial Norwegian farming facilities in the 1970s. Particularly, the Norwegian farmed Atlantic salmon has gained significant popularity worldwide, emerging as the most favored fish species (Norwegian Seafood Council, 2022). As one of Norway's largest export products, the importance of quality and safety of the A. salmon is undoubtedly prioritized. Already in 2016. the seafood industry had exceeded 12% of the total Norwegian exports by value, of which 8% was made up of A. salmon alone (Federation of Norwegian Industries). In 2022. the total value of seafood export in Norway amounted to an ever-growing 151.4 billion Norwegian kroner (Aandahl & Brækkan, 2023). Globally, the seafood industry has experienced large growth in recent times, with an annual growth rate of 3.3% since 1950, and as the world's population is increasing, this industry has the potential to become an even more important source of protein (Food and Agriculture Organization of the United Nations, 2022). Currently, the foremost requirement of our planet is the provision of healthy and nourishing food alternatives, produced in a sustainable manner. Seafood, with its inherent potential, can aptly fulfill this need.

The increasing pressure and need to expand aquaculture production has concurrently raised concerns regarding environmental impacts and animal welfare, only resulting in an escalation of these concerns in the future (Ahmed et al., 2019). These concerns need to be addressed, and solutions prioritized to ensure sustainable growth of the industry.
A range of viral and bacterial diseases has affected fish farmers for many years which threatens the ongoing expansion of the industry. Several disease outbreaks in different farm locations have affected the welfare of the farmed fish and the potential to spread to wild salmon (Murray & Peeler, 2005). Additionally, the economies, both of individual farmers, regional and national, are impacted by each outbreak (Murray & Peeler, 2005). Apart from disease outbreaks, the impact of the fish farm facilities on the surrounding environment constitutes a significant challenge. For example, the production of salmon produces organic

waste that will sediment to the seabed, and could potentially pose harm to the species living here (Grefsrud et al., 2018). Over the course of the last decade, a diverse array of frameworks, regulations and treatments have been implemented to make farmed salmon production more sustainable. Nonetheless, the menace of plastic pollution, originating from the farming facilities as well as other sources that generate plastic waste, has not been accorded sufficient consideration despite its potential adverse impacts on both the free-living and captive fish in the ocean. Additionally, the physical treatment of farmed salmon for parasites creates a risk of open wounds in the skin. This will in turn allow foreign substances, such as small plastic particles, a possibility for adhesion and internalization.

1.2 Atlantic Salmon (*Salmo salar*)

The Atlantic salmon (*Salmo salar*) is part of the Salmonidae family, which are physically typified by a laterally compressed body form and a dorsal adipose fin (Webb et al., 2007). These anadromous fish migrate from fresh water in the rivers as young smolt and return to their natal rivers as sexually mature adults to reproduce (Havforskningsinstituttet, 2019). For the salmon to adapt to the saltwater, they undergo a range of physiological changes. The fish farming industry has developed a system based on light and temperature to ensure the fish to efficiently develop the fish for life in the net pens.

The A. salmon genome is large and complex with an estimated size of about 3 billion base pairs (Davidson et al., 2010). The repeat content of A. salmon is 58-60%, which is among the highest found in any vertebrate genome (Lien et al., 2016). A final set of approximately 37 000 protein-encoding genes have been identified with high confidence, and these genes have all been assigned a likely function based on similarities to known genes in the Swissprot database (Lien et al., 2016). The Salmonidae family's unusually large genome size originates from a whole genome duplication of the ancestors of salmon and trout that happened about 88 million years ago (Christensen & Davidson, 2017). This event resulted in a doubling of their entire genome and has had significant evolutionary consequences for the species within the Salmonidae family. The salmon is still partly tetraploid from this duplication, and because of the large number of repeated genetic elements, it has been particularly complicated to

assemble their genome (Lien et al., 2016). Although the large and complex genome of the A. salmon has led to some challenges for genome sequencing, the recent advances in sequencing technologies and bioinformatics have made it possibly to generate a high-quality genome sequence that maps all genes in the A. salmon and can act as a reference for other salmonid species (Davidson et al., 2010).

In Norway, A. salmon is by far the most abundant commercially produced fish species. Atlantic salmon, Rainbow trout *(Oncorhynchus mykiss)*, and Arctic char (*Salvelinus alpinus)*, together constitute 98.8% of the total fish farming in Norway (Misund, 2023). The year 2021 was the best year so far for Norwegian seafood exports and it was recorded a total export of 3.1 million tons of seafood worth 120.8 billion Norwegian kroner (Norwegian Seafood Council, 2022). A. salmon makes up almost 70% of the total seafood export from Norway (Aandahl & Brækkan, 2023).

1.2.1 Teleost Head kidney

The teleost head kidney (HK) is an organ unique to teleost fish and analogous to the mammalian adrenal gland (Geven & Klaren, 2017). It is a significant important organ in the immune system of the fish and comprises cytokine-producing lymphoid cells and endocrine cells secreting cortisol, catecholamines and thyroid hormones (Geven & Klaren, 2017) (Figure 1). The head kidney is special in the way that the immune system and endocrine system is intimately organized in one single organ, which makes bidirectional signaling possible. This organ is also one of the main places in the body where hematopoiesis occurs and where immune cells are produced (Abihssira-García et al., 2020).

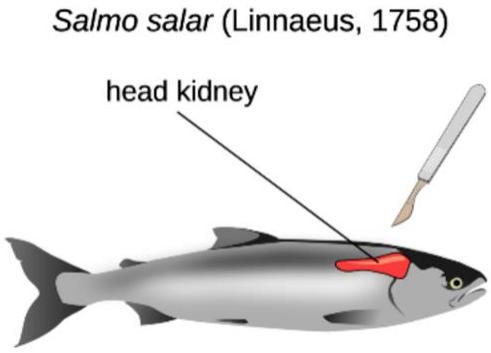

Figure 1: Illustration of the Atlantic salmon and the head kidney where both ASK-1 and SHK-1 cells are derived from (Jalili et al., 2020).

The HK is rich in macrophages which specifically plays an important role in both the innate and adaptive immunity (Cui et al., 2020). Head kidney-derived cells from a range of species are also known to play significant roles in non-specific defense mechanisms against pathogens and to be an important part of the endocrine response to stress. Studying the uptake of plastic particles and their impact on HK cells may provide an insight on how fish can be affected by similar particles in the ocean.

1.2.2 A. salmon derived cell lines

The ASK (Atlantic Salmon Kidney) is an epithelial cell line derived by B. Krossøy in 1998 from head kidney cells of the A. salmon (Devold et al., 2000). As the head kidney is an important immune organ in fish, the cell line was originally developed for studying immune responses in A. salmon (Krossøy et al., 1999). Since then, the cell line has been a valuable resource in research connected to the immune system, interactions with pathogens, and the effects of environmental stressors and pollutants. The ASK cell line have also previously been described to have "macrophage-like" abilities (Jørgensen et al., 2006).

SHK-1 is another macrophage-like cell line derived from head kidney of A. salmon (Levicán-Asenjo et al., 2019). This cell line has been shown to internalize some fish viruses such as infectious pancreatic necrosis (Levicán-Asenjo et al., 2019). Like ASK-1 cells, the SHK-1 cell line has been reported to have an epithelial-like morphology and is adherent, meaning that the cells attach to the surface of the growth flask or plate (Dannevig et al., 1997).

1.3 Chinook salmon (*Oncorhynchus tshawytscha*)

The Chinook salmon is the largest of the Pacific salmon species and can grow to approximately 13 kilograms (The National Wildlife Federation). Like the Atlantic salmon, the Chinook salmon is anadromous and migrates to the oceans after hatching. However, all Chinook salmon die after spawning because of all the energy they use for migration, breeding and protecting of the eggs (NOAA, 2023). Their living habitats include the upper reaches of the Pacific Ocean and the freshwater rivers of the Pacific Northwest (The National Wildlife Federation).

As with the A. salmon, the almost 90-million-year-old genome duplication still resonates in the modern genomes of Chinook salmon (Christensen et al., 2018). The total size of the genome is 2.3 Gb which makes it a bit smaller than the genome of A. salmon (National Library of Medicine, 2015). Despite the difference in size of the two genomes, the species have been found to share a considerable amount of genes and genomic regions that are known to be involved in important biological processes such as growth, metabolism, and immunity (Christensen et al., 2018; Davidson et al., 2010; Lien et al., 2016).

1.3.1 CHSE-214 cells

The CHSE-214 cell line is derived from a Chinook salmon embryo and has previously been used in scientific applications such as growth and titration of viruses and to carry out cell infection assays (Sigma Aldrich, 2023). As with SHK-1 cells, these cells have also been shown to internalize infectious pancreatic necrosis virus (Levicán-Asenjo et al., 2019). These cells have similar growth requirements compared to the ASK-1 cells; however, they divide faster and thus cultures need to be passaged more often. The CHSE-214 cell line is an epithelial-like cell line, originally from 1964, and has since then been used in a handful of studies mainly connected to antiviral responses (Monjo et al., 2017). The cells have also been documented to take up some other viruses, as was noted for the A. salmon cell lines as well (Levican et al., 2017). The documentation pertaining to the macrophage-like abilities of the CHSE-214 cell line, is relatively scarce when compared to cells derived from the head kidney of A. salmon. However, it is reasonable to anticipate that these cells possess the capacity to phagocytose small particles to a certain extent. Besides, embryonic cells from other aquatic species such as sea bass (*Dicentrarchus labrax* L.) (Picchietti et al., 2017) and zebrafish (*Danio rerio*) (Quevedo et al., 2021) has previously been shown to ingest nanoparticles. Conversely, based on the presently available information, it is challenging to determine which of these three salmonid cell lines would exhibit the highest level of nanoparticle uptake.

1.4 Cell marker staining

To examine different parts of a cell, one could use cell markers which will give color to a specific organelle of the cell. Cell staining is a highly versatile technique in cell biology and has the potential to distinguish cells and cell organelles from each other (Rodig, 2022).

Fluorescent dyes are commonly used to label and track acidic organelles in living cells, such as lysosomes, membranes and mitochondria. The dyes accumulate in acidic compartments as a result of a negative membrane potential, and a higher negative membrane potential will result in a higher accumulation (Perry et al., 2011). LysoTracker™ Deep Red is a fluorescent dye that allows scientists to visualize any changes in lysosomal morphology or function in live cells using advanced microscopy. Deep red has its maximal excitation and emission at 647/668 nm and is excited using a Cy5 filter (Table 3) (ThermoFisher Scientific).

1.5 Plastics in marine environments

Plastics have emerged as a ubiquitous material and have attained an indispensable status in numerous domains of our daily existence (Kershaw & Rochman, 2015). Regrettably, this progress has also resulted in a significant surge in anthropogenic plastic waste, thereby presenting a new set of environmental challenges.

It has been suggested that at least fourteen million tons of plastic end up in the ocean every year, and that 80% of all marine debris is made up of plastics (International Union for Conservation of Nature, 2021). Considerable attention has recently been directed towards the reduction of plastic waste and the remediation of plastic pollutants in marine ecosystems. However, despite these concerted efforts, significant quantities of plastic particles continue to circulate within our oceans. This poses a great threat to food safety, quality, and ultimately human health, while also aggravating the issue of climate change. The plastic materials polluting the oceans are made up of a range of polymers such as polypropylene, polyethylene, polystyrene, and polyethylene terephthalate (Quecholac-Piña et al., 2017).

The plastic pollution stemming from the aquaculture facilities has grown in tandem with the current expansion in the farmed fish industry. Fish farmers use a range of products and tools that can potentially add plastic pollution of varied sizes and types to the ocean. In the Norwegian seas, pollution from fisheries, aquaculture and shipping has been identified as the largest sources of marine littering (Nogueria et al., 2019). In 2017 alone, plastic pollution from aquaculture was estimated between 16 000 and 29 000 tonnes (Hognes & Skaar, 2017). There are still uncertainties connected to the tracking of marine litter, but the main products

causing microplastic (MPs) and nanoplastic (NPs) debris are the net pen constructions, feeding tubes and ropes. The reports compiled in the last few years, give reason to believe that the farmed species, and any surrounding wild species are exposed to these toxic particles (Lusher et al., 2017).

1.5.1 Nanoplastics

From a viewpoint of biological interactions, MPs and NPs are considered the most problematic type of plastic pollution when it comes to size (Clark et al., 2023). The definition of nanoparticles varies between different fields, however for the work described in this project, a nanoparticle is defined as particles less than 1000nm (Capaldi Arruda et al., 2015; Hartmann et al., 2019; Skåre et al., 2019). MPs and NPs are mainly incidental debris broken down from larger plastic objects (Figure 2).

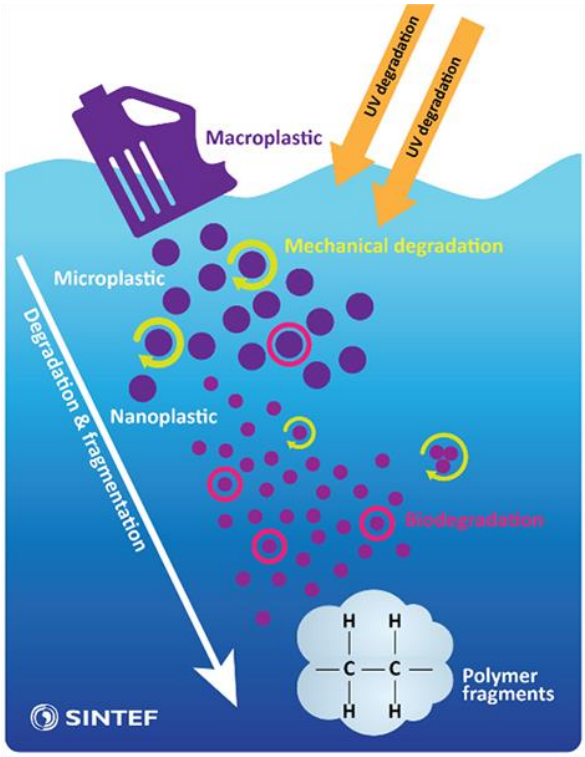

Figure 2: Breakdown of larger plastic products in the ocean; from macroplastics to tinier polymer fragments (Booth, 2017).

Recent advancements in tools and knowledge for analyzing marine pollutants have revealed the ubiquitous presence and accumulation of these small plastic particles, and this has become a source of great concern (Quecholac-Piña et al., 2017). Nano- and microplastics can be

ingested by marine organisms, and a positive correlation between the abundance of NPs and MPs and the number of particles ingested by fish has been established (Quecholac-Piña et al., 2017). Due to their smaller size and subsequent capability for internalization through endocytosis, nanoparticles possess the potential to pose a higher level of toxicological risk compared to relatively larger particles (Clark et al., 2023). Although the information regarding presence of MPs and NPs in tissues outside the digestive tract is currently limited, it has been documented that very fine microplastics can translocate across living cells into the circulatory or lymphatic system, which would result in dispersal of these possibly toxic particles throughout the fish body (Wright et al., 2020).

There has been documentation of ingestion of NPs in a variety of cells from different species, including gill epithelial cells from Rainbow trout (Felix et al., 2017), epidermal keratocyte-like cells from A. salmon (Åsbakk & Dalmo, 1998), intestine epithelial cells in several species (Gaiser et al., 2011), embryonic cells from sea bass (Picchietti et al., 2017), and more recently also in immune cells of A. salmon (Abihssira-García et al., 2020).

Collectively, the understanding of the effects exerted by NPs on fish and other animal species remains incomplete. However, the prevailing trajectory of plastic pollution portends an unfavourable outlook for the future (Ivar do Sul & Costa, 2014; Savoca et al., 2021; Shoiynbayeva et al., 2021). Consequently, it is imperative to further elucidate the impact of NP exposure on aquatic species, such as salmon, in order to deepen our comprehension of these ecological repercussions in marine environments.

1.5.2 Polystyrene

Polystyrene plastic is widespread and found in a variety of everyday products. This material takes hundreds of years to break down and makes up a one of the principal component of the marine debris in the world's oceans (Berger, 2009). Foamed polystyrene is lightweight, buoyant and water resistant and therefore also a popular choice for a wide range of plastic products. These properties unfortunately also make this plastic compound a common form of plastic pollutant (Akester, 2019). The likelihood of polystyrene MPs (PS-MPs) and NPs (PS-

NPs) to pollute the marine environment, increases with their wider use and inadequate waste disposal.

PS-MPs have been shown to not only be ingested by fish who perceive the particles as food, but also to adhere to fish tissue. The particles have been found adhered/taken up by the fish skin and gills, muscle, and liver (Yang et al., 2020). It has been found that PS-MPs can be taken up by epidermal and corneal keratocyte-like cells in salmon (Kjølstad & Svartaas, 2020; Åsbakk & Dalmo, 1998). This leads us to believe that other types of fish cells, which possess macrophage-like characteristics like the keratocyte-like cells, also can ingest these particles. Indeed, macrophage-like immune cells from intestine, blood, and head kidney, have recently been shown to phagocytize microplastics *in vitro* to varying extents (Abihssira-García et al., 2020).

1.6 Cellular internalization and intracellular transportation

Cellular internalization refers to the process of which cells take up substances or molecules. This includes passive diffusion and different forms of endocytosis mechanisms including phagocytosis, which is a process by which cells ingest or engulf other particles (Britannica, 2022) (Figure 3). Macrophages are a class of innate immune cells which are responsible for attaching to any foreign objects through the process of phagocytosis (Jarai & Fromen, 2022). Other forms of endocytosis include micropinocytosis, *clathrin-dependent* endocytosis, and *caveolae-dependent* endocytosis (Hua & Wang, 2022).

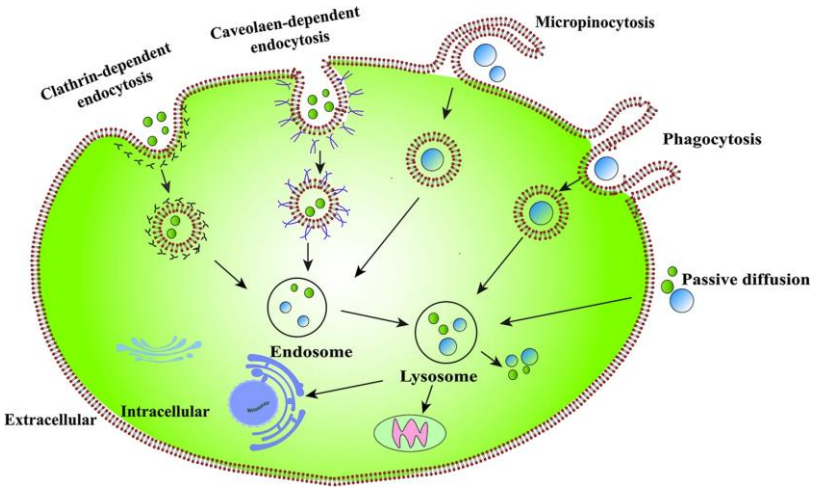

Figure 3: Eukaryotic cell with cellular uptake pathways and intracellular transport of MPs and NPs (Hua & Wang, 2022).

The major endocytic route for internalization of many types of cargoes is the clathrin-mediated endocytosis (Kaksonen & Roux, 2018). Clathrin is a protein which assembles into structures called clathrin-coated pits on the cell membrane in response to specific receptor reactions. Caveolae-dependent endocytosis on the other hand, involves invaginations called caveolae, which are enriched in a protein called caveolin (Nabi & Le 2003).

Both clathrin and caveolin dependent endocytosis trigger production of early endosomes, which in turn takes over the incoming cargo which has been internalized from the cell membrane (Quevedo et al., 2021).
It has been shown that passive diffusion and forms of endocytosis is involved in the cellular uptake of MPs and NPs, and that some organelles such as endosomes, autophagosomes, and lysosomes play an important role in the transportation of the particles inside the cell (Hua & Wang, 2022). Depending on the type of particle and its size, some MPs and NPs have also been documented to enter the cell through passive diffusion (Hua & Wang, 2022).

When nanoparticles are taken up by cells via some sort of endocytosis, they usually tend to accumulate in different compartments such as lysosomes or endosomes within the cell (Yue et al., 2016). The overloading of such compartments with external stressors can potentially lead to adverse cellular effects such as lysosomal dysfunction (Yue et al., 2016). MPs and NPs can also be transported through the autophagy process, where the internalization of NPs could trigger the formation of autophagosomes (Hua & Wang, 2022). This route of transportation could also lead to lysosomal damage and in turn release of lytic enzymes, by autophagosomes fusing with lysosomes (Schütz et al., 2016). Furthermore, from endosomes, autophagosomes or lysosomes, NPs can also escape and end up in other cellular organelles where they could cause further damage.

Uptake of particles may induce production of oxygen radicals. Oxidative stress is a state of imbalance of the production of reactive oxygen species (ROS) and the antioxidants defense (Birnie-Gauvin et al., 2017). ROS are highly reactive molecules which are generated as a byproduct of normal cellular metabolism but could also be produced as a response to external stressors (Birnie-Gauvin et al., 2017; Jakubczyk et al., 2020). With the increased attention

towards the environment and pollution of recent years, focus has been directed to the association between oxidative stress and external stressors. Some external factors that can affect oxidative stress of aquatic animals are temperature, oxygen availability, salinity, and lastly different forms of pollution.

Intake and accumulation of MPs in aquatic species has been found to induce an increase in oxidative damage and inflammatory markers (Solomando et al., 2020). Several studies have demonstrated that also nanoparticles can trigger oxidative stress by generation of ROS and cause mitochondrial damage, thus further inducing the oxidative stress (Linse et al., 2007; Nel et al., 2006). Apoptosis is one of the mechanisms that can be induced by mitochondrial damage, through a variety of pathways (Hua & Wang, 2022).

Proteomic and transcriptional responses in the form of up- or downregulation of stress-related proteins and genes, have been reported in salmon cells treated with a variety of external stressors (Beemelmanns et al., 2021; Dhamad et al., 2020). However, the proteomic and transcriptional responses to exposure and ingestion of polystyrene nanoparticles in salmon cells, is yet to be explored.

1.7 Protein pathways implicated in cellular uptake and stress responses

1.7.1 Apoptosis pathway (*map04210*)

The apoptosis signalling pathway consists of all the proteins involved in regulating this mechanism, and plays a critical role in tissue homeostasis, development, and elimination of damaged cells (Henson & Hume, 2006). Apoptosis, or programmed cell death, is a mechanism characterized by morphological and biochemical changes which all lead to cell death (Papaliagkas et al., 2007). It is highly involved in the deletion of cells with severely damaged DNA, auto-reactive cells in the immune system, and finally eliminate any infected cells (Papaliagkas et al., 2007). Apoptotic cells are also often characterized by specific morphological and biochemical changes, which are orchestrated by a family of cysteine proteases called *caspases* (Zimmermann & Green, 2001). The apoptotic pathways are usually

sectioned in two main pathways, the intrinsic and the extrinsic pathway, which are mainly distinguished according to whether caspases are involved or not (Hongmei, 2012). The two pathways can be activated independently or in conjunction with each other. Because apoptosis is responsible for eliminating infected cells, it means that a dysfunction of the mechanisms is implicated in many pathological conditions (Papaliagkas et al., 2007). The most important proteins that have been identified to play a vital role in apoptosis are the caspases, the amyloid-B peptide, the BCl-2 family of proteins, the p53 gene and the heat shock proteins. The apoptotic pathways can be activated by a variety of stimuli such as cellular stress signals, oxidative stress, DNA damage or nutrient deprivation.

1.7.2 p53 signalling pathway (*map04115*)

The p53 protein is a transcription factor that plays critical roles in the regulation of apoptosis, cell cycle, response to cellular stress and genomic stability (Wang et al., 2023). In response to stress signals, the p53 protein is activated and initiates a program of cell cycle arrest, cellular senescence, or apoptosis (Harris & Levine, 2005).

1.7.3 Autophagy pathway (*map04140*)

Autophagy is the process of intracellular degradation of unwanted or damaged components to remain cellular homeostasis (Mizushima, 2007). Autophagy also plays an important role in viral and cellular stress responses and has been shown to be involved in programmed cell death (Schiøtz et al., 2010). When the cell is in normal conditions, they maintain low levels of autophagosome formation, making this pathway suitable as a biomarker in response to external stress (Quevedo et al., 2021). The process is tightly regulated by a complex network of signalling pathways, including the insulin signalling pathway, AMP-activated protein kinase pathway (AMPK signalling pathway) and the mTOR signalling pathway, which are all regulated by factors such as nutrient availability, cellular stress, and intracellular signalling molecules (Kim et al., 2011).

1.7.4 Phagosome pathway (*map04145*)

As previously alluded to, phagocytosis is a cellular process by which large foreign particles are internalized. The mechanism is of great significance in both innate and adaptive immunity, and involves a sophisticated interplay of proteins, ultimately culminating in the

destruction and degradation of intracellular pathogens (Desjardins, 2003). The process initiating phagocytosis, is the binding of particles to receptors on the cell surface, which in turn generates a bunch of signal-transduction events, generally divided into a few key steps including recognition and binding of particle, engulfment of particle, phagosome maturation, fusion with lysosomes, and lastly degradation and processing of the engulfed particle (Rosales & Uribe-Querol, 2017). Although phagocytosis typically involves a series of maturation events including early and late endosomes leading to the formation of phagolysosomes, in some cases the phagosome fuses directly with the lysosome without passing through the intermediate stages. This is called direct phagolysosome fusion and is known to allow for rapid delivery of engulfed cargo to lysosome for further degradation (Greene et al., 2022). This process in known to happen in specialized immune cells, such as macrophages, and under special conditions where the pathogen needs to be dealt with quickly (Gutierrez et al., 2008).

A relatively recently discovered phagocytosis mechanism is the endoplasmic reticulum-mediated phagocytosis (ER-mediated phagocytosis). It has been found that fusion of ER with the membrane of the macrophage works as a distinct form of phagocytosis that relies on the participation of ER-associated proteins (Gagnon et al., 2002).

1.8 Cell imaging and microscopy

1.8.1 Fluorescence

Fluorescence is defined as the emission of light by a particular substance that has absorbed light of a specific energy (Lakowicz, 1999). The process happens from absorption of photons followed by the emission of photons from the fluorescent substance.

Cells contain molecules with natural fluorescence without any external labels or dyes. This is called autofluorescence (Monici, 2005). This means that when using fluorescent dyes or labels in research, it is crucial to include adequate controls to compare with the fluorescence in the samples in question (Catarino et al., 2019).

1.8.2 Deconvolution microscopy and three-dimensional imaging

Deconvolution microscopy is a method used to improve the resolution and reduce out-of-focus fluorescence in fluorescent microscopy (McNally et al., 1999). Three-dimensional imaging techniques allow researchers to visualize and study the cell and its surroundings in three dimensions, unlike traditional 2D imaging. These higher complexity cell models produced in 3D imaging will better mimic in vivo environments and responses to foreign substances (Belin et al., 2014). The DeltaVision™ Elite system allows you to specify the highest and lowest focal point, for example the bottom and the top of the cell. The entire height provided will then be separated into sections which comprise the z-plane. By choosing the right wavelengths based on where the sample should emit and excite light, the fluorescent parts of the sample will give an image that can be further analyzed and assembled into a three-dimensional model.

1.9 Fluorescence-activated Cell Sorting

Fluorescence-activated cell sorting (FACS) is a form of flow cytometry that sorts mixtures of cells based on emitted fluorescence. The method makes it possible to sort a heterogenous mixture of cells into homogenous cells by differentiating the cells based on the specific light scattering and fluorescent characteristic of each individual cell (SinoBiological). FACS methodologies have given researchers, scientists, and clinicians the opportunity to study individual cells in greater detail than previous methods (Tung et al., 2004).

1.10 Proteomic studies

Proteomics of cells or tissue exposed to an external factor provides the opportunity to compare protein expressions in samples, and thus might provide insights into the effects this factor has on the cells or tissues. Proteomic studies allow the monitoring of protein content in tissues, by identifying proteins and their differential abundance in response to different processes and conditions such as growth, feeding and external stress factors (Ahmed et al., 2019). Proteins related to stress and the immune system in fish are up or down regulated according to their function in the defense of pathogens or regulation of stress responses, and these mechanisms are thus useful in understanding the impacts of stressors (Ahmed et al., 2019).

Protein extraction kits are frequently used for the extraction of proteins from cells, followed by a protein quantification assay, and protein expression analysis which are often based on mass spectrometry.

Mass spectrometry has been frequently used for relative quantification in a range of different systems in the last decade (Lindemann et al., 2017). Isobaric tagging is a method for labelling peptides and usually used in combination with MS. Isobaric labelling is based on covalent labelling of the N-terminus and side chain primary amines on the peptide (Cheng et al., 2016). These techniques allow users to simultaneously assess changes in peptide abundances across different experimental conditions or time points through labelling multiple peptide samples from any source material (Cheng et al., 2016). Tandem mass tagging is a type of isobaric tagging where digested peptides from multiple samples are labeled, before they are mixed and analyzed with reversed phase high performance liquid chromatography (HPLC) in combination with a mass spectrometer capable of tandem MS analysis (Zhang & Elias, 2017).

1.10.1 BCA protein assay

The bicinchoninic acid assay (BCA) is a method for estimating protein concentration based on the reduction of Cu^{2+} to Cu^{1+} by protein in alkaline solution, and concentration-dependent detection of the monovalent copper ions produced (Novagen®). The reduction produces a purple-colored product and can be measured spectrophotometrically at 562 nm. The assay involves mixing protein samples with a BCA reagent containing bicinhoninic acid, copper sulfate, and sodium carbonate in an alkaline solution – following the instructions given by Novagen® (Novagen®). The intensity of color of the reaction will be proportional to the amount of protein in the sample, and thus can be quantified by comparing the absorbance of the sample to a standard curve of known protein concentrations.

1.10.2 Label-free Quantification

Label-free quantification methods determine the relative number of proteins in a range of samples without using a stable isotope or other labels for the chemical binding and labeling of proteins (Creative Proteomics). These quantification methods typically involve identifying and quantifying peptides, prior to being used to determine the abundance of their respective proteins.

Traditionally, the label free approaches are divided into either spectral counting methods or peptide peak intensity-based proteomics (Arike & Peil, 2014). Spectral counting quantification relies on the number of peptides identified from a given protein, while peptide peak intensity-based analysis quantifies the relative peptides from the area under the curve of a detected peptide ion (Mehta et al., 2020). Label-free quantification allows for limitless sample numbers and is applicable to any kind of sample. It has the advantage of not requiring expensive and time-consuming labeling reagents. However, compared to labeled quantification, the label-free quantification strategy has reduced ability to detect proteins with low abundance, and generally has lower accuracy and reproducibility (Al Shweiki et al., 2017). Another major limitation is the requirement for multiple runs, which again reduces the throughput.

1.11 Transcriptomic studies

The transcriptome is defined as the abundance and activities of all RNA molecules within a cell (Liang et al., 2011). Transcriptomics describes the techniques used to study the transcriptome and provides further information about the active cellular processes. The transcriptome includes all mRNA, rRNA, tRNA, and non-coding RNA produced in a single cell or in a population of cells. Studying the transcriptome will help us understand the functional elements of the genome, as well as giving us a further look into the molecular constituents of cells and tissues. Transcriptomic studies complements proteomic studies because the former evaluates cell/tissue response at RNA level while the latter provides information at protein level. In the current study, only a few genes were targeted for their expression by using qPCR since time did not allow us to do RNA sequencing analysis.

1.11.1 RNA extraction/isolation

RNA isolation is the process of extracting RNA from biological samples and mainly consists of homogenization of sample, isolating the RNA from other cellular components, purification of RNA and quantification of RNA.

1.11.2 cDNA synthesis

Reverse transcription-polymerase chain reaction (RT-PCR) is a widely used technique for mRNA detection and quantification. The method consists of mRNA being reverse transcribed, amplified, detected, and quantitated in real time (Gibson et al., 1996).

1.11.3 Impact of NP on immune-related genes

Genes and primers for PCR were chosen based on published literature (Abarghouei et al., 2021; Danilova et al., 2005; Natarajan et al., 1999; Piazzon et al., 2016; Ryo et al., 2010) supporting their connection with immune defense mechanisms and cellular stress in salmon, as well as to uptake of microplastics. Abarghouei et al. (2021)reported an induction in expression of antioxidant related genes, such as *hsp70*, as a response to exposure to polystyrene (Abarghouei et al., 2021). Heat shock proteins (HSP) are a group of proteins whose expressions are generally induced by an increase in temperature. However, several of these proteins also play important roles in the immune defense system of fish (Xie et al., 2015). A number of these *hsp* genes have been related to pathogen-specific infection, for example, bacterial infections (Xie et al., 2015). HSPs are also known to be crucial in protein folding and translocation within cells (Krone & Heikkila, 1988). *Hsp90* and *hsp70* have been linked to cellular survival and immune responses, as highlighted by Celi et al. (2012). Moreover, these proteins may be induced by environmental stimuli, including NPs, thereby exerting significant influence on the biological outcomes of stress.

In teleost species, including salmon, immunoglobulin genes, such as *igt* and *igm*, play a crucial role in the fish immune system. Cellular stress, such as exposure to pathogens, environmental changes or inflammatory signals, can trigger the activation of immune cells and the production of antibodies (Piazzon et al., 2016). Traditionally, the production of immunoglobulin has been restricted to B-cells of the immune system (Chen et al., 2009). However, recently immunoglobulin genes have been found expressed in some epithelial cells as well (Chen et al., 2009). These findings could potentially suggest a presence of these genes in the epithelial-like cell lines, such as the ones employed in the research, indicating a potential immunological response to NP exposure. However, it is important to note that there is limited documentation supporting the existence of these genes in salmonid cell lines, as

well as their general association with cellular stress response and NPs. Major Histocompatibility Complex (*mhc*) genes of different classes have been shown to have important immune functions in both fish, as well as mammals (Yamaguchi & Dijkstra, 2019). The mhc class I molecules, which normally present peptides from cytosolic origin, have functions related to cytotoxic T-ells (Natarajan et al., 1999). Nanoparticles may transverse the endosomal-lysosomal system into the cytosol (Singh et al., 2007), and thereby affect the expression of *mhc1*. This aspect has never been studied before.

1.11.4 Real-time PCR

To detect the PCR product, a two-dye tracking system is commonly used. SYBR™ Green dye is the main component of one of these tracking systems. The dye works by binding to double-stranded DNA formed during PCR and gives off fluorescence only when bound to the DNA (ThermoFisher Scientific, 2020) (Figure 4). When the target sequence is amplified by DNA polymerase during PCR, the SYBR™ Green binds to each new copy of double-stranded DNA. The resulting increase in fluorescence is therefore proportional to the amount of PCR product produced.

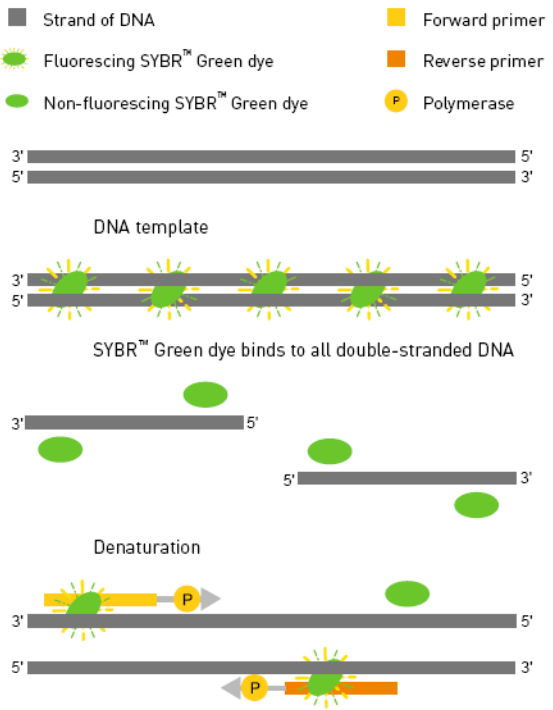

Figure 4: Overview of polymerization with SYBR Green dye binding to double-stranded DNA. Figure generated by ThermoFisher Scientific in PowerTrack SYBR™ Green Master Mix User Guide (ThermoFisher Scientific, 2020).

Real-Time PCR is an efficient method for amplifying cDNA products reverse transcribed from RNA (Pfaffl, 2001). The accumulation of the amplified product, here fluorescence, is measured in real time with a product quantification after each amplification cycle (Bio-Rad Laboratories, 2023). The real-time PCR system can monitor the reaction as it progresses and generates quick results for measuring low abundance gene expression.

A standard curve based on a C_q or Cp (Ct) value needs to be generated for the real-time PCR. This value represents the cycle number where the samples' reaction curve intersects the threshold line that is set (Oswald, 2020) (Figure 5). The threshold line represents the point

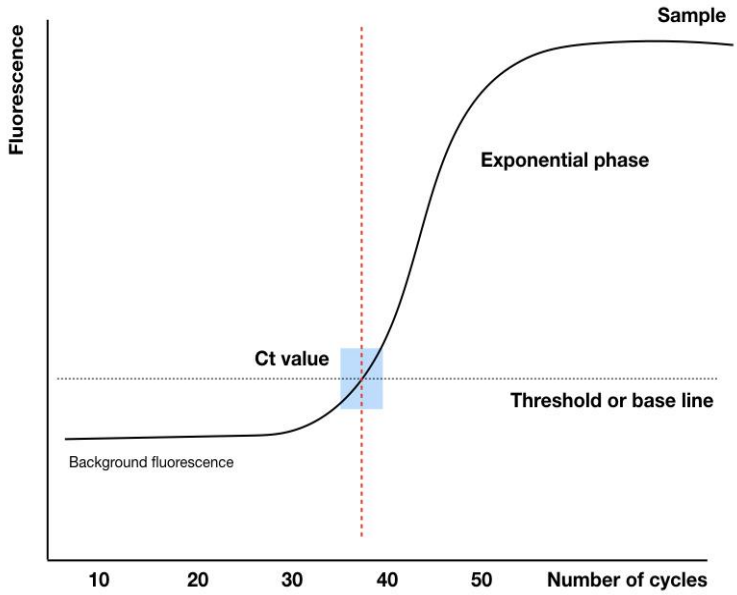

Figure 5: Example of standard curve for qPCR. The curve is generated based on fluorescence quantity and the number of PCR cycles. A Ct or Cp value is found where the curve intersects with a threshold or base line (Pfaffl, 2001).

where a reaction reaches a fluorescent intensity which is above the background levels (Oswald, 2020) There will be separate reaction curves for each sample in the PCR run, meaning there will be many Cp values which all represents a quantitative measure of the amount of DNA present in a sample.

The Lightcycler® real-time PCR system calculates the Cp values for the samples in an experiment and generates a curve for each sample and standard.
The PCR efficiency is calculated from Cp values and gives a quantitative value.
A mathematical model to determine the relative quantification of a target gene in comparison to a reference gene has been developed by Michael W. Pfaffl (Pfaffl, 2001).

$$ratio = \frac{(E_{target})^{\Delta CP_{target}(control-sample)}}{(E_{ref})^{\Delta CP_{ref}(control-sample)}} \qquad \textit{Equation 1}$$

This equation calculates the relative expression ratio of a specific gene compared to a known reference gene and is based on the PCR efficiency and Cp values.

1.12 Inspiration

This project is originally inspired by a study conducted by Roy A. Dalmo and Kjetil Åsbakk in 1998 investigating the internalization of latex beads by epidermal keratocyte-like cells of A. salmon (Åsbakk & Dalmo, 1998). Furthermore, this thesis is partly inspired by results from two previous master projects conducted by respectively Ole Kristian H. Svartaas & Eskil M. Kjølstad (Kjølstad & Svartaas, 2020), and Marie Stette (Stette, 2022). These projects focused on studying the uptake of a variety of MPs and NPs in corneal and epidermal keratocyte-like cells observed using advanced microscopy.
This study, although based on similar aims as these previous projects, is focused on a new range of salmonid cells, and generally utilizes a proteomic and transcriptomic view on how to gain new information about the uptake of NPs. The results from this project can improve the general understanding of the underlying mechanisms of NP toxicity on A. salmon. Moreover, this study has the potential to provide a scientific basis for further research within NP toxicity and identification of biomarkers related to the effects of exposure and uptake of NPs.

1.13 Scientific aim

The need for detailed knowledge on how marine organisms is affected by NPs, will continue to increase as the issues of plastic waste and its prevalence in the marine environment becomes more present. Based on cell imaging, proteomics and transcriptomics, this study will aim to investigate the uptake of polystyrene NPs in salmonid cells. The thesis will aim to study the uptake of nanoparticles of plastic waste in A. salmon and Chinook salmon-derived cells, with the goal of learning more about how these marine organisms are affected by plastic waste, and in turn how this information could become an important part in improving fish health and welfare. It is desirable to study and compare the uptake of plastic particles in ASK-1, SHK-1 and CHSE-214 cell lines, to detect any possible differences in protein and genetic expression of the exposed and non-exposed cells.

The goal of this thesis is to (i) evaluate whether the salmonids-derived cells ASK-1, CHSE-214 and SHK-1 are capable of taking up NPs, (ii) identify differentially expressed proteins of ASK-1, CHSE-214 and SHK-1 cell lines caused by exposure to NP; (iii) evaluate the effect of NP on relative expression of selected stress response genes of ASK-1.

The goal will be sought achieved using different approaches:

- Expose and monitor uptake of fluorescent plastic particles (polystyrene, 503 nm) in cells through imaging and microscopy.
- Enrich cells that have taken up the fluorescent plastic particles through Fluorescent activated cell sorting (FACS).
- Identify differentially expressed proteins of cells following plastic exposure and uptake.
- Determine the effects on relative expression of some stress-and immune related genes in ASK-1 cells.
- Optimize methods and protocols for plastic exposure and cell sorting of the specific cell lines.

2 Materials and methods

2.1 Biological material

Three salmonids-derived cell lines, namely, Atlantic salmon kidney 1 (ASK-1), salmon head kidney 1 (SHK-1) and Chinook salmon embryo 214 (CHSE-214) were used in the study. The ASK-1 cell was obtained from the Federal Research Institute for Animal Health, Germany, and is an adherent immortalized cell line from A. salmon. The SHK-1 cell is also an immortalized cell line from A. salmon and a gift from the Norwegian Veterinary Institute, Oslo. The CHSE-214 cell line obtained from Sigma-Aldrich, United Kingdom, is an adherent immortalized cell line from Chinook salmon (*O. tshawytscha*).

2.2 Chemicals, kits

Table 1: List of Chemicals and kits used in this project with associated manufacturer and product number.

Chemical/ kit	Product ID	Manufacturer
Ethanol (99,9%)	-	Antibac
Tryphan Blue (0,4%)	EBT-001	Bio-Rad (Oslo, Norway)
Lysis Buffer (1M Urea, 0.5% Sodium deoxycholate (SDC), 100mM TEAB)	Self-made	
BCA Protein Assay Kit	TB380	Novagen® (Darmstadt, Germany)
PowerTrack™ SYBR™ Green Master Mix	MAN0018826	ThermoFisher Scientific (Massachusetts, USA)
High-capacity cDNA reverse transcription kit	4368814	ThermoFisher Scientific (Massachusetts, USA)
RNAqueous™ RNA isolation kit	AM1912	ThermoFisher Scientific (Massachusetts, USA)
Quantitech Reverse Transcription Kit	No. 205311	Qiagen, Netherlands

2.3 Media, buffers, solutions

Table 2: List of media, buffers and solutions used in this project with associated concentration/amount (if applicable) and manufacturer.

Reagent	Concentration/ amount	Product ID	Manufacturer
Dulbecco's Phosphate Buffered Saline (PBS) w/o calcium chloride and magnesium chloride	N/A	D8537	Sigma-Aldrich (Missouri, USA)
Leibovitz L15 (1x) with 4mM L-Glutamine and L-amino-Acids	N/A	11415-049	Gibco™ (NY, USA)
Fetal Bovine Serum	10%-20% diluted in L15 medium for cell cultures	S00K910331	Biowest (Nuaillé, France)
Trypsin-EDTA	EDTA in HBSS w/ Phenol Red	T4049	VWR (Pennsylvania, USA)
Sequencing grade Trypsin (for LC-MS)	-	V511A	Promega (Madison, USA)
Lysyl Endopeptidase®, Mass Spectrometry Grade (Lys-C)	-	125-05061	Wako (Tokyo, Japan)
Plum Purple Polystyrene (503 nm)	1% particles	FSPP003	Bangs Laboratories (Indiana, USA)
CellMask™ Green (CMG)	1:2000, diluted with L15 medium	C37608	Invitrogen/ThermoFisher Scientific (Massachusetts, USA)
LysoTracker™ Deep Red (LTDR)	1:2000, diluted with L15 medium	L12492	Invitrogen/ ThermoFisher Scientific

2.4 Experimental description

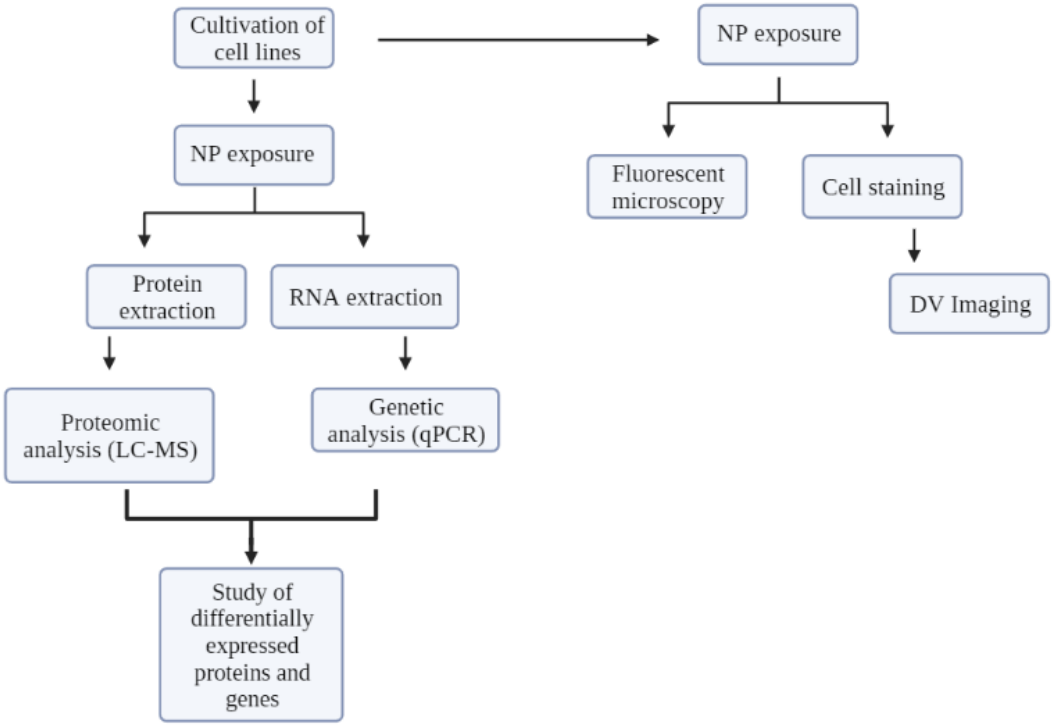

Figure 6: Workflow of experimental procedures from cultivation of salmonid cell lines to exposure to NPs and studies of the following effects.

2.5 Growing cell cultures

All three cell lines were cultivated and passaged according to previously developed protocols. Frozen cells were taken from -80°C and quickly thawed in a water bath heated at approximately 60-70 ºC until a small piece of ice was left in the vial. Cells were then transferred to a T-25 culture flask under sterile conditions in a laminar flow cabinet. All three cell lines were cultivated in the Leibovitz L15 media supplemented with 10% Fetal Bovine Serum (FBS) with penicillin/streptomycin (0.5%) as antibiotics. Cell cultures were incubated in the dark at 22°C without adding CO_2.

Routine sub-culture of ASK-1 and SHK-1 cells involved growing the cells to 60-80% confluence before splitting in 1:2 ratio. Phosphate Buffered Saline (PBS) was used to wash cells, and 0.25% Trypsin was used to detach cells from flask. Thereafter, cells were observed in a light microscope while Trypsin was added, to check that cells were detaching from the

surface of the culture flask. Once the cells had detached, a volume of fresh L15 medium with 10% FBS was added to the culture flask. The total volume was then split into two parts and transferred to new culture flasks. Flasks were incubated as described previously.
The routine CHSE-214 cell passaging was similar to the passaging of ASK-1 and SHK-1cells described above, except that the CHSE-214 cells were split in a 1:3 ratio.
All freeze-preserved cells were passaged at least three times before used in experiments.

2.5.1 Exposure of fish cells to plastic particles

Before exposure to plastic nanoparticles, cell density was estimated manually using the hemocytometer, or by the automated NanoEnTek EVE™ PLUS cell counter. For the hemocytometer, 20 µl of cell culture was mixed with 20uL of Tryphan blue and pipetted under a glass slide on the hemocytometer. Cells were counted in the microscope and cell density was calculated using Equation 2.

$$Cell\ density = Average\ of\ cells\ on\ grid * \frac{100\,000}{mL\ of\ culture} \qquad \textit{Equation 2}$$

The cell culture was then diluted as needed with an end concentration of around 10^5 -10^6 cells/ml.

Amid the project, the lab acquired a new cell counter, NanoEnTek EVE™ *PLUS* Automated cell counter. The cell counts performed after this equipment arrived, was done using this cell counter.
For the automated cell counter, 10ul of the aliquoted cell culture was mixed with 10ul of Tryphan blue. Then, 10 µl of this mixture was added to each side of the cell counter slide and the slide was inserted into the cell counter. The counter was set to automatic cell count and counting was initiated. Once the counting of the first side of the slide was completed, the slide was turned around and the second side was counted. Finally, the average of counted cells was calculated from counted cells on both sides of the counting slide.

Plum purple-stained fluorescent polystyrene particles with excitation of 360 nm and emission of 420 nm, and with a mean diameter of 503 nm were used in NP exposure of ASK-1, SHK-1

and CHSE-214 cells. The plastic particles were delivered from the supplier in a 1 ml suspension containing 1% plastic and this was then diluted to 10^{-5} (1:100 000) before exposure to cells.

Cells at approximately 75% confluency were exposed to the NPs and incubated with L-15 media in 6-well plates as described in Figure 7. Briefly, cells detached by trypsinization as described above were washed with PBS and resuspended in L-15 media supplemented with 10% FBS before being transferred to tubes for NP exposure. A volume of 150 µl of diluted polystyrene particles was added to one of the tubes to a final volume of 15 ml. Both a negative and a positive control were initially included for the fluorescent microscopy. The negative control consisted of cells in tube to which polystyrene particles were not added. Both NP-exposed and non-exposed cells were transferred to 6-well plates and incubated in the dark at 22ºC without CO_2 for seven days. The positive control was only included for fluorescent microscopy to check for fluorescence and was not used in further experiments. This control was made by diluting stock particle suspension of polystyrene with L15 media to a relationship of 1:10 000. The 6-well plates were used for the following fluorescent microscopy of exposed cells (Figure 7). This procedure was individually repeated for all three cell lines.

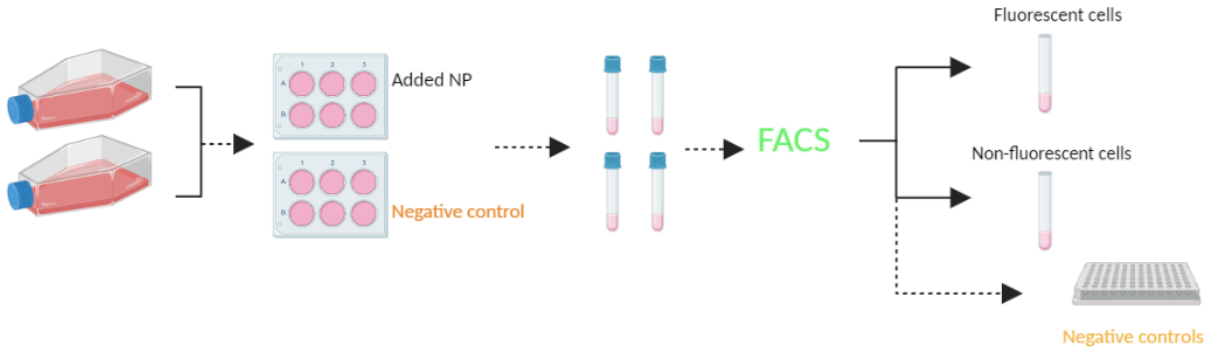

Figure 7: Experimental setup of NP exposure to cell cultures for both Proteomics and Transcriptomics. A total of four T-75 flasks of cells was used in the nanoplastic exposure experiment. Cells cultivated with or without antibiotics were seeded into 6-well plate.

2.5.2 Microscopy of cells

The 6-well plates containing cells exposed to NP as well as controls were observed in the fluorescent microscope (Zeiss, Axiocam 202 mono) after 24 hours incubation, and then every 48 hours for 9 days for the first exposure experiment. Once the method was further optimized, pictures of the cell cultures were taken only after 7-9 days of incubation with NP particles.

Composites fluorescence micrographs were created in ImageJ (Fiji) to combine the fluorescent channel pictures with the light channel pictures. Subsequently, pictures from the fluorescent channel were stacked on top of the pictures from the light channel, and the fluorescent parts were colored purple to enhance any visible particles. This was performed on all pictures taken for both the samples and the controls. The fluorescent pictures could not clearly distinguish ingested particles and particles bound to the surface of the cell.
In order to evaluate whether particles were bound to cell surface or ingested by the cells, imaging of NP-exposed cells was done using the DeltaVision™ (DV) Elite deconvolution microscope (GE Healthcare Life Sciences, Marlborough, USA). The cell markers CellMask™ Green (CMG) and LysoTracker™ Deep Red (LDTR) were used for staining cell membranes and lysosomes in the cells respectively at a concentration of 1:2000.

NP-exposed cells incubated for one week were stained with LDTR and CMG as follows: Briefly, 1.5 µl each of CMG and LDTR were added to 3 ml of L15 media, mixed thoroughly and added to cells in the 35 mm glass culture dishes. After incubation for 30 minutes, the media containing CMG and LDTR was replaced with fresh L15 media after washing three times with PBS to enable observation of cells under the microscope.

The microscope captured widefield fluorescence images and applied a deconvolution algorithm to improve resolution and contrast (Hira et al., 2020). The microscope system used a 60 x 1.42NA oil immersion objective and a sCMOS camera. The images with fluorescence were captured with DAPI (diamidino-2-phenylindole) and Cy5 (Cyanine-5) filter sets with excitation from respectively 390/18 nm and 632/22 nm, and emission from 435/48 nm and 679/34 nm (Table 3). Any areas where fluorescent particles seemed to be in close relation to cell organelles were saved in the DV software and further explored. The acquisition software

DeltaVision SoftWoRx™ (GE & Healthcare, 2014) was used to deconvolve the images, and Fiji was subsequently used to perform image analysis.

Table 3:Excitation and emission ranges of the most common filters used in DV imaging. A combination of the DAPI and Cy5 filters was used for this purpose and cells were stained with LysoTracker™ Deep Red, and Cell Mask Green.

	DAPI	FITC	TRITC	CY5
Excitation	405 *(381-399)*	488 *(464-489)*	568 *(531-556)*	642 *(621-643)*
Emission	411-459	501-549	574-620	662-696

2.5.3 Flow cytometry: enrichment of fluorescent cells

To augment the population of fluorescent cells that had internalized nanoparticles, a fluorescence-based flow cytometry technique was employed. Fluorescent cells resulting from uptake of NPs were sorted into a separate tube by the fluorescent-activated cell sorting (FACS) on the BD FACSAria™ III (BD, NJ, USA) as follows. After 6-9 days incubation, depending on the cell type, cells exposed to NPs as well as unexposed control cells were washed 2-3 times with PBS, trypsinized and transferred to 15 ml tubes. Conditioned media was prepared for culturing the sorted cells. Approximately 5 mL of the cells suspension were passed through a cell filter cap into a glass tube prior to FACS in order to de-clump the cells. These tubes were centrifuged at 100g for 3 minutes, and ~60% of the supernatant was removed. The fluorescent cells identified through FACS, were first sorted into 5 mL tubes containing approximately 100 µL of conditioned L15 media with 0.5% pen/strep before the entire suspension was transferred into a single well on a 96-well plate. The surrounding wells were filled with PBS to keep them from drying. All non-fluorescent cells were firstly sorted into a separate tube, before diluted and plated onto a separate 96-well plate. For the cells not exposed to plastic particles (negative controls), a number of 3000 cells was sorted into each well on a 96-well plate according to the scheme described in Figure 8.

Fluorescent cells were sorted by using the violet 405-nm laser of the FACSAria™ cell sorter. This laser generally detects wavelengths of 450 and 510 nm.

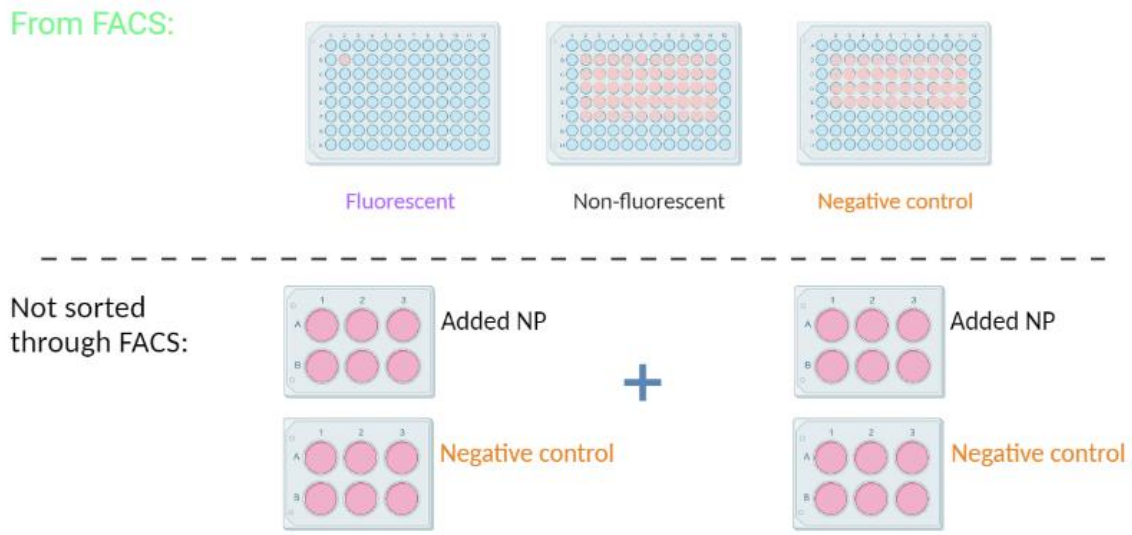

Figure 8: Setup of all cells resulting from FACS (cell sorting) as well as the 6-well plates left for RNA- and protein extraction. Cell sorting was performed on all the prepared samples, resulting in a total of three 96-well plates of sorted cells for each cell type (ASK-1, SHK-1 and CHSE-214). One of the plates contained cells that had been exposed for plastic particles and showed fluorescence, and one plate contained cells not giving emitting fluorescence. The last plate contained negative controls with no plastic particles. As described previously, the cells exposed to plastic was firstly sorted into two separate tubes and then plated out in the 96-well plates as described above. All surrounding wells on the 96-well plates were filled with PBS which prevented them from drying.

2.6 Label free proteomic analysis of NP-exposed vs. non-exposed ASK-1 cells

As a preliminary proteomic study within this project, a comparison of salmon cells exposed to NPs and those not exposed to NPs was performed using label free mass spectrometric proteomic analysis method. ASK-1 cells in 6-well plates incubated with and without NP particles for 7 days (Figure 9) were washed three times in PBS after aspiration of old L15 media. Approximately 50 µl lysis buffer (1M Urea, 0.5% Sodium Deoxycholate (SDC), 100 mM Triethylammonium bicarbonate (TEAB)) was used to lyse cells. Lysed cells were transferred to Eppendorf tubes and subjected to 25 cycles of sonication (1 minute on and 30 seconds off) with 100% amplitude in a cuphorn sonicator, with watercooler (cuphorn/watercooler: Qsonica. Sonicator: Fisherbrand FB705 sonicator, Fisher). Protein concentrations in lysed samples were estimated by the Bicinchoninic acid (BCA) protein assay method.

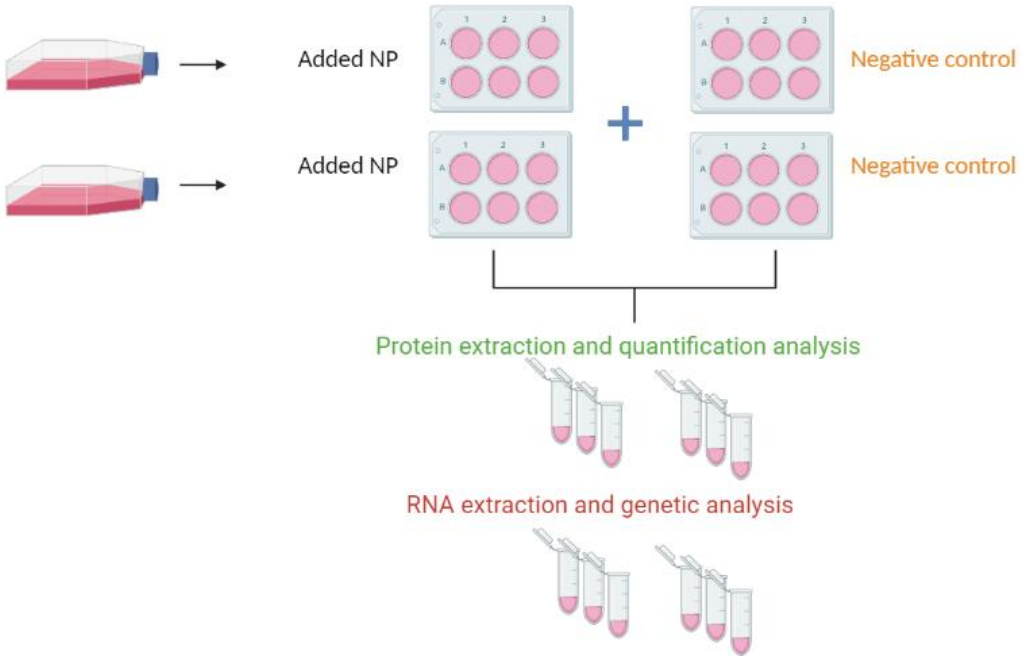

Figure 9: Experimental setup of cell cultures for non-labelled proteomic analysis and transcriptomic analysis. Cells from two T-175 cell culture flasks were used for NP exposure followed by protein extraction about a week later.

The BCA Protein Assay was used to determine the protein concentration in the samples employing a microtiter protocol supplied by the manufacturer protocol (Table 1). Optical densities were measured at 595 nm using a FLUOstar OPTIMA plate reader (BMG LABTECH) to measure the absorbances of the copper complexes in both samples and standards. The protein concentration of each sample was calculated based on the standard curve constructed from readings from the BCA assay with premade dilutions of bovine serum albumin (BSA) (Figure 10). All concentrations/dilutions for the proteins assay, including the setup of samples and standards, are given in Appendix – A.

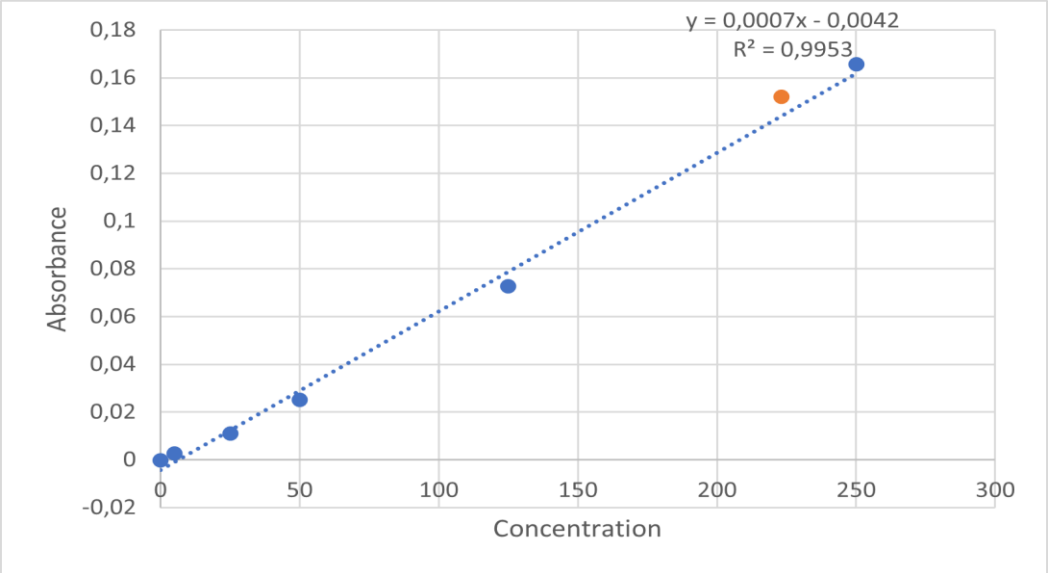

Figure 10: A standard curve based on the known BSA concentrations was plotted to make it possible to generate an equation for the slope which was used to calculate the specific protein concentrations.

2.6.1 Sample preparation and Mass spectrometry

Mass spectrometric analysis of protein samples was conducted on protein extracts retrieved from ASK-1 cells exposed to polystyrene particles, and coherently on cells not exposed to the particles. The analysis was performed at the Proteomics and Metabolomics Core Facility (PRiME) of UiT. The protein samples were analyzed with Orbitrap *Exploris 480.* This is a high-performance mass spectrometer used for analysis of complex biological samples (ThermoFisher Scientific). Label-free protein quantification was performed on protein extracts retrieved from ASK-1 cells exposed to NP particles. Non-exposed cells served as controls.

Briefly, cells were sonicated for 25 cycles (1 minute on and 30 seconds off) with 100% amplitude in a cuphorn sonicator, with watercooler (cuphorn/watercooler: Qsonica. Sonicator: Fisherbrand FB705 sonicator, Fisher). Disulfide bridges in the protein extracts were reduced with 1.4-dithiothreitol (DTT) with a final concentration of 5 mM and in incubation at 54ºC for 30 minutes. Cysteins were then alkylated with 15 mM iodoacetamide (IAA) followed by incubation for 30 min at room temperature in the dark. To remove excess IAA, DTT solution corresponding to a final concentration of 5 mM was added. Calcium chloride solution was

added to the sample to a final concentration of 1 mM, and proteins in samples were digested with 100ng of Lys-C (Wako, 125-05061) for 5 hours.

Lysozyme C and Trypsin digestion of samples was achieved by treatment with 1.5 µg Trypsin (V511A, Promega) and overnight (16 hours) incubation under gentle agitation at 37 °C. After digestion, SDC was precipitated by adding 50 % formic acid to the sample (final concentration of 2.5 % v/v). Samples were then incubated for 10 min and centrifuged at 13.000 rpm for 15 min. Supernatants containing peptides were transferred to new Protein Low Bind tubes. The peptides were concentrated and cleaned up using DPX C18 pipette tips (DPX Technologies, XTR tips 10 mg C18AQ 300) on a Tecan Fluent pipetting robot. Purified peptide samples were dried in a vacuum concentrator and dissolved in 20 µL 0.1 % formic acid. Peptide concentration was measured on a spectrophotometer (Nanodrop ONE, Thermo Fisher Scientific, Massachusetts, USA) at 205 nm, 31 methods with baseline. Thereafter, 0.5 µg peptides per sample were loaded for liquid chromatography-mass spectrometric (LC-MS) analysis.

The peptide mixtures containing 0.1% formic acid were loaded onto a ThermoFisher Scientific EASY-nLC1200 system and EASY-Spray column (C18, 2 µm, 100 Å, 50 µm, 50 cm). Peptides were fractionated using a 5-80% acetonitrile gradient in 0.1% formic acid over 60 minutes at a flow rate of 300 nl/min. The separated peptides were analysed using a ThermoFisher Scientific Orbitrap Exploris 480 mass spectrometer. The resulting data was collected in data dependent mode using a Top20 method. Data was searched the uniprot *Salmo salar* database using Proteome Discoverer™ 3.0. Protein identification was done with the Sequest search engine. A volcano plot analysis was used to determine significantly up- and downregulated proteins.

2.6.2 Protein pathway and network analysis

From the data retrieved from MS analysis in the software Proteome Discoverer™, it was possible to identify interesting up and down regulated proteins which could be further studied. To identify correlation between differentially expressed proteins in A. salmon ASK-1 cells after exposure to NPs, the publicly available programs STRING and Kyoto Encyclopaedia of

Genes and Genomes (KEGG) was used to search and visualize relevant protein pathways and networks. These programs made it possible to find correlations between the differently expressed proteins and thus connect the proteins to biological functions and systems.

2.6.3 Transcriptomics of NP-exposed and non-exposed ASK-1 cells

Transcriptomics analysis was done in order to evaluate differential expression of selected genes when ASK-1 cells were exposed to NPs. The targeted genes, namely *hsp70, hsp90* are stress related genes, while *igm, igt*, and *mhcI are immune related* genes (Abarghouei et al., 2021; Danilova et al., 2005; Natarajan et al., 1999; Piazzon et al., 2016; Ryo et al., 2010). Gene-specific forward and reverse primers were utilized for these genes (Table 4).

Table 4: Primer sequences of target genes used in qPCR reaction. Information provided by Sigma-Aldrich®.

Gene		Forward sequence (5'-3')	Reverse sequence (5'-3')
hsp70		TGACGTGTCCATCCTGACCAT	CCAGCCGTGGCCTTCAC
hsp90		TTGCGTGGAACTAAGGTGA	CCAATGAACTGAGAGTGCT
igm		TGAGGAGAACTGTGGGCTACACT	TGTTAATGACCACTGAATGTGCAT
igt		CAACACTGACTGGAACAACAAGGT	CGTCAGCGGTTCTGTTTTGGA
mhc1		ATGGTGGAGCACATCAGCC	CTCAGCCTCAGGCAGGGAC

Elongation factor 1α (*ef-1α)* was used as the internal reference gene, chosen from a selection of available housekeeping genes based on its PCR efficiency (Table 5). A total of two qPCR runs were performed.

Table 5: Primer sequence and accession number for the gene used as reference gene in the qPCR reaction (Ingerslev et al., 2006).

Housekeeping gene	Abbreviation		Sequence (5'-3')	GenBank accession no.	Species
Elongation factor 1a	*ef-1α*	Fwd. Rev.	GCTGTGCGTGACATGAGG ACTTTGTGACCTTGCCGC	AF321836	A. salmon

RNA extraction was performed on ASK-1 cells exposed to polystyrene and controls not exposed to polystyrene, using the RNAqueous RNA isolation kit according to the manufacturer´s instructions. Briefly, cells in 6-well plates incubated with and without NP particles for 7 days (Figure 9) were washed three times in PBS after aspiration of old L15 media. Cell lysis buffer (400 µl) was added to each of the wells. The cells were then scraped

away with a cell scraper and transferred to Eppendorf tubes. Cells from two wells were pooled into one tube to a total volume of 800 µl in each of the tubes.
An equal volume of 800 µl of 64% ethanol was added to all the tubes with lysate mix, making a total volume of 1.6 ml. The tube was briefly vortexed to mix the reagents. Fresh collection tubes with a filter cartridge were prepared and marked. Subsequently, 700 µl of the lysate mix was pipetted onto the filter and the tubes were centrifuged for 1 minute at 1400 rpm. The flow-through was discarded. This process was then repeated until all the lysate mix had gone through the filter. A volume of 700 µl of wash solution #1 was applied to the filter, the tubes were centrifuged as above and flow-through discarded. Following this, 500 µl of wash solution #2/3 was added to the filter, the tubes were centrifuged again and flow-through was discarded. The tubes were then centrifuged an additional time for 30 seconds and any flow-through left in the tube was discarded. The filter was transferred to a new collection tube and 20 µl of Elution buffer was added to the filter in two rounds. In between the addition of elution buffer, the tubes were centrifuged for another 30 seconds.
Lastly, the filter was discarded, and the RNA concentration was measured in all samples using NanoDrop. Samples was stored in -80ºC over-night until cDNA synthesis was performed.

2.6.4 cDNA synthesis

cDNA synthesis was performed with the high-capacity cDNA reverse transcription kit/ QuantiTect Reverse Transcription kit. The RNA samples were thawed on ice while all reagents in the kit was thawed in room temperature. The RNA concentration of the samples was measured again on the day of cDNA synthesis. The reagents in the kit were mixed gently by flicking the tubes and briefly centrifuging if needed. The genomic DNA elimination reaction was prepared on ice. A volume of 2 µl wipe out buffer was mixed with 2 µl water and 10 µl of the RNA extract. This mixture was then incubated at 42ºC for two minutes. After the incubation time the samples were put directly on ice. A mixture of 1 µl Reverse Transcriptase, 4 µl of Reverse Transcriptase Buffer and 1 µl Reverse Transcriptase Primer mix, was mixed with the 14 µl of template RNA sample. The tubes were incubated at 42ºC for 15 minutes, followed by 3 minutes at 95ºC. The samples were put directly on ice again

after incubation time. The cDNA concentration was measured with NanoDrop before samples was placed in -20ºC until further analysis.

2.6.5 Real-time qPCR

Real-time PCR was performed in combination with the two-dye tracking system PowerTrack™ SYBR™ Green Master Mix kit supplied by Thermo Fischer Scientific. PowerTrack™ master mix reagents and cDNA samples were thawed before preparation of standards and dilutions for qPCR. From the previously synthesized cDNA, a concentration of 2.5 ng/µl was made for each of the samples used in the PCR. Standards was prepared with concentrations given in Table 6. Triplicates was implicated for all standard concentrations, as well as the unknown samples.

Table 6: Standard dilutions and final starting quantities of cDNA used for PCR.

Standard dilution	Starting Quantity (SQ) ng/µl
1:1	2.5
1:10	0.25
1:100	0.025
1:1000	0.0025

A Master mix of 12.5 µl Yellow Sample Buffer, 250 µl Power Track™ SYBR™ Green Master Mix, 72.5 µl of nuclease free water, and 20 µl of forward and reverse gene-specific primer. The master mix was vortexed before 15 µl was added to the wells in the 96-well PCR plate. Samples and standards were then vortexed before 5 µl of these were added to the master mix in the wells. The setup of samples and standards are shown in Table 7.

Table 7: Setup of qPCR in 96-well plate. Dilution relationships indicate the correlated standard triplicates. There were two sets of NP exposed samples and two sets of control samples in total, and triplicates of each sample was included in the qPCR.

		1	2	3	4	5	6	7	8	9	10	11	12
Hsp70	A	1:1	1:1	1:1	1:10	1:10	1:10	1:100	1:100	1:100	1:1000	1:1000	1:1000
Hsp70	B	NP-A	NP-A	NP-A	NP-B	NP-B	NP-B	C-A	C-A	C-A	C-B	C-B	C-B
Hsp90	C	1:1	1:1	1:1	1:10	1:10	1:10	1:100	1:100	1:100	1:1000	1:1000	1:1000
Hsp90	D	NP-A	NP-A	NP-A	NP-B	NP-B	NP-B	C-A	C-A	C-A	C-B	C-B	C-B
IgM	E	1:1	1:1	1:1	1:10	1:10	1:10	1:100	1:100	1:100	1:1000	1:1000	1:1000
IgM	F	NP-A	NP-A	NP-A	NP-B	NP-B	NP-B	C-A	C-A	C-A	C-B	C-B	C-B
Mhc I	G	1:1	1:1	1:1	1:10	1:10	1:10	1:100	1:100	1:100	1:1000	1:1000	1:1000
Mhc I	H	NP-A	NP-A	NP-A	NP-B	NP-B	NP-B	C-A	C-A	C-A	C-B	C-B	C-B

The qPCR was in accordance with the Power Track™ SYBR™ Green (ThermoFisher) Protocol; (Table 8).

Table 8: PCR cycles with associated temperatures and duration.

PCR profile	Degrees	Time	Cycles	Ramp rate (degrees/sec)
Pre-incubation	95	2 min	1	
Amplification	95	15 sec		4.4
Annealing	65	60 sec	40	4.4
Extension	72	10 sec		
Default dissociation step				
Step 1	95	15 sec	1	1.6
Step 2	60	1 min		1.6
Step 3	95	15 sec		0.1
Cooling	40	10 sec	1	2.2

The data from qPCR was downloaded and analyzed in the LightCycler® 480 software (Roche Diagnostics, Germany).

2.6.6 Gene expression analysis

The PCR efficiency and the relative expression ratio of the target gene compared to a reference gene, was calculated based on the Cp values given in the LightCycler® software. PCR efficiency was calculated using Equation 3.

$$PCR\ efficiency = 10^{\frac{-1}{slope\ of\ standard\ curve}} \qquad \textit{Equation 3}$$

The relative expression of target genes were then calculated with Equation 4.

$$Ratio = \frac{E_{target}^{\Delta CP_{target}(control-sample)}}{E_{reference}^{\Delta CP_{target}(control-sample)}} \qquad \textit{Equation 4}$$

With a stable reference gene, Equation 3 can be shortened to Equation 5.

$$Ratio = E_{target}^{\Delta CP_{target}(control-sample)} \qquad \textit{Equation 5}$$

The calculated relative expression was then used to observe any upregulations of target genes in the sample compared to the control.

3 Results

3.1 Cell culture

The protocols and methods for cultivation of ASK-1. SHK-1 and CHSE-214 cells as described in section “Growing cell culture” of the Materials and Methods are well established in the project group at NORCE (Strømsnes et al., 2022). Routinely, cells are passaged at least three times after resuscitation from the cold before being exposed to NPs. ASK-1 and SHK-1 cells seeded in T25 tissue culture flask at approximately 10^4 cells/ml in Leibovitz L15 medium with 10% FBS achieved 70-90% confluency after 10 days. CHSE-214 cells seeded at the same cell density achieved similar confluency in 6 days (Figure 11).

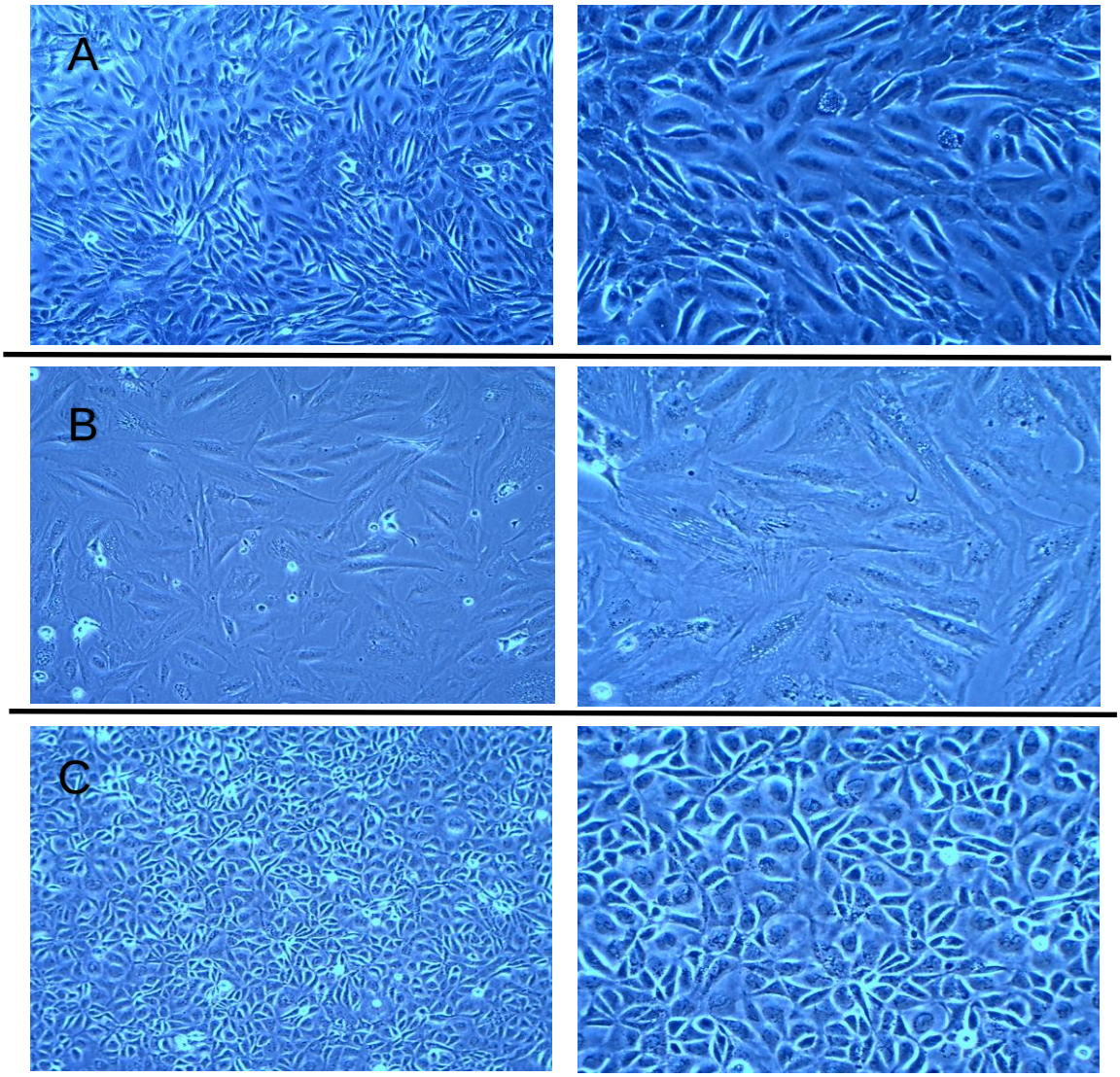

Figure 11: ASK-1, SHK-1 and CHSE-214 cells. All pictures were acquired with light microscope. ***A:*** *ASK-1 cells 4 days after passage.* ***B****: SHK-1 cells 7 days after passage.* ***C****: CHSE-214 cells 7 days after passage. Magnification: x10 (left column), x20 (right column)*

The growth characteristics of SHK-1 cells were found to be comparable to those of ASK-1 cells; however, the cultivation of SHK-1 cells required some initial adjustments due to some distinct characteristics. Notably, SHK-1 cells exhibited a higher degree of sensitivity and demonstrated a faster response to Trypsin treatment during passage of cell cultures compared to ASK-1 cells. SHK-1 cells, similarly, to ASK-1 cells, took 7-14 days to reach 70-90% confluency and was incubated with NPs for seven days.

3.2 Uptake of fluorescent polystyrene particles in fish cells

3.2.1 Fluorescent microscopy

Comparison of the images acquired with the light and fluorescent channels revealed some fluorescent particles either adherent on the cell surface or ingested and thus internalized within the cells. Through image processing using Fiji adding the fluorescent channel image on top of the light channel image, it could be inferred that the particles were internalized (Figure 12). Further, the particles were neither dislodged nor their positions changed following vigorous washes with PBS. Figure 12 through 17, shows the pictures acquired from

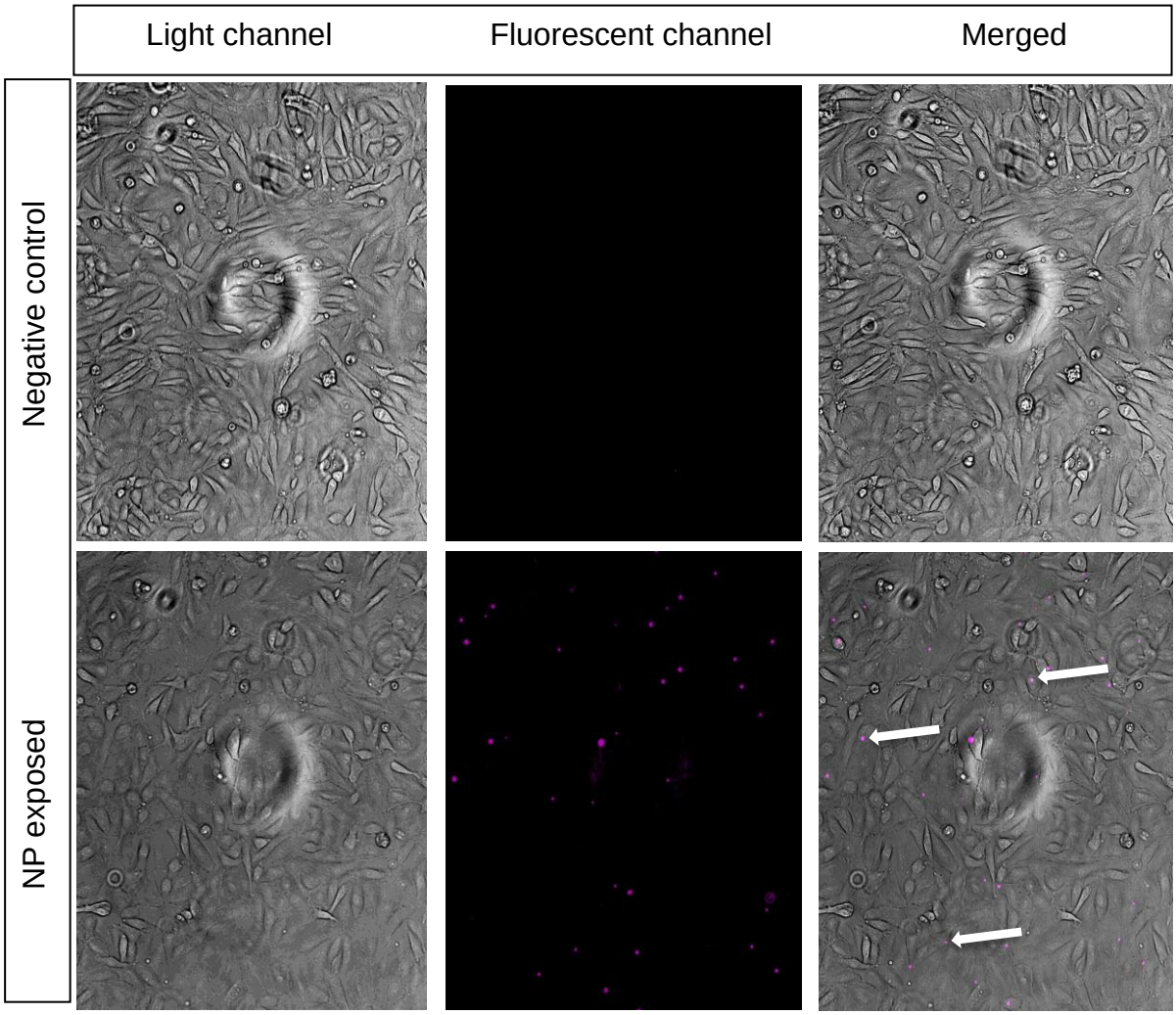

Figure 12: ASK-1 cells exposed to polystyrene nanoparticles of 503 nm with Plum Purple fluorescence. Images acquired with fluorescent microscope (magnification: x20). Top row includes controls. Bottom row includes cell culture exposed to NPs. Both cultures were incubated for seven days before fluorescent microscopy. Pictures were edited in Fiji to make the fluorescent particles purple, and to merge the picture from the fluorescent channel together with the picture form the light channel (on the right). The circle in the middle of the pictures taken with the light channel, is a shadow from the microscope and is not a part of the cell cultures.

fluorescent microscopy processed in Fiji. Although it was clear that some particles was in close proximity with some cells, it was still difficult to determine whether the particles were adhered to the surface of the cell or if it was in fact ingested.

In order to confirm whether the NPs were internalized or adhered to cell surfaces, the NP-exposed cells were lysosome stained with LysoTracker ™ Deep Red (LTDR) and imaged with the DeltaVision™ deconvolution imaging.

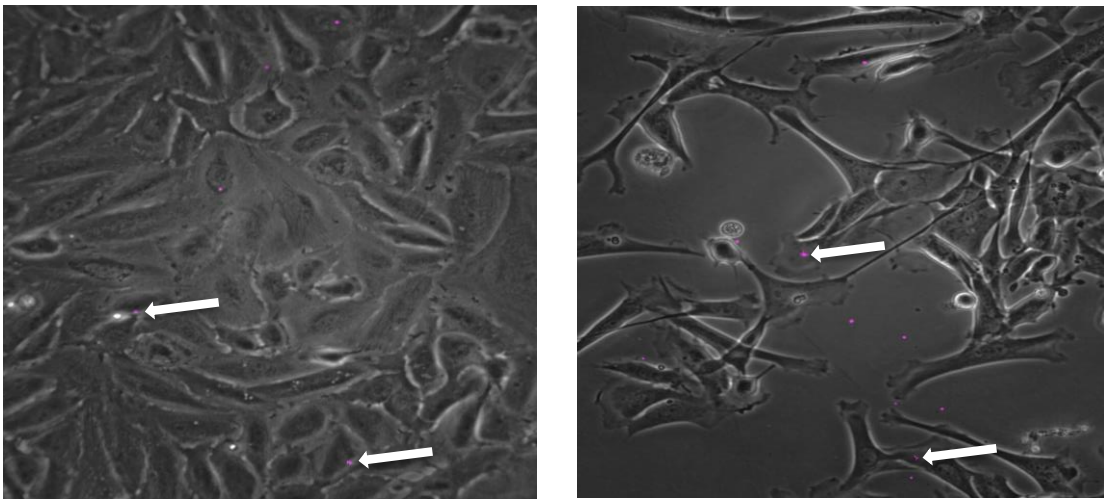

Figure 13: Fluorescent microscopy of ASK-1 cells exposed to fluorescent NPs. Images are taken in x40 magnification, seven days after exposure to NPs. Fluorescent polystyrene is coloured purple and fluorescent channel image is merged with light channel image through editing in Fiji. Arrows mark some particles that seemed to be colocalized with the cells.

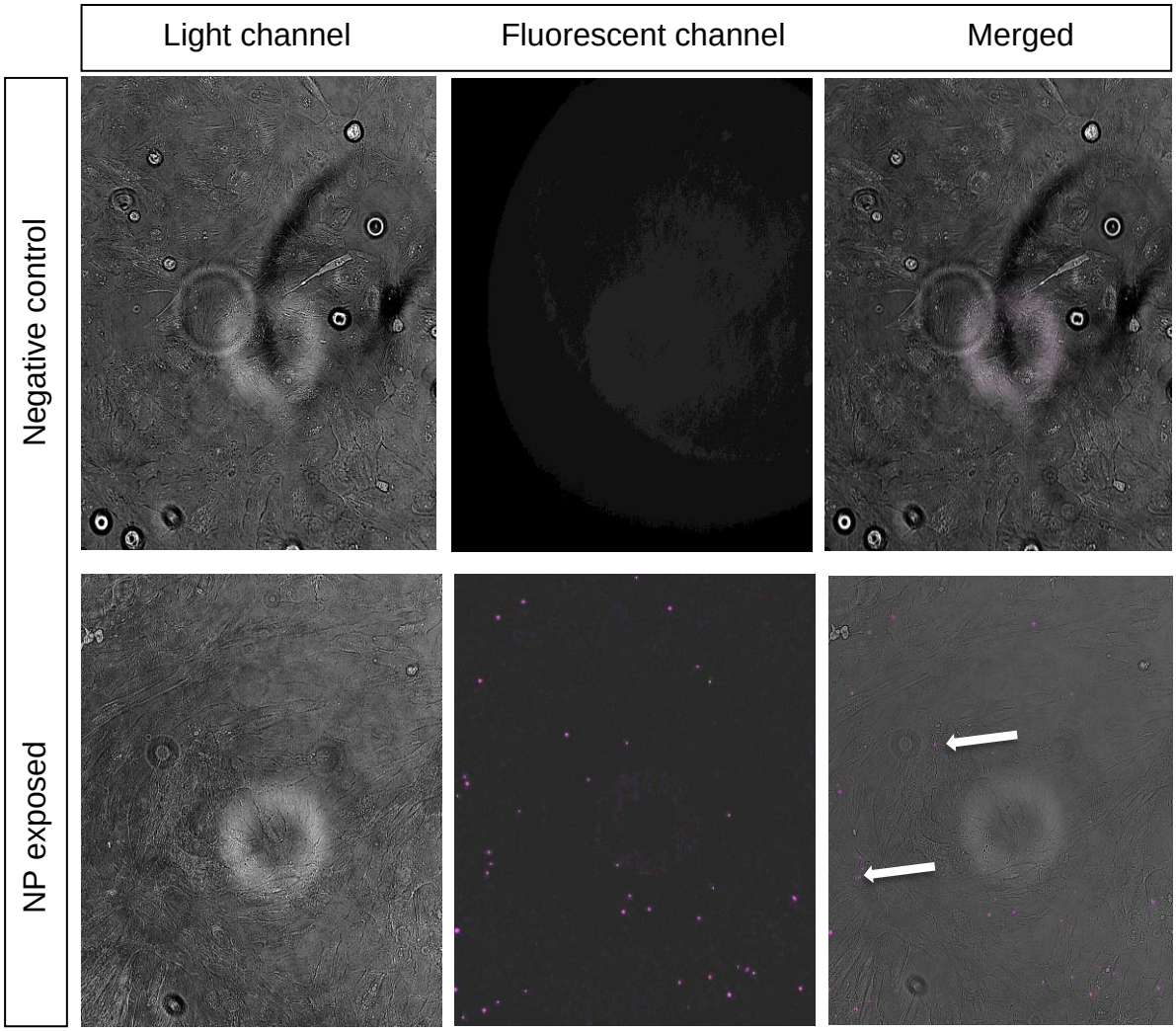

Figure 14: SHK-1 cells exposed to polystyrene nanoparticles of 503 nm with Plum Purple fluorescence. Images acquired with fluorescent microscope (magnification: x20). Top row includes controls. Bottom row includes cell culture exposed to NPs. Both cultures were incubated for seven days before fluorescent microscopy. Pictures were edited in Fiji to make the fluorescent particles purple, and to merge the picture from the fluorescent channel together with the picture form the light channel (on the right). The circle in the middle of the pictures taken with the light channel, is a shadow from the microscope and is not a part of the cell cultures.

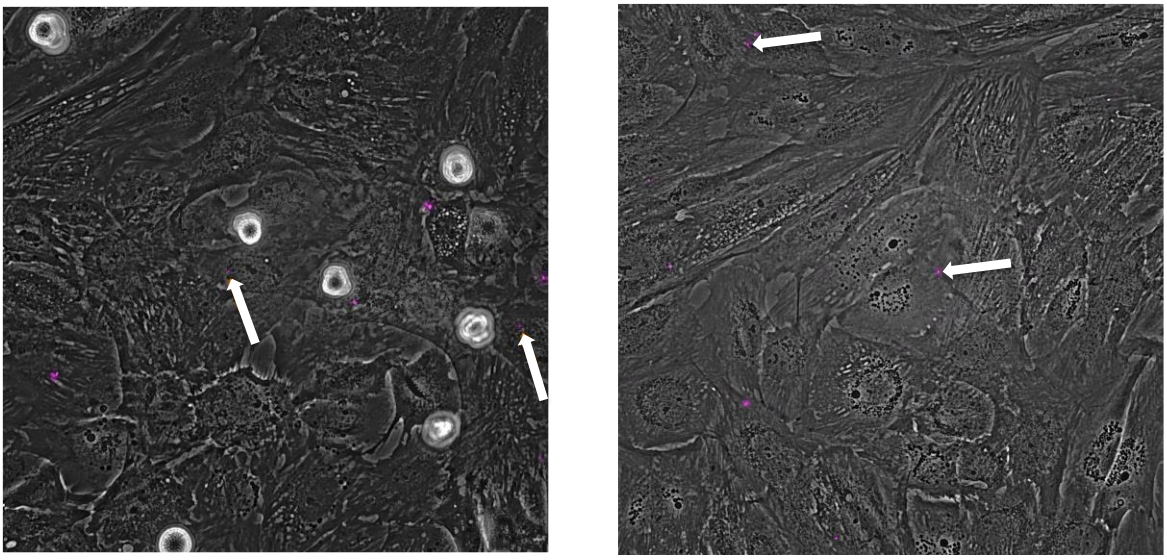

Figure 15: Fluorescent microscopy of SHK-1 cells exposed to fluorescent NPs. Images are taken in x40 magnification, respectively three (left) and seven (right) days after exposure to NPs. Fluorescent polystyrene is coloured purple and fluorescent channel image is merged with light channel image through editing in Fiji. Arrows mark some particles that seemed to be colocalized with the cells.

Initial observations during the early rounds of polystyrene exposure and subsequent fluorescent imaging of CHSE-214 cells indicated a general lack of particle ingestion or adherence. This conclusion was drawn based on the observed movement of particles within the floating media of the cultures, rather than their static adherence to the cells at the bottom of the culture flasks. However, noteworthy changes were observed in the later stages of the exposure experiment, once the procedure had been repeated several times. After 4-7 days post-exposure, it became evident that certain fluorescent particles had indeed been ingested by or adhered to the CHSE-214 cells (Figure 16, Figure 17). This observation suggests a potential time-dependent uptake process, wherein particles were internalized by a prolonged exposure.

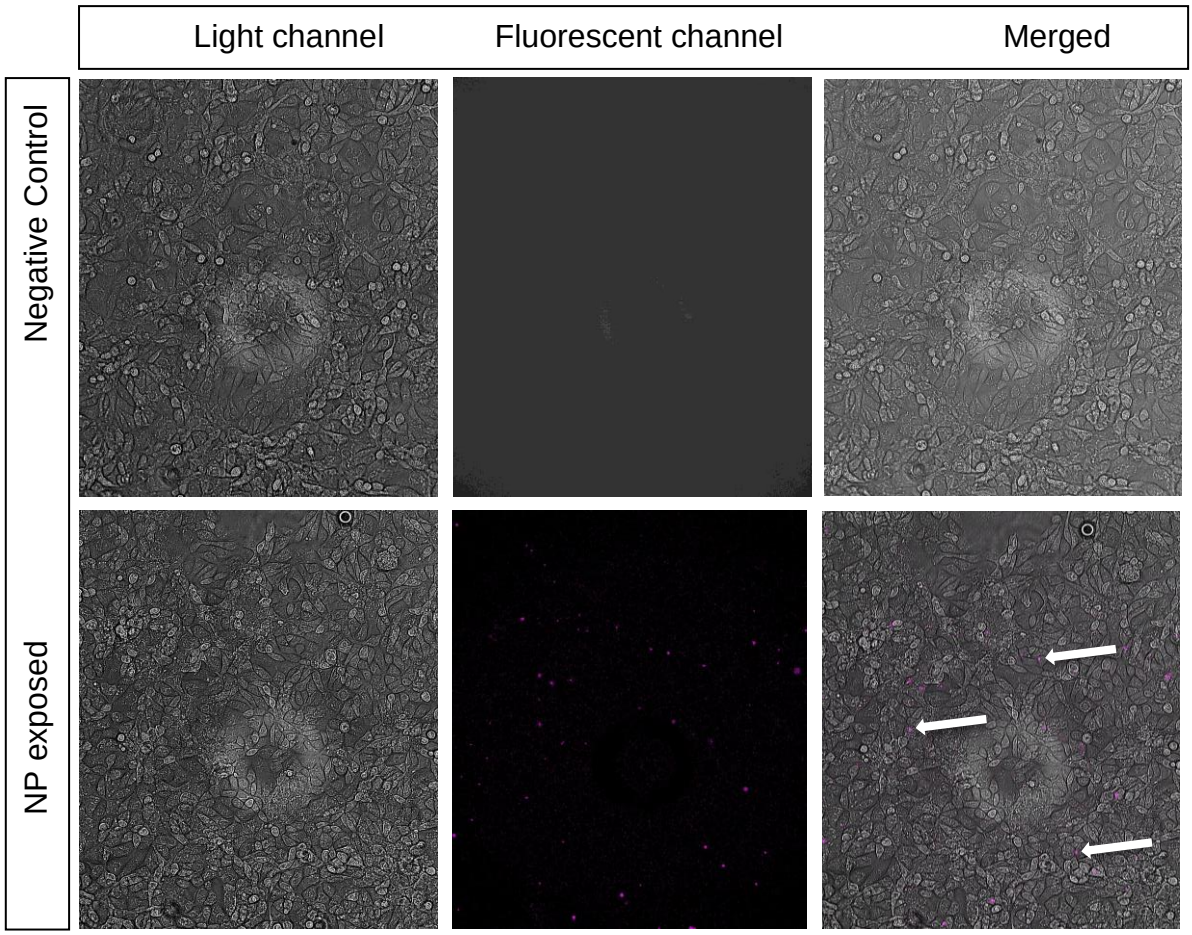

Figure 16: CHSE-214 cells exposed to polystyrene nanoparticles of 503 nm with Plum Purple fluorescence. Images acquired with fluorescent microscope (magnification: x20). Top row includes controls. Bottom row includes cell culture exposed to NPs. Both cultures were incubated for seven days before fluorescent microscopy. Pictures were edited in Fiji to make the fluorescent particles purple, and to merge the picture from the fluorescent channel together with the picture form the light channel (on the right). The circle in the middle of the pictures taken with the light channel, is a shadow from the microscope and is not a part of the cell cultures.

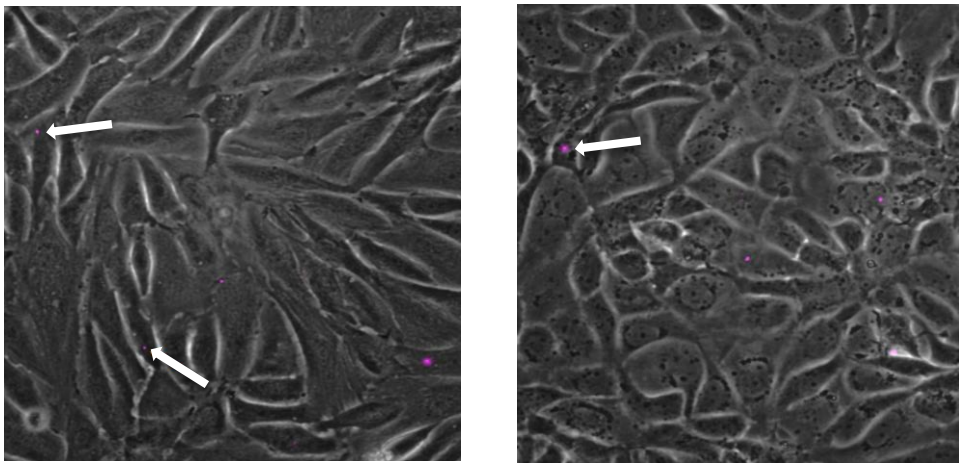

Figure 17: Fluorescent microscopy of CHSE-214 cells exposed to fluorescent NPs. Images are taken in x40 magnification, seven days after exposure to NPs. Fluorescent polystyrene is coloured purple and fluorescent channel image is merged with light channel image through editing in Fiji. Arrows mark some particles that seemed to be colocalized with the cells.

3.2.2 DeltaVision™ Imaging of polystyrene particles colocalized with lysosomes

Through lysosome staining with LysoTracker ™ Deep Red (LTDR) and 3D imaging with DV, it was possible to localize the polystyrene particles associated with or in stained lysosomes in the cells. For all three cell types, the NP particles showed up close to or were confined in the lysosomes. The three-dimensional images also indicated that the particles lied in between lysosomes, suggesting there were lysosomes both underneath and over the NPs (Figure 18-24).

Lysosomes stained with LTDR was edited to magenta, and polystyrene particles were made turquoise for colour blind viewers.

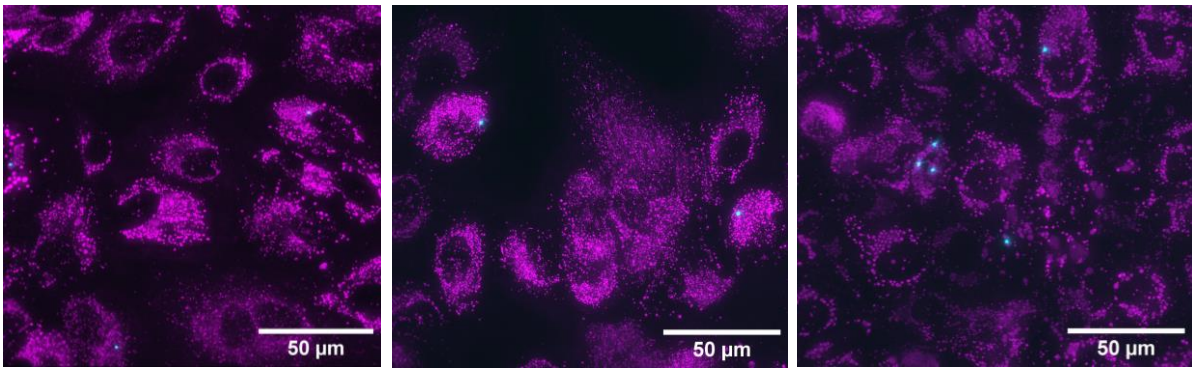

Figure 18: Images of stained lysosomes (magenta) and polystyrene NPs (turquoise) in respectively ASK-1 (A), SHK-1 (B) and CHSE-214 (C) respectively. Images taken in DeltaVision™ and processed in Fiji.

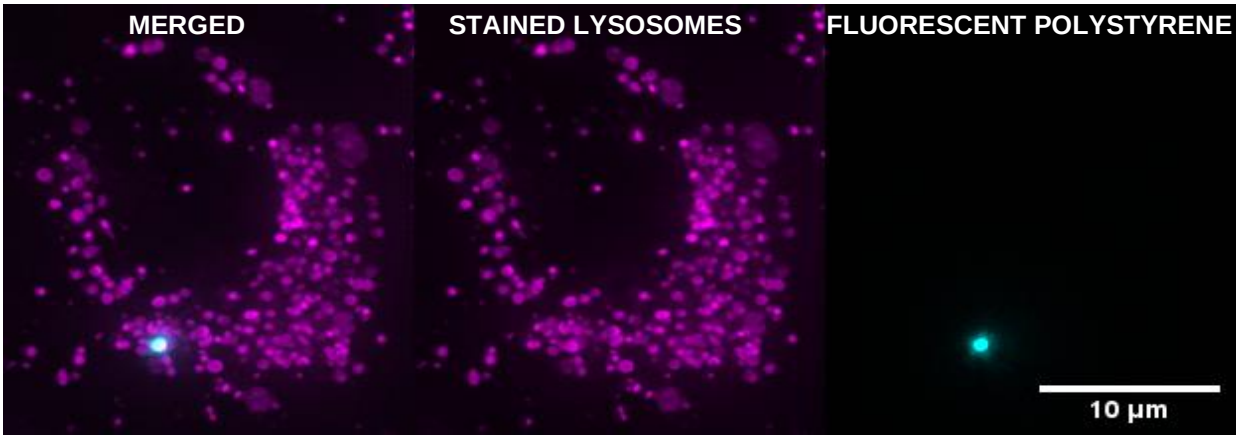

Figure 19: 2D images from DeltaVision™ of ASK-1 cells. Lysosomes are stained with LysoTracker™ Deep Red (LTDR) before imaging. Images are edited in Fiji and colours are changed for visualization purposes.

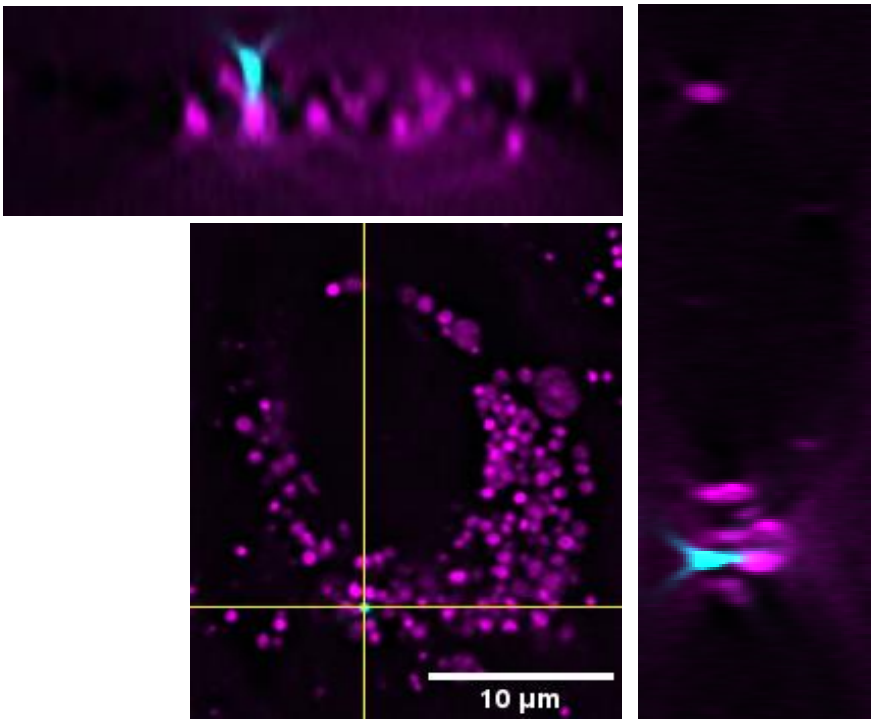

Figure 21: 3D images of ASK-1 cells with fluorescent polystyrene particles. Lysosomes are stained with LysoTracker™ Deep Red (LTDR) and edited to show up as magenta. Polystyrene particles are edited to show up in turquoise.

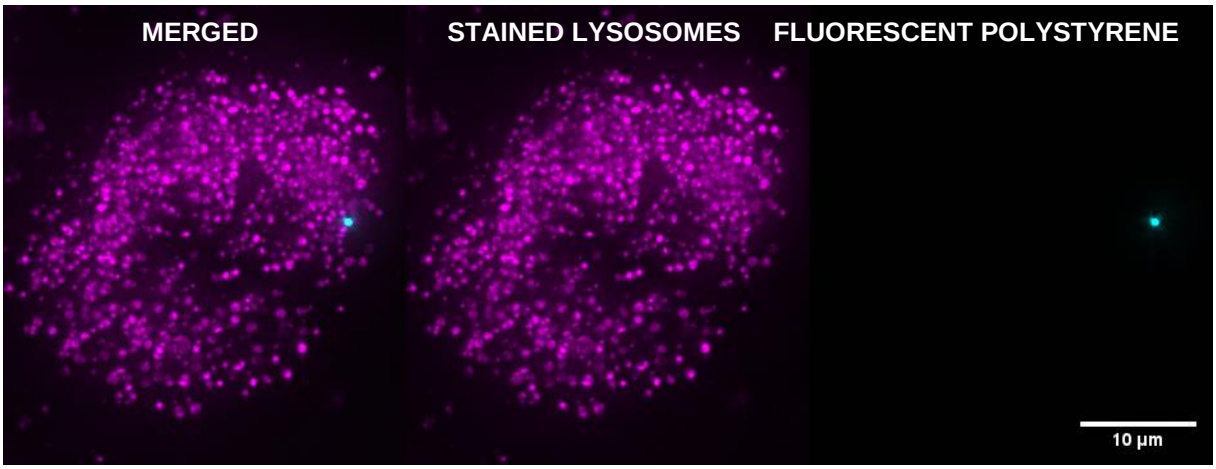

Figure 20: 2D images from DeltaVision™ of SHK-1 cells. Lysosomes are stained with LysoTracker™ Deep Red (LDTR) before imaging. Images are edited in Fiji and colours are changed for visualization purposes.

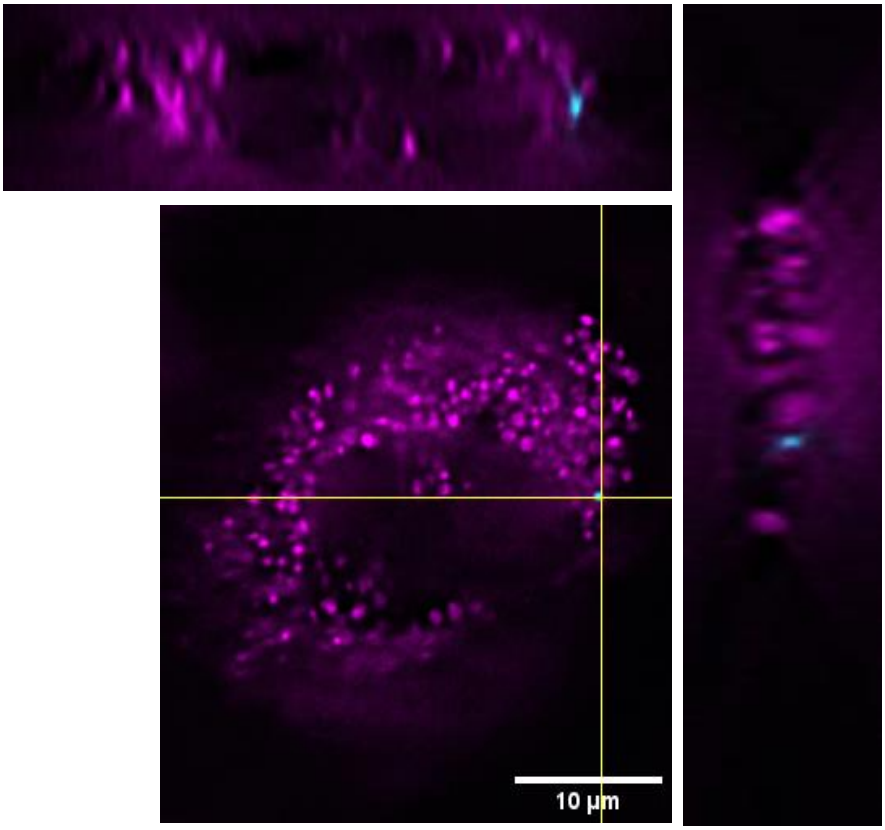

Figure 22: 3D images of SHK-1 cells. Lysosomes are stained with LysoTracker™ Deep Red (LTDR) and polystyrene particle shown in turquoise.

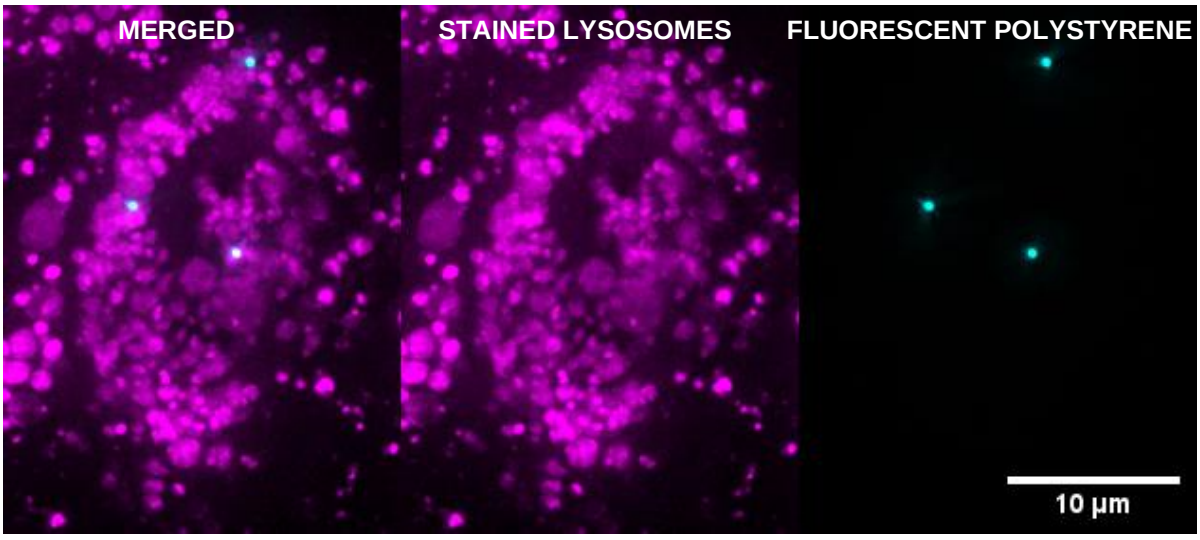

Figure 23: 2D images from DeltaVision™ of CHSE-214 cells. Lysosomes are stained with LysoTracker™ Deep Red (LTDR) before imaging. Images are edited in Fiji and colours are changed for visualization purposes.

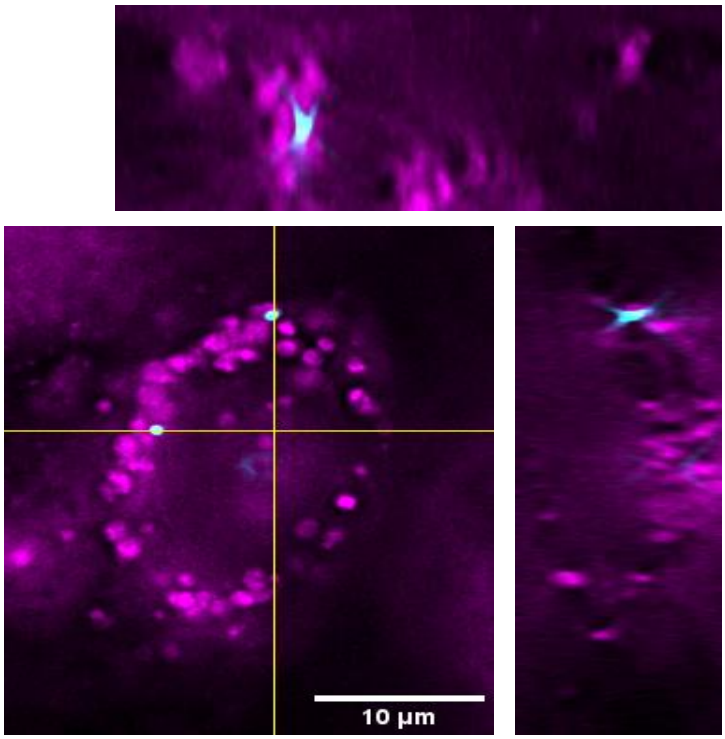

Figure 24: 3D images of CHSE-214 cells with fluorescent polystyrene particles. Lysosomes are stained with LysoTracker™ Deep Red (LTDR) and edited to show up as magenta. Polystyrene particles are edited to show up in turquoise.

Altogether, the results for all three cell lines show NPs that are associated to lysosomes, indicating that particles are ingested. The 3D view of the cells shows particles in contact with lysosomes which would support the assumption that NPs are transported to/into lysosomes.

3.3 Enrichment of fluorescent cells

Another method to find out whether the cells contained particles is using flow cytometry method based on fluorescence (FACS). By leveraging the violet laser functionality of the BD FACSAria™, it became feasible to isolate all cells emitting a distinct violet fluorescence from the remaining cell population (Figure 25). In the FACSDiva software, one gate excluding everything but particles with the size of a cell was set up (P1). One gate excluding all cells that did not fluorescence (P2) within the chosen spectra (Figure 25) was also established.

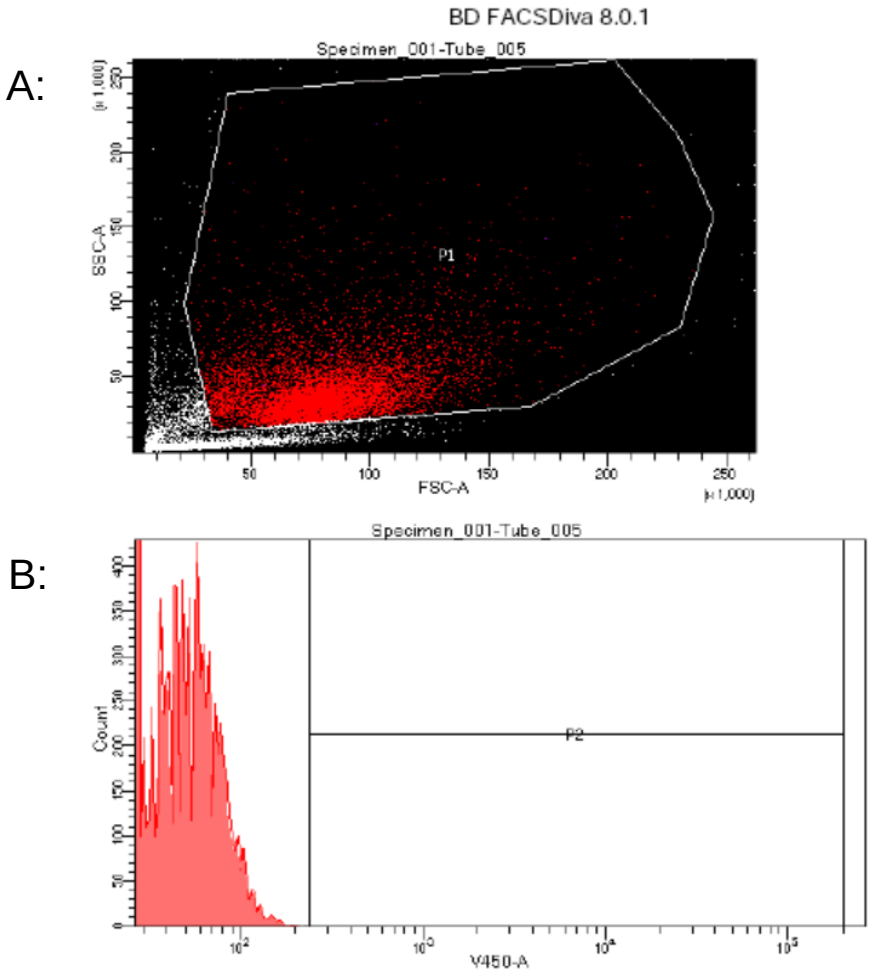

Figure 25: Display of data collected during cell sorting of ASK-1 cells through the BD FACSAria™ system. A: The gate named "P1" encloses all particles considered cells based on size. The x-axis gives the forward-scatter and y-axis the side-scatter which combined defines the size of the particles. B: The gate named "P2" encloses all cells with a fluorescence greater than the threshold levels which are set based on the negative controls which should not have any fluorescence. The laser used in this analysis was the Violet450 laser which optimally detects wavelengths of 450 nm. The x-axis of the histogram shows the intensity of the fluorescent signal detected, while the y-axis represents the cell count.

The first couple of attempts of cell sorting of ASK-1 cells exposed to fluorescent polystyrene particles was relatively unsuccessful and they showed very low numbers of fluorescent cells. However, after increasing plastic concentration, incubating cells for longer time to achieve higher confluency, and generally acquiring more practice with the performed methods, the cell sorting eventually gave more "promising" results. Thus, in the second try of cell sorting of cells that have been exposed to a polystyrene diluted by 10^{-5}, a total number of 320 cells with particle-derived fluorescence was sorted. This was an improvement from the first cell sorting try which only gave about 25 cells with fluorescence. In the third and final attempt, a total number of 1001 fluorescent cells was enriched. These cells were all collected in one

single well on separate 96-well plates and incubated until further analysis. A total of 1001 fluorescent cells compared to a total of 1 840 000 non-fluorescent cells, made a percentage of cells that had ingested the polystyrene particle to 0.05% (Table 9).

Conditioned media was also used in this third trial, unlike in the two first attempts. Non-fluorescent cells, which was considerably higher in number, was also kept for possible further analysis. As such, a higher number of non-fluorescent cells were brought to wells of the 96-well plates. Control cells, not exposed to particles, were also sorted through FACS, and transferred directly into a 96-well plate. The wells all contained 3000 cells each, as this was set in the FACSDiva software. These cells were also distinguished between cells cultured in media with and without antibiotics.

Once cell sorting had been successfully performed on ASK-1 cells, the same procedure was repeated for SHK-1 and CHSE-214 cells. This cell sorting gave a total of 448 fluorescent SHK-1 cells out of a total number of 603 910 sorted cells, which amounted a percentage of 0.074% fluorescent cells. For CHSE-214 cells, there was a total of 116 fluorescent cells out of 426 414 totally sorted cells. This means the percentage of fluorescent CHSE-214 cells was 0.027% (Table 9).

Table 9: Numbers of sorted cells through FACS. Cell lines ASK-1. SHK-1 and CHSE-214 are included. Percentage of total fluorescent cells is calculated from the number of fluorescent cells divided by the total number of sorted cells.

Cell line	Fluorescent cells	Non-fluorescent cells	Total number of cells	Percentage of cells with fluorescence
ASK-1	1001	1 840 000	1 841 001	0.05%
SHK-1	448	603 462	603 910	0.074%
CHSE-214	116	426 298	426 414	0.027%

After ASK-1 cells had been enriched from the FACS and cultured in 96-well plates, the growth of the cells was varying. Non-fluorescent cells reached 75-85% confluency in approximately 14 days and was then transferred to two wells on a 12-well plate. Subsequently, negative control cells reached 75-85% confluency after about four weeks. From this point, these cells were transferred to larger wells and split into several wells as they reached confluency. Because of the low number of enriched fluorescent cells, this culture had a somewhat delayed growth (Figure 26). Fluorescent CHSE-214 cells reached 75-85% confluency and could be transferred to bigger wells, after 20 days.

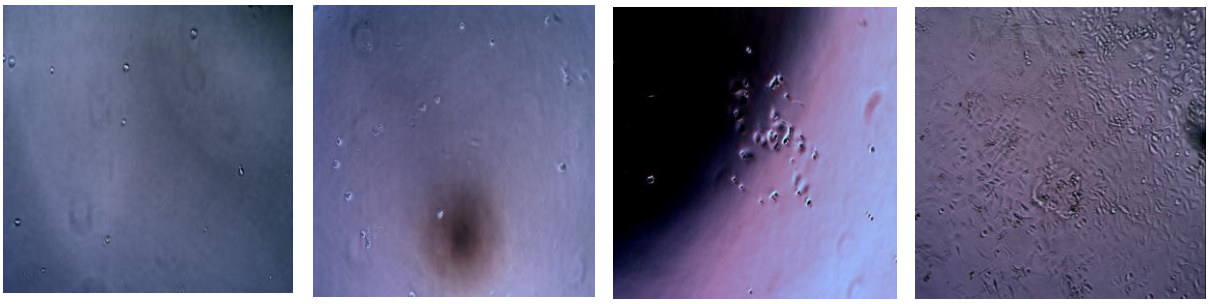

1 day after FACS | 10 days after FACS | 13 days after FACS | 5 weeks after FACS

Figure 26: Microscopic images of ASK-1 cells enriched through FACS. A total of 1000 fluorescent cells were sorted and cultivated into one single well on a 96-well plate. Pictures were taken frequently to observe any cell division and culture growth. Images are taken with x10 magnification.

3.4 Differential protein expression of NP-exposed cells

Due to time constraint, CHSE-214 and SHK-1 cells were not subjected to proteomic analysis. The concentration of proteins in the isolated protein from ASK-1 cells exposed to plastic particles, was analyzed by the BCA Protein Assay. The measured absorbance of BSA standards and protein samples, associated standard curve, and calculated concentrations, are presented in Appendix – A. Protein concentrations of the three samples used in the assay was respectively 2091.14, 1951.43 and 2231.43 µg/ml.

The equation of the slope from the standard curve used to calculate protein concentration is given in Equation 6.

$$y = 0.0007x - 0.00042 \qquad \textit{Equation 6}$$

The mass spectrometry analysis conducted on cells exposed to NPs and cells not exposed to NPs yielded a repertoire of expressed proteins. A total of approximately 8800 proteins were identified in the samples. To assess the impact of plastic particle exposure on protein expression, the ratio of proteins expressed in the cells exposed to plastic particles was compared to proteins expressed in cells not exposed to the particles. This calculation was performed using Proteome Discoverer software (PD), allowing for a quantitative evaluation of the differential protein expression between the two conditions. The software also made it possible to filter out non-significant hits based on the number of unique peptides, their abundance ratios, and a preset p-value of 0.05. All proteins with an abundance ratio higher than 1 were considered upregulated, and any proteins with abundance ratios lower than 1 were considered downregulated. These proteins are given in Appendix – B.

To investigate whether the protein expression in NP exposed samples was significantly different to the protein expression in the controls, a Principal Component Analysis (PCA) plot was generated (Figure 27). The plot visualizes the triplicates of both NP exposed sample and control cells as separate dots. The function of a PCA plot is to visualize high dimensional data and reducing the complexity by finding patterns and correlations between the variables. There were two outliers in the plot, referring to the two data points, one from each variable, deviating from the overall pattern or distribution of the data. Nonetheless, one could disregard these outliers because the placement of the other points in the plot could identify a difference between the two variables.

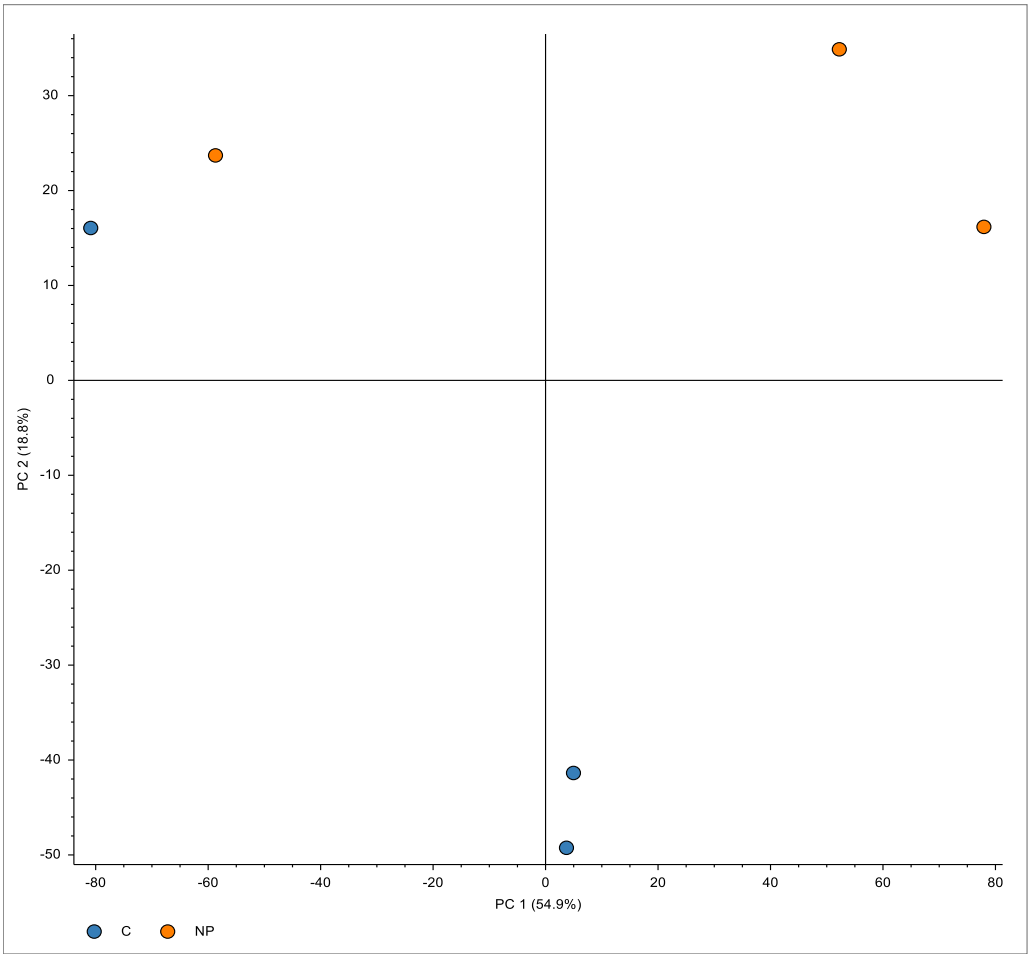

Figure 27: PCA plot visualizing the difference in expression of proteins between the NP exposed samples and the negative controls not exposed to NPs. The majority of the points representing the replicates, are far apart from each other in the graph, which means there is reason to believe that there is a significant difference in expression between the two variables. The two points found in the top left part of the plot were identified as outliers but could be disregarded based on the visible difference between the rest of the points within the two variables.

The Proteome Discoverer™ 3.0 Software analysis generated a comprehensive range of protein function categories. These categories provided insights into the specific functional pathways represented by the identified proteins. To visually represent the distribution of expressed proteins within each category and facilitate a comparison of highly expressed protein functions, a pie-chart was constructed. Figure 28 showcases this diagram, which highlights the diverse functions of the proteins expressed in the samples, enabling a deeper understanding of the pathways associated with the experimental conditions. The graph shows that several of the categories of biological processes includes both upregulated and downregulated proteins. However, some categories are only found in either of the groups. For both upregulated and downregulated proteins, the biological process that included most proteins expressed, was the one called “other metabolic processes”. As these categories are generated by the PD software, there can be issues with connecting all proteins to one specific biological function or process.

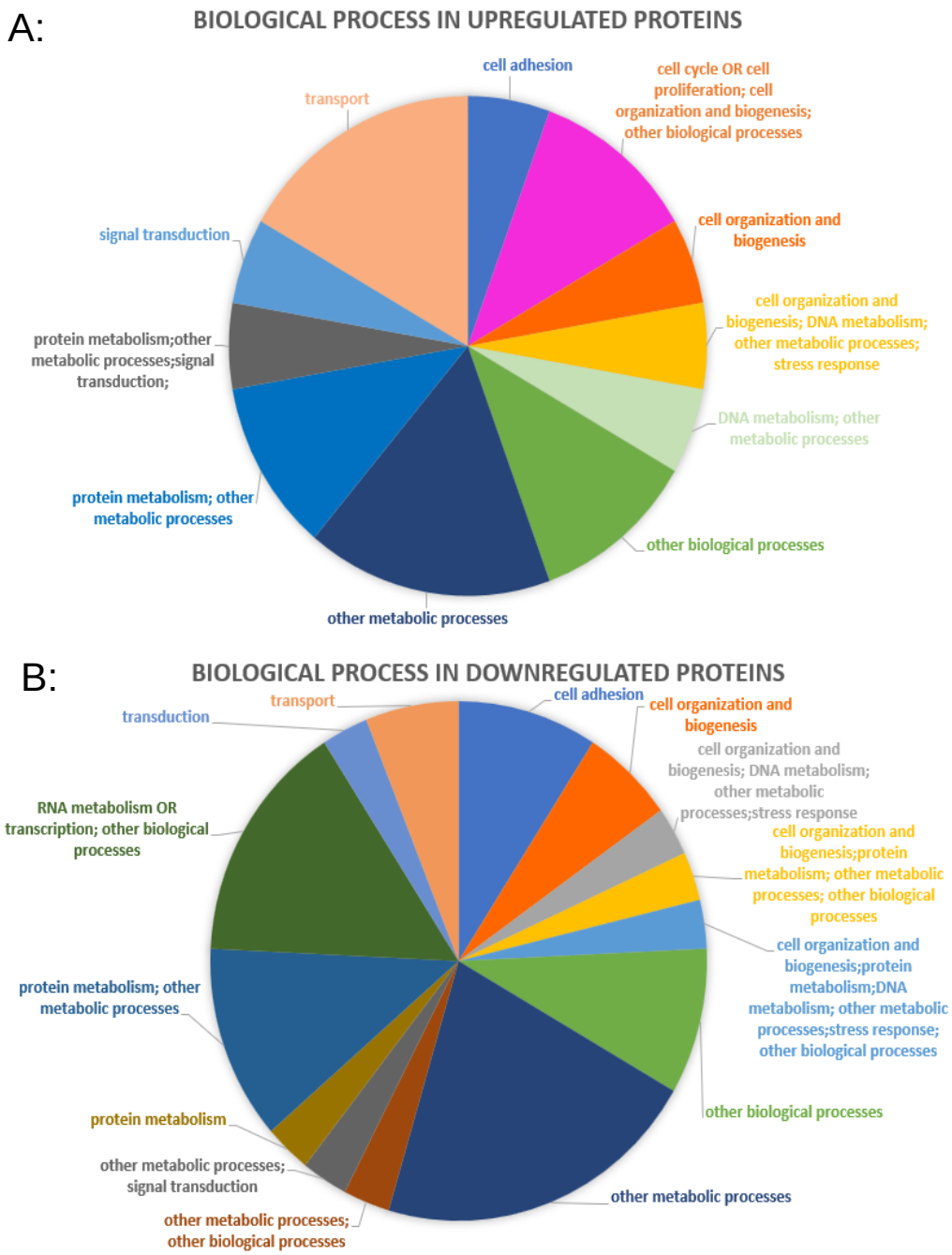

*Figure 28: **A**: Biological processes connected to significantly upregulated proteins in NP sample compared to control. **B**: Biological processes connected to significantly downregulated proteins in NP sample compared to control. The biological functions are generated by the Proteome Discoverer™ software connected to the MS analysis. Both diagrams are colour sorted in the same colours. Only the 118 significantly expressed proteins are included in this diagram.*

A volcano plot was used to filter out proteins that for different reasons would not be viewed as significant (Figure 29). Firstly, all proteins that were expressed in only one of the variables were removed. Then, a p-value of 0.05 was included to filter out any statistically non-significant results. This resulted in a total of 36 upregulated proteins, and 82 downregulated proteins. From this selection of expressed proteins, it was possible to further study the details about each specific protein.

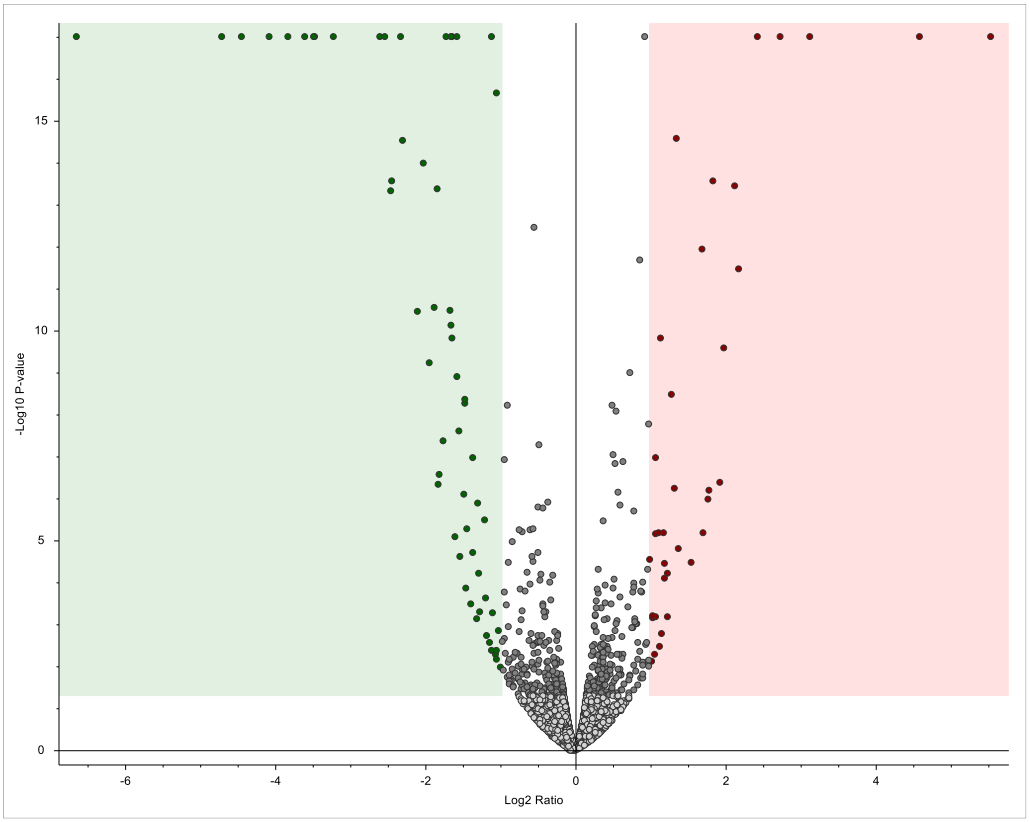

Figure 29: Volcano plot presenting all significantly differentially expressed proteins in the samples. Each dot represents a separate protein which are placed along the x-axis based on their logarithmic abundance ratio. Y-axis shows the P-value which has a lower limit of 0.05. The green area covers all significantly downregulated proteins, while the red area covers all the significantly upregulated proteins. Model is generated in Proteome Discoverer™ software.

To visualize the relationships between upregulated and downregulated proteins, a bar graph based on the abundance ratios of the significantly expressed proteins was created (Figure 30). The zero point of the graph is set at 1, which is the point separating upregulated proteins from downregulated ones. Although there was a higher number of downregulated proteins compared to upregulated, the bar graph show that the abundance ratio is generally further from 1 for the upregulated proteins than for the downregulated proteins.

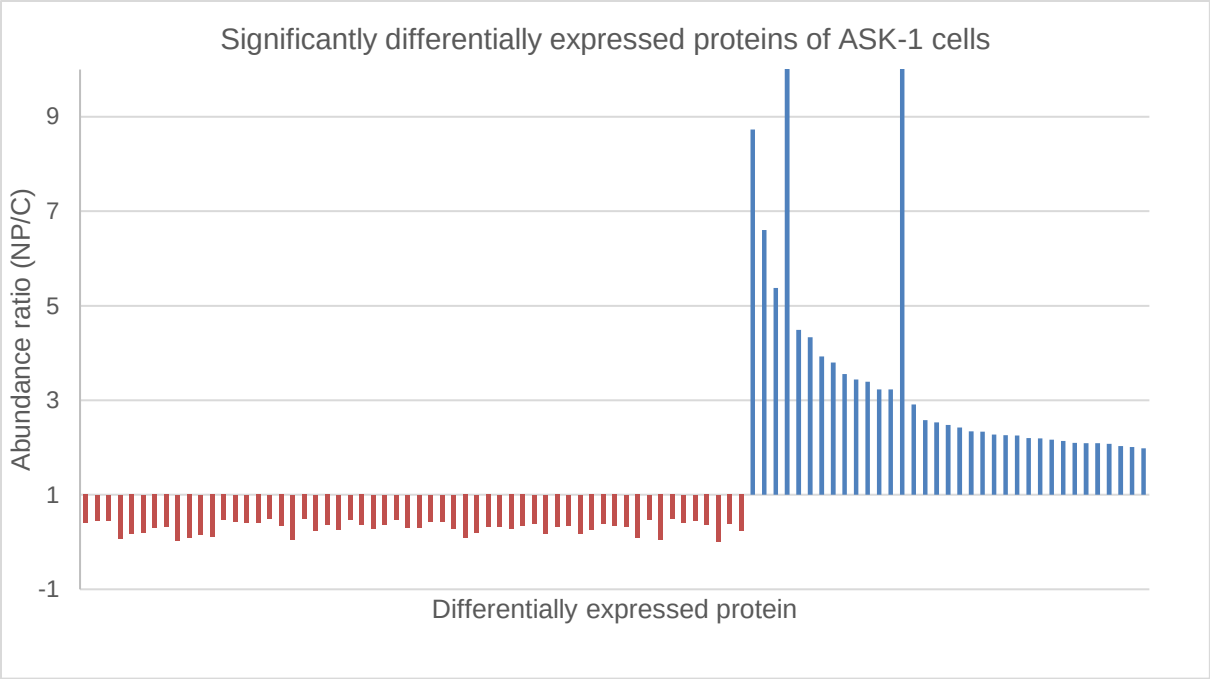

Figure 30: Bar graph showing all significantly expressed proteins in the protein samples from ASK-1 cells. Red bars represent all proteins with an abundance ratio (NP/C) less than 1. meaning they are downregulated. Blue bars represent all proteins with an abundance ratio higher than 1. meaning they are upregulated. Threshold for abundance ratio value was set at 1. Proteome Discoverer™ software was used to generate the values accounted for in this graph.

Furthermore, it was favorable to further study a selection of differentially expressed proteins which could act as biomarkers in the unknown responses to exposure to NPs in the salmon ASK-1 cell line. The protein pathways: apoptosis pathway (*map04210*), p53 pathway (*map04115*), autophagy pathway (*map04140*) and phagocytosis pathway (*map04145*) were further investigated through the KEGG online database (KEGG: Kyoto Encyclopedia of Genes and Genomes). Table 10 shows a selection of differentially expressed proteins which have previously been documented as stress-related in response to some external factors.

Table 10: A selection of differentially expressed proteins found in samples of ASK-1 cell line exposed to NPs. Proteins are selected based on relevant literature stating their role in stress-related responses. Differentially expressed proteins which have a role in given protein pathways are also included. A combination of the Proteome Discoverer™ software and the online KEGG database was used to generate the information.

Gene symbol	Description of protein	Abundance ratio (NP/C)	Documented stress-relation	Biological function	Supporting literature	Protein pathway
casp3	Caspase-3 OS=Salmo salar OX=8030 GN=CASP3 PE=2 SV=1	1.072	Apoptosis immune-related,	Protein metabolism	(Beemelmanns et al., 2021; Dhamad et al., 2020)	• P53 • Apoptosis • MAPK signaling pathway • Cytosolic DNA-sensing pathway • Salmonella infection • Herpes simplex virus
jak1	Tyrosine-protein kinase OS=Salmo salar OX=8030 GN=jak1 PE=3 SV=1	1.105	Apoptosis, immune related	Protein metabolism, signal transduction	(Beemelmanns et al., 2021; Dhamad et al., 2020)	• Necroptosis • NOD-like receptor signaling pathway • Herpes simplex virus 1 infection
cyp1a	Cytochrome P450 1A OS=Salmo salar OX=8030 GN=CYP1A PE=2 SV=1	1.075	Oxidative stress and hypoxia-related		(Beemelmanns et al., 2021)	
prdx6	Peroxiredoxin-6 OS=Salmo salar OX=8030 GN=PRDX6 PE=2 SV=1	0.641	Oxidative stress and hypoxia-related		(Beemelmanns et al., 2021)	• Metabolic pathways • Glutathione metabolism pathway
rraga	Ras-related GTP-binding protein OS=Salmo salar OX=8030 GN=RRAGA	0.970	Oxidative stress and hypoxia-related		(Beemelmanns et al., 2021)	• Autophagy pathway • mTOR signaling pathway
txnd1	Thioredoxin domain-containing protein 1 OS=Salmo salar OX=8030	1.072	Oxidative stress		(Beemelmanns et al., 2021)	
sod1	Superoxide dismutase [Cu-Zn] OS=Salmo salar OX=8030 GN=SOD1 PE=2 SV=1	0.908	Oxidative stress	stress response	(Beemelmanns et al., 2021; Sendra et al., 2021)	• Peroxisome pathway
cata	Catalase OS=Salmo salar OX=8030 GN=cata PE=3	0.892	Oxidative stress	stress response	(Beemelmanns et al., 2021)	
grp75	Stress-70 protein, mitochondrial OS=Salmo salar OX=8030 GN=GRP75 PE=2 SV=1	1.010	Oxidative stress, hypoxia		(Dhamad et al., 2020)	• RNA degradation

A number of the proteins included in the apoptosis pathway (*map04210*) (Figure 31), was found differentially expressed in the ASK-1 samples (Table 11).

*Table 11: Proteins found differentially expressed in the ASK-1 samples exposed to NPs, with a role in the apoptosis pathway (*map04210*). Information generated through the Proteome Discoverer™ software and KEGG database.*

Protein	Gene symbol	Involvement in pathway	Abundance ratio
CASP3	*casp3*	Pro-apoptotic gene	1.072
FAP1	*ptpnI3*	Pro-survival gene	1.0977
IAP/XIAP	*birc4*	Pro-survival gene	0.977
P53	*tp53rk*	Pro-apoptotic gene	0.861
BAX	*bax*	Pro-apoptotic gene	0.799
α-tubulin	*tba*	Cleavage of substrates	0.947
α-tubulin	*tuba812*	Cleavage of substrates	0.827
Fodrin	*sptan1*	Cell shrinkage and membrane blebbing	1.022
Lamin	*lmnb1*	Loss of integrity of nuclear	0.955
Lamin	*lmnb2*	Loss of integrity of nuclear	0.982
PARP	*parp1*	Protein modification	1.031
PARP	*parp2*	Protein modification	1.641
ICAD	*dffa*	DNA fragmentation during	0.976
IKK	*ikbkb*	NF-κ B signaling pathway	0.957
Ras	*rask*	PI3K-Akt signaling pathway	0.983
Cathepsin	*catb*	Antioxidative mechanism	1.026

The apoptosis pathway (*map04210*) (Figure 31) is a complex network of proteins and genes, and as a range of proteins within this pathway were differentially expressed in the samples exposed to NPs, there would be reason to believe that this network is impacted by the exposure and possibly ingestion of the particles.

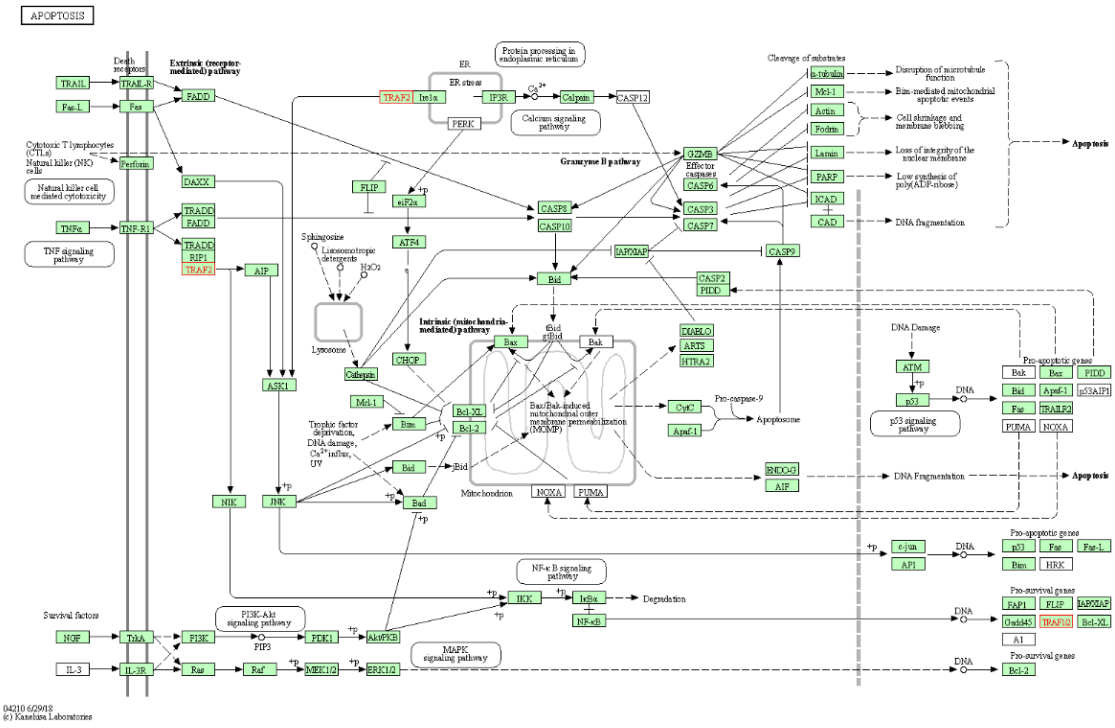

*Figure 31: Apoptosis pathway (*map04210*). Network of proteins involved in the mechanisms related to programmed cell death, apoptosis. Network is retrieved from the KEGG genetic database; (KEGG: Kyoto Encyclopedia of Genes and Genomes).*

A selection of proteins involved in the p53 signaling pathway (*map04115*) (Figure 32) was found differentially expressed in the ASK-1 cells exposed to NPs (Table 12). The protein CASP3, which is a known pro-apoptotic protein, was found up-regulated in the NP exposed samples.

*Table 12: Proteins found differentially expressed in the ASK-1 samples exposed to NPs, with a role in the p53 signalling pathway (*map04115*). Information generated through the Proteome Discoverer™ and KEGG software.*

Protein	Gene symbol	Involvement in pathway	Abundance ratio
CASP3	*casp3*	Apoptosis	1.072
P53	*tp53rk*	Pro-apoptotic gene	0.861
BAX	*bax*	Apoptosis	0.799
AIFM	*aifm2*	Apoptosis	0.958
P53R2	*rrm2*	DNA repair and damage prevention	0.964
TSAP6	*steap3*	Exosome mediated secretion	0.010
PERP	*perp*	Apoptosis	1.057
CDC2	*cdc2*	Cell cycle arrest	1.011
CDK2	*cdk2*	Cell cycle arrest	0.792

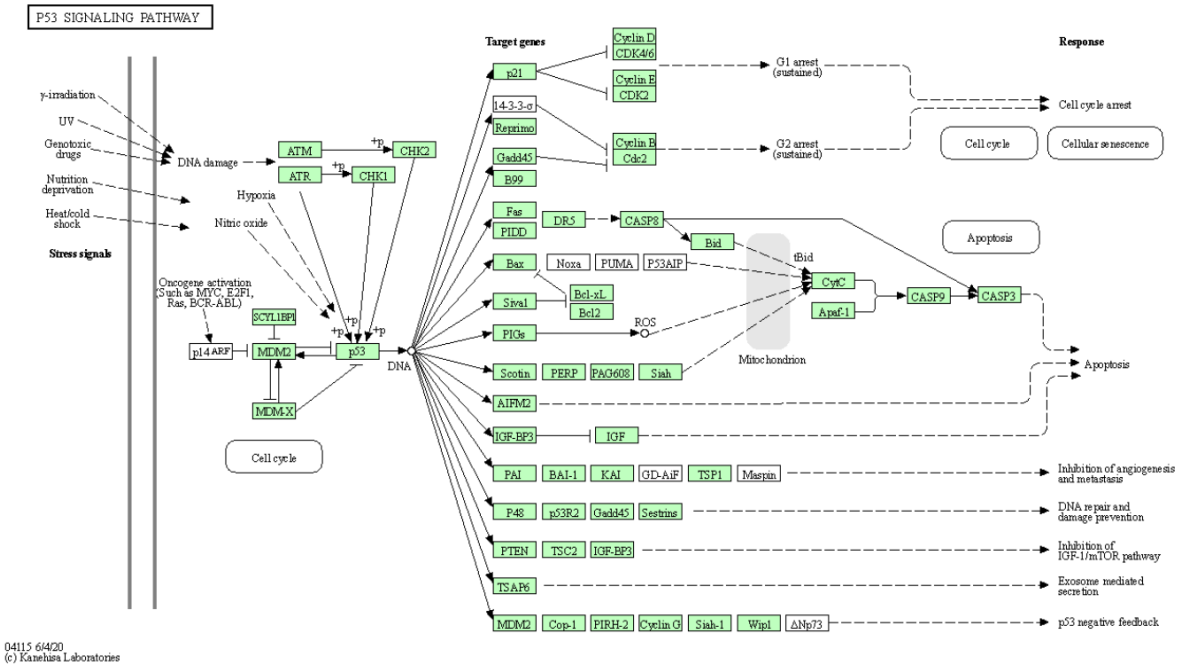

*Figure 32: P53 signalling pathway (*map04115*). Network of proteins involved in the mechanisms related to the p53 gene and its functions. Network is retrieved from the KEGG genetic database; (KEGG: Kyoto Encyclopedia of Genes and Genomes).*

From the selection of protein pathways studied in this project, the autophagy pathway (*map04140)* (Figure 33) was the one that contained the highest number of proteins with an up- or downregulation in the ASK-1 samples (Table 13).

Table 13: Proteins found differentially expressed in the ASK-1 samples exposed to NPs, with a role in the autophagy pathway (map04140). Information generated through the Proteome Discoverer™ software and KEGG database. ER = Endoplasmic reticulum.

Protein	Gene symbol	Involvement in pathway	Abundance ratio
IGFR	*igf1r*	Insulin signaling pathway	0.691
RAS	*rask*	MAPK signaling pathway	0.983
MEK1/2	*mp2k2*	MAPK signaling pathway	0.591
ERK	*mk03*	MAPK signaling pathway	100
ERK	*mapk1*	MAPK signaling pathway	1.044
Rheb	*rheb*	Regulates mTOR pathway	0.976
Rheb	*rhebl1*	Regulates mTOR pathway	0.906
PKCς	*kpcd*	Protein processing in ER	0.956
RagA/B	*rraga*	Nutrient starvation	0.970
AMPK	*prkaa1*	AMPK signaling pathway	1.289
eIF2α	*if2α*	ER stress/ Nutrient starvation	1.101
ATG5	*atg5*	Autophagosome formation	1.036
ATG16	*atg16I1*	Autophagosome formation	0.757
ATG3	*atg3*	Autophagosome formation	0.917
ATG4	*atg4b*	Autophagosome formation	0.994
ATG4	*atg4c*	Autophagosome formation	1.257
ATG7	*atg7*	Autophagosome formation	0.972
LC3	*map1Ic3a*	Microtubule-associated	1.040
LC3	*gbrI2*	Microtubule-associated	0.918
RAB7	*rab7a*	Ras-related	0.907
VAMP8	*vamp8*	Lysosome-associated	1.002
LAMP	*lamp2*	Lysosome-associated	0.899
LAMP	*lamp1*	Lysosome-associated	0.810
SNAP29	*snap29*	Lysosome-associated	1.043
CATD	*catd*	Peptidase	1.110
CTSD	*catId*	Degradation of the inner vesicle	1.136
CATB	*catb*	Antioxidative mechanism	1.026
MTOR	*mtor*	mTOR signaling pathway	0.946
HMGB1	*hmgb1*	ROS	0.950
Beclin	*becn1*	Autophagy	0.975
Bif-1	*sh3gIb1*	Apoptosis	1.045
ATG2	*atg2b*	Autophagy	0.952
mlST8	*mlst8*	mTOR signaling pathway	1.125
PP2A	*pp2aa*	ULK complex	1.717
TBK1	*tbk1*	Innate immunity	0.932
Rab8a/39b	*rab8a*	GDP→GTP	0.929
P62	*sqstm*	Autophagy	1.069

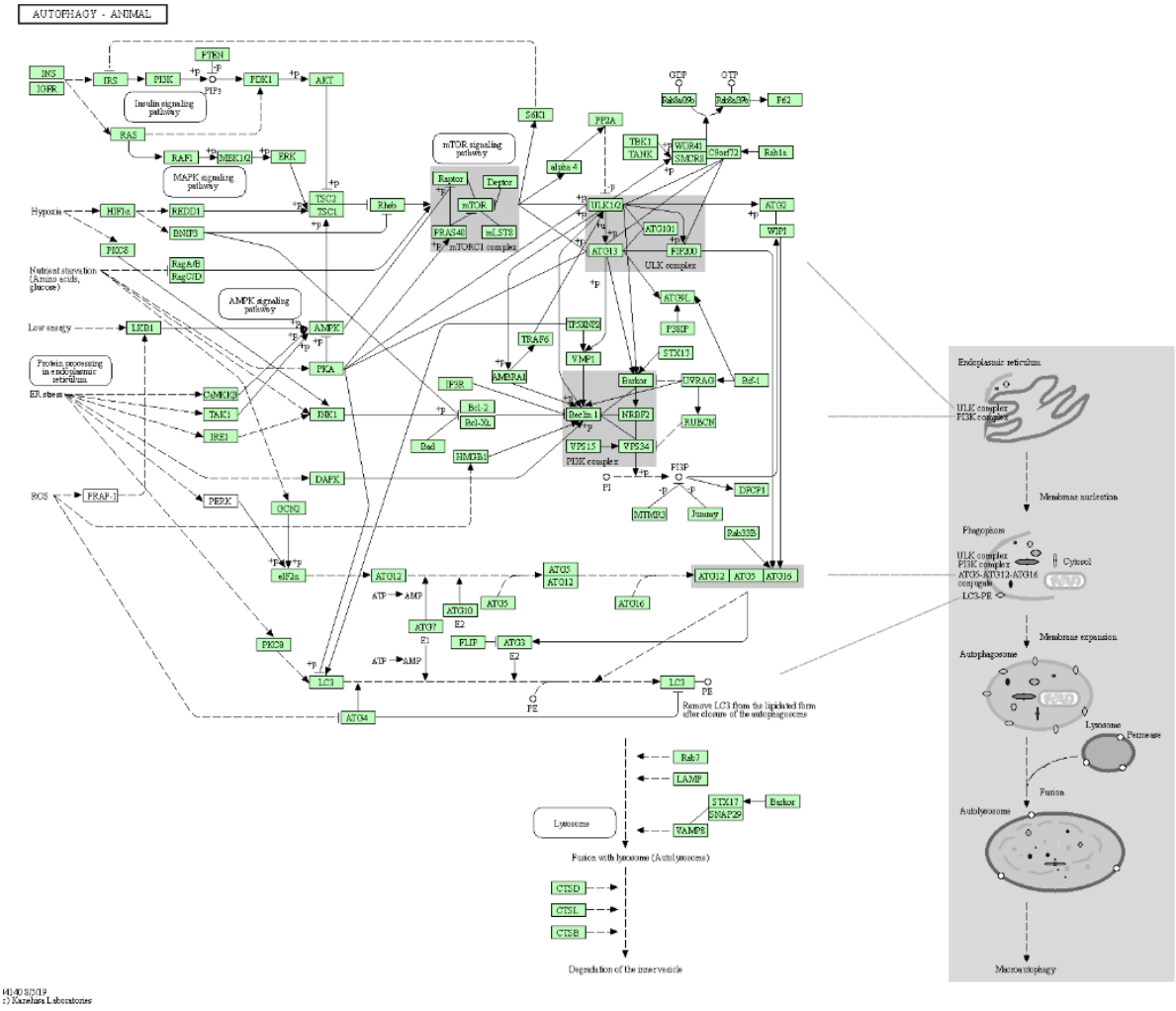

Figure 33: Autophagy pathway (map04140). Network of proteins involved in the mechanisms related to autophagy. Network is retrieved from the KEGG genetic database; (KEGG: Kyoto Encyclopedia of Genes and Genomes).

A range of differentially expressed proteins were also found in the Phagosome pathway (*map04145*) (Table 14). More specifically, there was a general upregulation in proteins involved in ER-mediated phagocytosis. The phagosome pathway is illustrated in (Figure 34).

Table 14: Proteins found differentially expressed in the ASK-1 samples exposed to NPs, with a role in the phagosome pathway (map04145). Information generated through the Proteome Discoverer™ software and KEGG database.

Protein	Gene symbol	Function in pathway	Abundance ratio
F-actin	*actb*	Internalisation and formation of the phagosome	1.127
Rab5	*Rab5*	Microtubule – Early phagosome	0.994
vATPase	*vat1*	Early phagosome/Mature phagosome	1.075
vATPase	*vath*	Early phagosome	1.048
Calnexin	*canx*	Endoplasmic reticulum	1.125
TAP	*tap1*	Endoplasmic reticulum, lysosomal acid hydrolases	1.456
Stx7	*stx7*	Late endosome	0.978
Rab7	*rab7a*	Microtubule – Mature phagosome	0.907
Dynein	*dc1i2*	Microtubule – Mature phagosome	0.998
TUBA	*tuba8l2*	Microtubule – Mature phagosome	0.827
LAMP	*lamp2*	Microtubule - Phagolysosome	0.899
LAMP	*lamp1*	Microtubule - Phagolysosome	0.810
Cathepsin	*cysp2*	Lysosomal acid hydrolases - Phagolysosome	1.022
Sec61	*S61a1*	Lysosomal acid hydrolases - Phagolysosome	1.019
Rac	*Rac1*	The activation mechanism of NADPH oxidase	1.053
SRB1	*sr-bi*	Scavenger receptors	0.825
α2β1	*itb1*	Integrins	0.960
αVβ3	*itgav*	Integrins	0.943

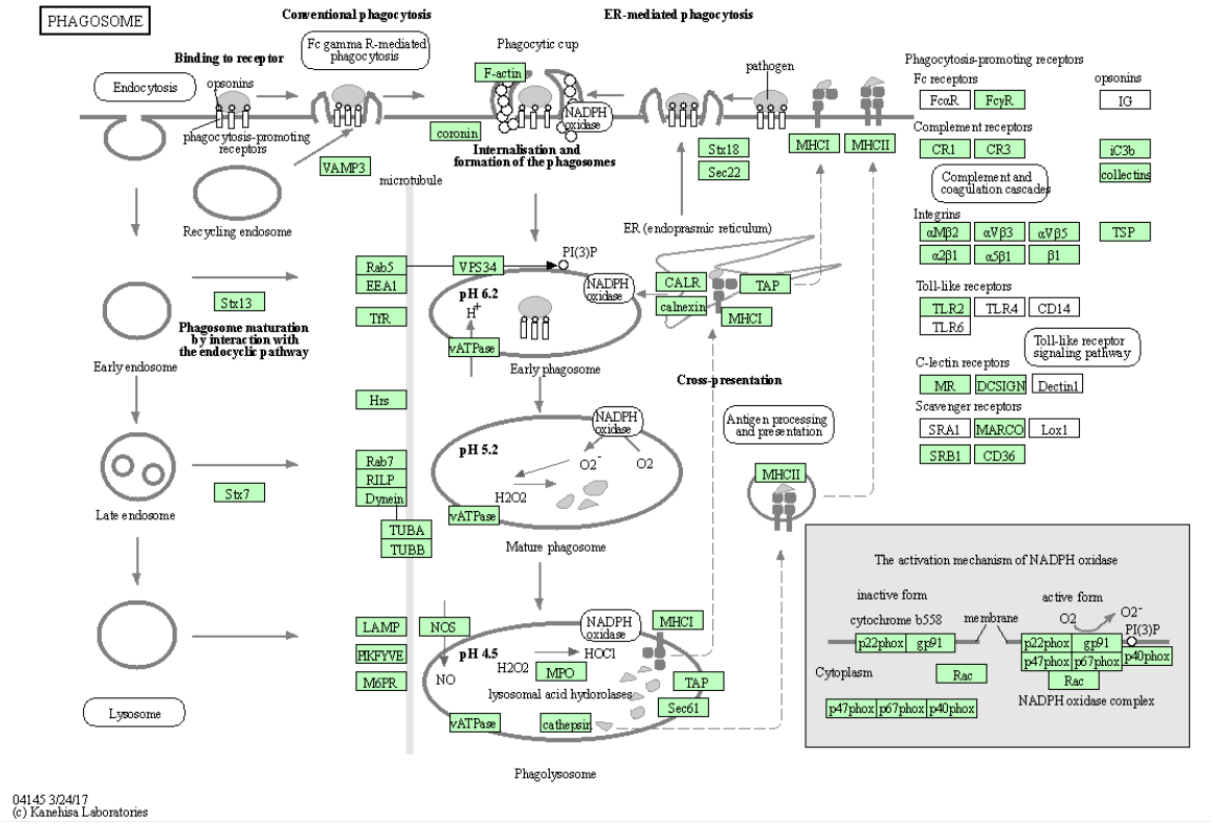

Figure 34: Phagosome pathway (map04145). Network of proteins involved in the mechanisms related to phagosome synthesis and transportation. Network is retrieved from the KEGG genetic database; (KEGG: Kyoto Encyclopedia of Genes and Genomes)

3.5 Differential gene expression of NP-exposed cells

The five genes assessed using qPCR analysis were chosen based on literature (Abarghouei et al., 2021; Danilova et al., 2005; Natarajan et al., 1999; Piazzon et al., 2016; Ryo et al., 2010) stating that these genes could be stress-related and/or have important immune functions in salmonids. The genes tested in qPCR analysis were respectively *hsp70, hsp90, igm, igt* and *mhc1*. A standard curve was generated based on the measured cp-values and the logarithmic values of the starting concentrations made (Appendix - C).

mRNA isolated from ASK-1 cells exposed and controls not exposed to polystyrene particles was used as starting material. The qPCR assay showed that the expression of *hsp90* was higher in cells exposed to polystyrene compared to control cells not exposed to the particles,

in both qPCR runs performed, meaning the Cp-values were higher in controls compared to treated samples for all sample numbers (Appendix - C) (Figure 35). The amplification curves of the remaining gene showed some questionable variations that might indicate methodological mistakes in the procedure.

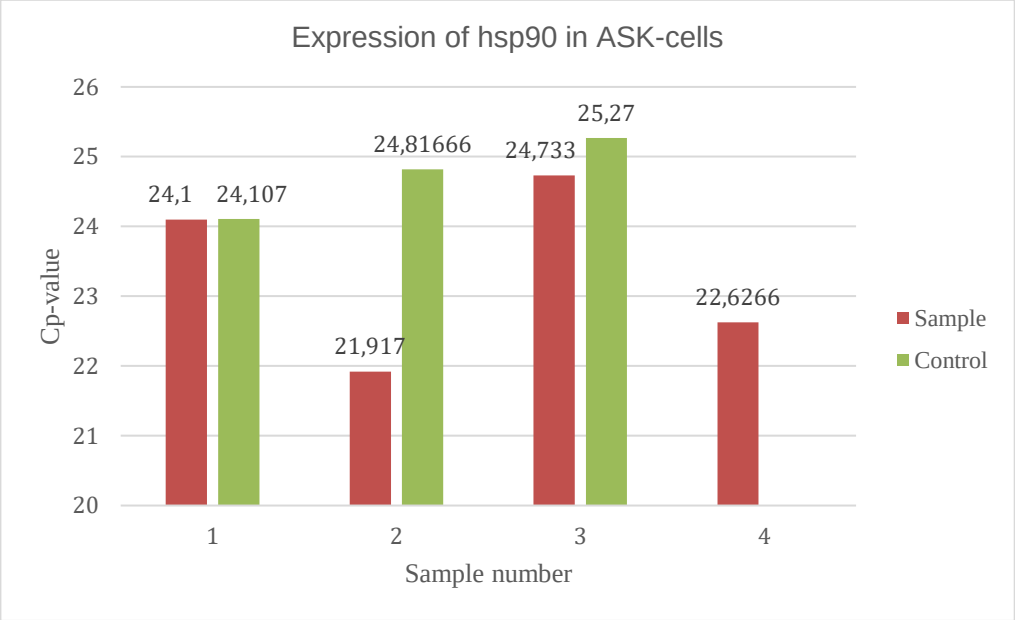

Figure 35: Expression of target gene hsp90 in ASK-1 cells exposed to NPs based on mean Cp-values. Red bars represent the treated samples and green bars represents untreated controls. A higher Cp-value means a lower expression of the gene in question. Sample number 4 is missing a control sample as there was included only one control sample in this run.

The relative expression for *hsp90* was calculated based on a standard curve generated for each of the qPCR runs (Appendix – C). From the PCR efficiency, the slope of the standard curve, and the difference in cp-values between control and sample, it was possible to calculate a relative expression value for four samples of *hsp90* (Appendix – C). The relative expression of *hsp90* in treated samples compared to controls were 4.022, 0.987, 1.059 and 4.467. All samples gave positive relative expression values, meaning the expression of *hsp90* was higher in all NP exposed samples compared to the controls.

4 Discussion

Extensive research in recent years has focused on the detrimental effects of MPs and NPs on aquatic animals (Abarghouei et al., 2021; Bagheri et al., 2020; Clark et al., 2023; Hua & Wang, 2022; Liu et al., 2019; Savoca et al., 2021; Solomando et al., 2020). However, the intricate cellular responses to these small particles in fish remain inadequately understood (Abihssira-García et al., 2020; Felix et al., 2017; Quevedo et al., 2021; Sendra et al., 2021). The present investigation endeavors to shed light on the cellular-level impacts of NPs on salmonid species, while concurrently employing the analysis of differentially expressed proteins to discern crucial pathways associated with NP uptake and cellular stress responses. By doing so, this study aimed to unveil novel insights into the intricate mechanisms underlying the interactions between NPs and salmonid cells.

4.1 Microscopy and imaging of NP exposed Salmonid cells

Initially, the observation of NP nanoparticle ingestion posed challenges due to limited experience and prior knowledge specific to this experiment. However, through method optimization, indications of NP ingestion or adherence to the cell surface were successfully obtained. This was achieved using fluorescent microscopy coupled with image processing in Fiji software. To facilitate interpretation, both negative and positive controls for fluorescent imaging were included, enabling adequate comparisons to be made. This approach enhanced the clarity and confidence in interpreting the acquired images.

The images and videos obtained through fluorescence microscopy revealed stationary particles in close proximity to cells, suggesting either surface adhesion or cellular internalization of the particles. Yet, it could not be ascertained through these pictures whether the NPs were within the cell or just in close relation to it. For this purpose, three-dimensional imaging combined with lysosome staining of the three cell lines using DeltaVision™ deconvolution microscope was applied (Figure 18-Figure 20), and successfully revealed colocalization of polystyrene particles and lysosomes. The close interaction of the particles and this particular cell organelle, strongly indicates that the polystyrene particles have been taken up by the cell. As the image clearly showed stained lysosomes both underneath and on

top of the fluorescent particles, it indicates that the particles were engulfed within the cell and not adhered to the surface.

Lysosomes have previously been classified as the main organelle colocalizing with nanoparticles (Chung et al., 2012; Sendra et al., 2021), and this is supported by the images captured in this study. However, it would be preferable to additionally stain different cell organelles, such as mitochondria and cellular membranes to further explore this statement and the exact positioning and behavior of the NPs. Lysosomes contains diverse hydrolysis enzymes that can break down foreign polymers or cellular waste (Chung et al., 2012).

The observed colocalization of NPs and lysosomes can possibly be related to the upregulation of the lysosome proteolytic enzyme CTSD, as brought up in more detail in section 4.3. It is known that some NPs can induce lysosomal dysfunction, and that lysosomal alkalization as a response to the dysfunction, is a part of a bidirectional interplay with ROS production (Li et al., 2008; Stern et al., 2012). This means that the production of ROS can lead to pH increase of lysosomes, and this alkalization would trigger oxidative stress in the cell. Hence, the lysosomal colocalization could possibly be an indication of oxidative stress as a response to imbalance of oxidants (ROS) and antioxidants, also referred to as oxidative stress. The antioxidant and detoxifying defenses to prevent excessive production of ROS is a complex network, but a variation in level of antioxidant enzyme activities have been suggested as biomarkers of aquatic contamination (Solomando et al., 2020). The expression of the enzyme proteins CATA and SOD has been used as reference proteins to detect MP-induced oxidative stress and toxicological consequences, which again can lead to inflammation and cell death (Ding et al., 2018; Kim et al., 2021). Both these proteins were found differentially expressed in the NP exposed samples, further supporting the hypothesis of the occurrence of oxidative stress and antioxidative responses as a reaction to the NP exposure. Moreover, Solomando et al. (2020) documented protein damage and elevated oxidative stress in *Sparus aurata* (gilt-head seabream) subsequent to exposure to MPs, despite the activation of antioxidant reactions and detoxification systems. This finding suggests that cells encounter cellular stress upon exposure to MPs and nanoparticles (NPs), even when their defense systems are engaged as a response.

4.2 Flow cytometry supports the assertion of polystyrene internalization.

Previous studies on the interaction of plastic particles with fish cells have shown that some cells have the ability to ingest particles with sizes similar to the polystyrene particles used in this project. Åsbakk and Dalmo (1998) reported that keratocyte-like cells from Atlantic salmon engulfed latex beads in vitro. suggested that polystyrene particles of both 503 nm and 956 nm was taken up by keratocyte-like cells. Sendra et al. (2021) showed uptake of NPs of 50 nm and 1 µm sizes by ZF4 cells of zebra fish. Altogether, results from microscopy and fluorescent-activated cell sorting, gave adequate proof that ASK-1, SHK-1 and CHSE-214 cells ingested the NPs.

For the cell lines, ASK-1 and SHK-1, originating from head kidney of A. salmon, with keratocyte-like and phagocytic abilities, it was expected that the cells would ingest the plastic particles to a more or less extent as an innate immune defense mechanism. There is no documentation on how the embryonic cells from Chinook salmon, CHSE-214, would response to NP exposure. Nevertheless, these cells have been described as epithelial-like cells and have also been shown to have the ability to internalize some fish virus particles (Levicán-Asenjo et al., 2019; Monjo et al., 2017), although virus and polystyrene particles are dissimilar. The latter has distinct and well characterized mode of cell infection whereby it induces its internalization via, e.g., cell receptors whilst it is yet to be determined whether the internalization of NPs was via phagocytosis or involvement of other mechanisms of particulate uptake such as cell receptors.

In all three cell lines evaluated via FACS, a number of cells exhibited violet fluorescence, confirming the observations made through microscopy that the NPs were ingested by the salmonid cells. While the proportion of fluorescent cells relative to non-fluorescent cells was very low, it can still be concluded that the cells were capable of internalizing the NP particles. The limited uptake may potentially be attributed to a variety of causes. One hypothesis could be that the cells have the ability to sense, discern and discriminate between potentially injurious particles such as nanoparticles from non-injurious particles such as food particles, although such specificity has not been reported previously. Time of flow cytometry is another possible cause as to why there was a low number of fluorescent cells. Within the seven-day

interval following NP exposure, it is plausible that cells may have already exocytosed the ingested particles or initiated cell death as a response to NP internalization. Consequently, discerning the detectable fluorescence emitted by such cells, as well as their classification as fluorescent entities, becomes challenging.

There was an element of uncertainty related to the behavior of the cells after ingestion of particles and sorting of the ingested particles, and whether it will be possible to perform proteomic analysis on the sorted cells. Throughout the project, it was observed that the cells had difficulties surviving and dividing after cell sorting. This is attributable to the relatively low number of cells sorted into wells, or the stress of the cell sorting. These salmonid cells prefer close proximity to their neighboring cells when dividing and multiplying and attempting to cultivate a small number of cells could therefore prove challenging. Strømsnes et al. (2022) described the growth of the salmonid cell lines as slow and difficult in some respects.

There was a difference in optimal wavelength spectrum for the plum purple particles and the violet laser used in the BD FACSAria™ which could potentially have contributed to a low number of fluorescent cells during sorting. Plum purple has its greatest excitation at 360nm and greatest emission at 420nm, while the violet laser in the flow cytometer detects optimum wavelengths at 450 nm. Due to limited options, this particular flow cytometer was employed for the project, despite its suboptimal wavelength spectrum for the incorporated fluorescent dyes.

Although of low probability, another concern was the possibility of leakage of fluorescence from the particles into the cell (Florence, 1998). Conversely, it has recently been sufficiently proven that these polystyrene particles are not prone to fluorescent leakage and can be used safely as a tracer in organisms and live tissue (Feng et al., 2021). Further, autofluorescence is another phenomenon that could possibly serve as a concern in NP cellular uptake study based on fluorescence. These concerns supports the necessity for adequate control samples when designing these types of studies. In this project, the negative control samples with cells not exposed to NPs served to preclude any autofluorescence during microscopy or cell sorting.

As this study can be considered novel in many of its aspects, there is a dart of knowledge on the fate of the cells following NP exposure. It has been established, in this study, that polystyrene NP particles are not toxic to the salmonid cells to the extent that cells die or are unable to divide and propagate after been exposed to the particles or after cell sorting to enriched for NP-internalized cells.

4.3 Differential expression of proteins revealed intracellular response to NP exposure

Protein samples from ASK-1 cells exposed to NPs, and negative controls were analyzed through mass spectrometry, and a wide range of differentially expressed proteins was found. The high number of differentially expressed proteins in response to NP exposure showed a strong response of ASK-1 cells to the particles. Several of the strongly regulated proteins are connected to cellular internalization, intracellular transport, and stress response pathways, indicating perturbation of these pathways by the NP particles. Among others, he following proteins CASP3, P53 , Ras and Cathepsin, involved in apoptosis were strongly regulated, which is not surprising as apoptosis have been connected to cell responses to exogenous substances (AnvariFar et al., 2017; Gopinath et al., 2010; Nobeli et al., 2009; Patil et al., 2010). In particular, Chen et al. (2018) highlighted the biosafety of NPs related to cytotoxicity and apoptosis, and the upregulation of Caspase-2 (CASP3) in the NP exposed samples from the present study supports this assertion.

CASP3 plays an important part in the regulation of both the apoptosis pathway (*map04210*) and the p53 pathway (*map04115*) (Gopinath et al., 2010). It is involved in initiation and execution of apoptosis. CASP3 is activated by an initial damage of the cell membrane integrity followed by an activation of pro-apoptotic genes, including P53 and Bax *(Gopinath et al., 2010)*. This activation will finally lead to an induction of the DNA fragmentation, and thus apoptosis. Because the proteins P53 and BAX are known to be a part of the cascade finally activating caspase-3, it would be expected to see an upregulation of P53 and Bax as well. However, P53 and Bax were not identified in the differentially expressed proteins induced by NP in ASK-1. There could be several reasons to why only some of the pro-apoptotic genes were activated. Firstly, the cells were exposed to NPs seven days before proteins were extracted, meaning it is difficult to estimate at what stage the cellular pathways

was active at the point of protein extraction. As far as we know, apoptosis could have already been activated, and a number of cells may have died before proteins were extracted and analyzed.

Due to its crucial role in physiological processes including tissue homeostasis, immune responses, and the elimination of damaged cells, the disruption of apoptotic pathways can give rise to significant organismal ramifications. In humans, inappropriate apoptosis have shown to be a factor in many conditions including neurodegenerative diseases, autoimmune disorders, ischemic damage, and several types of cancer (Elmore, 2007). Apoptosis is critically important during developmental processes and there is reason to believe that NPs may cause membrane disruption in fish cells as well.

In zebra fish models, it has recently been documented that the main uptake mechanism for 50 nm sized NPs, was dynamin-dependent internalization, which generally induced a modification in the expression of *cathepsin* and *catalase* genes (Sendra et al., 2021) Dynamin-dependent internalization is a form of clathrin-dependent endocytosis, and the disruption of this process could have profound effects on cellular processes. In the study described in this thesis, a differential expression in the antioxidant cathepsin enzymes SOD and CATA was found, possibly indicating similar uptake mechanism with corresponding cellular stress responses.

Upregulation of the lysosome proteolytic enzyme CTSD (cathepsin D), strengthens the indication of involvement of lysosomes in transporting and degrading the NPs, as these proteins are important in an extensive range of degradative functions of lysosome. In agreement with the observed upregulation, Sendra et al. (2021), and Wang et al. (2023) also found increase in the cathepsin and lysosomal protease expression in response to exposure to PS or metallic nanoparticles, respectively.

The proteins Rab5 and Rab7 are typically related to early and late endocytic structures, respectively (Poteryaev et al., 2010). Therefore, their differential expression is expected in the current study, but this was not the case. In previous studies where the upregulation of Rab5 and Rab7 was reported, the analysis was performed at an earlier timepoint. For example,

Sendra et al. (2021) did not report an upregulation of Rab5 in zebrafish cells at a 5-hour timepoint, on the other hand, there was an upregulation in the Rab7 protein at the same time point. This suggests that early endosomes had been in contact with the particles, but that they had not reached the time of late endosomes yet. In this study there was no upregulations in either of these endosome proteins, which may point towards non-involvement of Rab5 and Rab7 in the endocytosis of the NPs, or that the internalization of the NPs by ASK-l cells was not by endocytosis. However, the observed up- and downregulation of a diverse array of proteins associated with phagocytosis (*map04145*) and autophagy pathways (*map04140*) indicated internalization process of NP particles by ASK-1 cells via these mechanisms. As described in the introduction, autophagy differs from phagocytosis, which is a type of endocytosis characterized by the ingestion of solid particles, by its role in processing, degrading, and recycling the cellular components. This means that the ingestion of foreign particles, and the following mechanisms of managing these components, is co-regulated by these two cellular mechanisms.

The observed upregulation of F-actin and vATPase, as well as the increased expression of phagolysosomal-associated proteins such as Cathepsin and Sec61, suggests the possibility of direct phagolysosome fusion. This mechanism entails the direct transport of cargo from phagosomes to lysosomes for efficient degradation, thereby potentially explaining the absence of upregulation in endosome-related proteins in cells exposed to NP.
Direct phagolysosome fusion is typically induced when cells encounter pathogens such as bacteria or viruses, and are under pressure to swiftly transport and degrade foreign materials (Greene et al., 2022; Gutierrez et al., 2008). If this mechanism is indeed at play, it indicates that the cells recognized the particles as pathogens and aim to degrade them with maximum efficiency. ER-mediated phagocytosis is another method of endocytosis which does not involve activation of the endosomes and endosome-related proteins. This could have been an alternative route through which the observed ingestion of the NPs by the ASK-1 cells was achieved. There was a clear upregulation in several ER-associated proteins, including TAP and Calnexin, which further supports the mechanism of phagocytosis of NPs in the macrophagic cell lines.

Furthermore, the general change in expression of a range of proteins related to oxidative stress and immune response of the NP-exposed ASK-1 cells strongly indicated that the NPs induced stress in the cells, leading to a cascade of tightly regulated intracellular responses. It was surprisingly that the antioxidant enzymes SOD and CATA, which are known to be highly involved in oxidative stress responses, were downregulated. The downregulation of these proteins by ASK-1 in response to NP exposure, as opposed to an expected upregulation is unclear. However, any disruption in the expression of such proteins would mean that the network of proteins involved in oxidative stress responses, and thus cellular homeostasis, is affected. Moreover, a possible reasoning as to why there was a downregulation in these enzymes, could be that cellular resources were allocated elsewhere to upregulate the expression of other stress-related enzymes, such the oxidative stress response proteins Cyp1a, Txnd1 and Grp75, which were upregulated (Table 10). Together, the perturbation of the oxidative stress response proteins strongly indicates that the NPs induced oxidative stress in the ASK-1 cells.

4.4 Transcriptomic analysis revealed enhanced expression of *hsp90* gene in NP exposed cells

A gene expression study of expressed RNA transcripts was conducted as an additional part to this project to validate the findings from proteomic analysis. A selection of stress-related genes, spanning diverse fish species, was chosen for the gene expression analysis. Because of logistics, the proteomic research part of this project was delayed, and therefore the genetic analysis was performed before the results of differentially expressed proteins were acquired. This meant that some of the target genes chosen for qPCR analysis, was chosen based on somewhat inadequate prior knowledge. Moreover, the inclusion of these genes in the project was primarily based on their availability as potential candidates at the time, as the information obtained from proteomic analysis was not yet accessible during the genetic analysis phase. If this was not the case, the genetic research in this project would include genes associated with the differentially expressed proteins found. This limitation ultimately led to a less than optimal genetic analysis.

For the majority of genes analyzed, the abundance of variations, and in some cases absence of adequate cp-values, led to the conclusion that these results were not credible and was therefore not included in this section. Nonetheless, the findings revealed elevated expression levels of the hypoxia- and stress-associated gene *hsp90* in ASK-1 cells exposed to nanoparticles, when compared to the control group. This validates the findings from proteomic analysis which showed differential regulations in the related heat shock proteins in response to stress in the form of NP exposure.

In addition to HSPs being tightly associated with heat and responses to heat changes, apoptosis plays an important role in synthesizing of HSPs to prevent damage or initiate recovery in order to maintain cell survival (AnvariFar et al., 2017). Both in mammals and in fish, the Hsp90 and Hsp70 have been associated with cell survival and immune responses (Celi et al., 2012). These proteins can also be induced by environmental factors, such as NPs, and will have profound effects on the biological consequences of stress. The upregulation in expression of hsp90 thus indicates that the cells are activating stress response mechanisms in an attempt of coping with the NPs. However, further investigation is needed to fully understand the implications and downstream effects of the upregulated expression of *hsp90* in

ASK-1 cells exposed to NPs. This result, combined with the documented differential expression of HSPs from MS analysis, could indicate that the NP exposure may affect protein denaturation and degradation within the cell.

4.5 Limitations and future perspectives

This study encountered some limitations, which are as follows:

- There could be potential effects of cultivating cells in flasks and plates partially made with polystyrene material. To mitigate this potential influence, it would be advantageous to employ culture dishes devoid of polystyrene.
- The combination of cell staining with DV imaging presented limitations due to the unsuccessful staining of cell membranes with CMG. There could be several reasons as to why this was not ideal, but ultimately the successful staining of the lysosomes gave a good indication of particle ingestion on its own.
- Fluorescent microscopy and DV imaging of the cells exposed to polystyrene particles was performed at UiT, located a 10-minute walk from the NORCE labs at SIVA Innovation Centre where the cell cultures was kept and where all other cell work was performed. Although there were minimal visible effects of this transportation, it could in turn possibly affect the cells negatively.
- Ultimately, a proteomic analysis of all three cell lines in this study would be included. However, because of time constraints this analysis could only be carried out for the ASK-1 cell line.
- As salmon is a species with a complex genome, the protein analysis gives a very high number of expressed proteins and can in some cases be misleading. There is a lot of splice variants, which means some proteins could be double or triple analysed, and this needs to be considered.

For further research, a TMT labelled protein analysis on enriched cells, would be preferable compared to the non-labelled analysis performed in this project. This is mainly because the labelled method enables multiplexing, a simultaneous measurement and comparison of protein expression changes. TMT labelling enhances the accuracy and sensitivity of a protein quantification, and the results will be a highly accurate measurement of protein abundance,

where also subtle changes in protein expression will be detected. Generally, the outcome of this analysis would give a more concentrated and accurate range of differentially expressed proteins in response to NP exposure and uptake, which would enable a more thorough understanding of the cellular responses.

As briefly mentioned, it would be preferable to further optimize the gene expression studies of exposure and uptake of NPs in salmonid cells. Including target genes such as *cat, sod1. ctsf, ctsd, gabarap, casp, rab5 and rab7* which have known roles in uptake of compounds and cellular stress responses (Olsvik et al., 2005; Poteryaev et al., 2010; Sendra et al., 2021), would provide a better basis for determining the effects of NPs on cellular level. Another important addition to this study could be to measure the production of ROS. Quantitively measuring the production of ROS in tissue after exposure to NPs would provide significant support for the results from protein and gene analysis at cellular level.
The production of reactive oxygen species (ROS) is frequently associated with lysosomal alkalization. Given that lysosomal degradation processes contribute to alkalization, it would be advantageous to incorporate pH measurements alongside the assessment of lysosome-related cathepsin gene expression.

Given the significant role of the HK in both the endocrine system and immune defences, exploring the hormonal responses to nanoparticle (NP) exposure and uptake as a stressor presents an additional intriguing avenue for investigation. Teles et al. (2017)observed elevated cortisol levels in the plasma of the head kidney in Gilthead seabream, following exposure to gold nanoparticles. This finding prompts the inquiry as to whether a similar response would occur in A. salmon cells exposed to polystyrene, thereby suggesting the potential utility of measuring cortisol production in future studies.

Adopting a broader approach that includes *in vivo* studies of this nature, would provide additional insights into the impact of NPs on salmon species. Such comprehensive investigations would contribute significantly to advancing our understanding of the effects of NPs on salmon physiology and provide a more comprehensive assessment of cellular and organismal responses to NP exposure.

Given the inherent dissimilarities between primary fish cells and tissues, and immortalized cell lines as employed in this study, it is imperative to consider the potential disparities in responses that may arise during *in vivo* investigations and the inclusion of primary cells. So far, the studies conducted on cellular uptake and responses in salmon have been done on primary cells (Abihssira-García et al., 2020), as opposed to the immortalized cell lines utilized in this study. This means that the results need to be interpreted with caution, and further analysis with a broader scope and inclusion of primary cell cultures is necessitated. The findings obtained from this project, have provided valuable insights into the potential stress responses associated with nanoplastic internalization in salmonid cells. However, significant knowledge gaps persist, necessitating further investigation to fully understand the ramifications of plastic pollution on marine species. An inter- and transdisciplinary approach to the research of nanoplastic pollution is necessary to further elucidate the increasingly concerning issue. By adopting a holistic approach to this field of research, it is possible to integrate biological, ecological, socioeconomic, and cultural perspectives, allowing for an even more comprehensive assessment of the effects of plastic pollution and how it can affect the entire ecosystem.

5 Conclusion

In summary, this study provides the first insight into impacts of exposure of salmonid cell lines to NPs *in vitro*. Uptake of fluorescent polystyrene nanoparticles by the A. salmon head kidney cell lines ASK-1 and SHK-1, and Chinook salmon embryonic cell line, CHSE-214, were successfully observed with fluorescent microscopy and cell staining in combination with DeltaVision™ deconvolution microscopy. This was confirmed with fluorescent flow cytometry using the FACSAria™. The differential expression of proteins, by ASK-1, related to different biological functional groups and signaling pathways, including endocytosis, apoptosis and stress responses in the NP exposed cells provided further evidence of the phagocytic cells' capability to internalize NPs and that the NPs acted as a stressor. However, the analysis of responses to NP exposure in this project had certain limitations. It is recommended to incorporate more comprehensive protein and transcriptomic analysis of cells exposed to NPs versus NP-internalized cells. This would allow for a more detailed understanding of the cellular mechanisms involved in NP uptake and associated stress responses. It is also important to acknowledge that the use of immortalized cell lines, such as the ones employed in this study, may not fully represent the fish response to NPs. However, and in terms of fish welfare, proof-of-principle study as was conducted in the project described in this thesis, are best conducted using cell lines. To this extent and to better mimic events in the fish in response to NPs, primary cell lines are recommended for future investigations.

6 References

Abarghouei, S., Hedayati, A., Raeisi, M., Hadavand, B. S., Rezai, H., & Abed-Elmdoust, A. (2021). Size-dependent effects of microplastic on uptake, immune system, related gene expression and histopathology of goldfish (Carassius auratus). . *Chemosphere*, *275*. https://doi.org/https://doi.org/https://doi.org/10.1016/j.chemosphere.2021.129977

Abihssira-García, I. S., Park, Y., Kiron, V., & Olsvik, P. A. (2020). Fluorescent Microplastic Uptake by Immune Cells of Atlantic Salmon (Salmo salar L.) [Original Research]. *Frontiers in Environmental Science*, *8*. https://doi.org/10.3389/fenvs.2020.560206

Ahmed, N., Thompson, S., & Glaser, M. (2019). Global Aquaculture Productivity, Environmental Sustainability, and Climate Change Adaptability. *Environmental Management*, *63*(2), 159-172. https://doi.org/10.1007/s00267-018-1117-3

Akester, H. (2019). How big a problem is ocean polystyrene pollution? . *Fauna and Flora International*. https://phys.org/news/2019-12-big-problem-ocean-polystyrene-pollution.html

Al Shweiki, M. H. D. R., Mönchgesang, S., Majovsky, P., Thieme, D., Trutschel, D., & Hoehenwarter, W. (2017). Assessment of Label-Free Quantification in Discovery Proteomics and Impact of Technological Factors and Natural Variability of Protein Abundance. *Journal of Proteome Research*, *16*(4), 1410-1424. https://doi.org/10.1021/acs.jproteome.6b00645

AnvariFar, H., Amirkolaie, A. K., Miandare, H. K., Ouraji, H., Jalali, M. A., & Üçüncü, S. İ. (2017). Apoptosis in fish: environmental factors and programmed cell death. *Cell and Tissue Research*, *368*(3), 425-439. https://doi.org/10.1007/s00441-016-2548-x

Arike, L., & Peil, L. (2014). Spectral Counting Label-Free Proteomics. In D. Martins-de-Souza (Ed.), *Shotgun Proteomics: Methods and Protocols* (pp. 213-222). Springer New York. https://doi.org/10.1007/978-1-4939-0685-7_14

Bagheri, T., Gholizadeh, M., Abarghouei, S., Zakeri, M., Hedayati, A., Rabaniha, M., Aghaeimoghadam, A., & Hafezieh, M. (2020). Microplastics distribution, abundance and composition in sediment, fishes and benthic organisms of the Gorgan Bay, Caspian sea. *Chemosphere*, *257*, 127201. https://doi.org/https://doi.org/10.1016/j.chemosphere.2020.127201

Beemelmanns, A., Zanuzzo, F. S., Xue, X., Sandrelli, R. M., Rise, M. L., & Gamperl, A. K. (2021). The transcriptomic responses of Atlantic salmon (Salmo salar) to high temperature stress alone, and in combination with moderate hypoxia. *BMC Genomics*, *22*(1), 261. https://doi.org/10.1186/s12864-021-07464-x

Belin, B. J., Goins, L. M., & Mullins, R. D. (2014). Comparative analysis of tools for live cell imaging of actin network architecture. *BioArchitecture*, *4*(6), 189-202. https://doi.org/10.1080/19490992.2014.1047714

Berger, M. (2009). *Nano-Society: Pushing the Boundaries of Technology*. The Royal Society of Chemistry. https://doi.org/10.1039/9781847559609

Bio-Rad Laboratories, I. (2023). *What is Real-time PCR (qPCR)?* https://www.bio-rad.com/en-no/applications-technologies/what-real-time-pcr-qpcr?ID=LUSO4W8UU

Birnie-Gauvin, K., Constantini, D., Cooke, S. J., & Willmore, W. G. (2017). A comparative and evolutionary approach to oxidative stress in fish: A review. *Fish and Fisheries*, *18*(5), 928-942. https://doi.org/https://doi.org/10.1111/faf.12215

Booth. (2017). Visual representation of plastic degradation in water. *SINTEF.no*.

Britannica, T. (2022). Phagocytosis. *Britannica Encyclopedia*. https://www.britannica.com/science/phagocytosis

Capaldi Arruda, S. C., Diniz Silva, A. L., Moretto Galazzi, R., Antunes Azevedo, R., & Zezzi Arruda, M. A. (2015). Nanoparticles applied to plant science: A review. *Talanta*, *131*, 693-705. https://doi.org/10.1016/j.talanta.2014.08.050

Catarino, A. I., Frutos, A., & Henry, T. B. (2019). Use of fluorescent-labelled nanoplastics (NPs) to demonstrate NP absorption is inconclusive without adequate controls. *Science of The Total Environment*, *670*, 915-920. https://doi.org/https://doi.org/10.1016/j.scitotenv.2019.03.194

Celi, M., Vazzana, M., Sanfratello, M. A., & Parrinello, N. (2012). Elevated cortisol modulates Hsp70 and Hsp90 gene expression and protein in sea bass head kidney and isolated leukocytes. *General and Comparative Endocrinology*, *175*(3), 424-431. https://doi.org/https://doi.org/10.1016/j.ygcen.2011.11.037

Chen, L., Wu, L. Y., & Yang, W. X. (2018). NAnoparticles induce apoptosis via mediating diverse cellular pathways. *Future MEdicine*, *13*. https://doi.org/ https://doi.org/10.2217/nnm-2018-0167

Chen, Z., Qiu, X., & Gu, J. (2009). Immunoglobulin Expression in Non-Lymphoid Lineage and Neoplastic Cells. *The American Journal of Pathology*, *174*(4), 1139-1148. https://doi.org/10.2353/ajpath.2009.080879

Cheng, L., Pisitkun, T., Knepper, M. A., & Hoffert, J. D. (2016). Peptide Labeling Using Isobaric Tagging Reagents for Quantitative Phosphoproteomics. *Methods Mol Biol*, *1355*, 53-70. https://doi.org/10.1007/978-1-4939-3049-4_4

Christensen, K. A., & Davidson, W. S. (2017). Autopolyploidy genome duplication preserves other ancient genome duplications in Atlantic salmon (Salmo salar). *PLOS ONE*, *12*(2), e0173053. https://doi.org/10.1371/journal.pone.0173053

Christensen, K. A., Leong, J. S., Sakhrani, D., Biagi, C. A., Minkley, D. R., Withler, R. E., Rondeau, E. B., Koop, B. F., & Devlin, R. H. (2018). Chinook salmon (Oncorhynchus tshawytscha) genome and transcriptome. *PLOS ONE*, *13*(4), e0195461. https://doi.org/10.1371/journal.pone.0195461

Chung, H. E., Park, D. H., Choy, J. H., & Choi, S. J. (2012). Intracellular trafficking pathway of layered double hydroxide nanoparticles in human cells: Size-dependent cellular delivery. *Applied Clay Science*, *65-66*, 24-30. https://doi.org/https://doi.org/10.1016/j.clay.2012.06.007

Clark, N. J., Khan, F. R., Crowther, C., Mitrano, D. M., & Thompson, R. C. (2023). Uptake, distribution and elimination of palladium-doped polystyrene nanoplastics in rainbow trout (Oncorhynchus mykiss) following dietary exposure. *Science of The Total Environment*, *854*, 158765. https://doi.org/https://doi.org/10.1016/j.scitotenv.2022.158765

Creative Proteomics. *Label-free Quantification Service*. https://www.creative-proteomics.com/services/label-free-quantification-2.htm?msclkid=5a0294427d631279d55ff7ad188b2a19&utm_source=bing&utm_medi

um=cpc&utm_campaign=Proteomics%2BPeptides%20Services&utm_term=label%20free%20proteomics&utm_content=PR-%20Quantification-%20Label-free
Cui, K., Li, Q., Xu, D., Zhang, J., Gao, S., Xu, W., Mai, K., & Ai, Q. (2020). Establishment and characterization of two head kidney macrophage cell lines from large yellow croaker (Larimichthys crocea). *Developmental & Comparative Immunology*, *102*, 103477. https://doi.org/10.1016/j.dci.2019.103477
Danilova, N., Bussmann, J., Jekosch, K., & Steiner, L. A. (2005). The immunoglobulin heavy-chain locus in zebrafish: identification and expression of a previously unknown isotype, immunoglobulin Z. *Nat Immunol*, *6*(3), 295-302. https://doi.org/10.1038/ni1166
Dannevig, B. H., Brudeseth, B. E., GjØEn, T., Rode, M., Wergeland, H. I., Evensen, Ø., & Press, C. M. (1997). Characterisation of a long-term cell line (SHK-1) developed from the head kidney of Atlantic salmon (Salmo salarL.). *Fish & Shellfish Immunology*, *7*(4), 213-226. https://doi.org/10.1006/fsim.1996.0076
Davidson, W. S., Koop, B. F., Jones, S. J. M., Iturra, P., Vidal, R., Maass, A., Jonassen, I., Lien, S., & Omholt, S. W. (2010). Sequencing the genome of the Atlantic salmon (Salmo salar). *Genome Biology*, *11*(9), 403. https://doi.org/10.1186/gb-2010-11-9-403
Desjardins, M. (2003). ER-mediated phagocytosis: a new membrane for new functions. *Nature Reviews Immunology*, *3*(4), 280-291. https://doi.org/10.1038/nri1053
Devold, M., Krossøy, B., Aspehaug, V., & Nylund, A. (2000). Use of RT-PCR for diagnosis of infectious salmon anaemia virus (ISAV) in carrier sea trout. *Diseases of aquatic organisms*, *40*, 9-18. https://doi.org/10.3354/dao040009
Dhamad, A. E., Greene, E., Sales, M., Nguyen, P., Beer, L., Liyanage, R., & Dridi, S. (2020). 75-kDa glucose-regulated protein (GRP75) is a novel molecular signature for heat stress response in avian species. *American Journal of Physiology-Cell Physiology*, *318*(2), C289-C303. https://doi.org/10.1152/ajpcell.00334.2019
Ding, J., Zhang, S., Razanajatovo, R. M., Zou, H., & Zhu, W. (2018). Accumulation, tissue distribution, and biochemical effects of polystyrene microplastics in the freshwater fish red tilapia (Oreochromis niloticus). *Environmental Pollution*, *238*, 1-9. https://doi.org/10.1016/j.envpol.2018.03.001
Elmore, S. (2007). Apoptosis: A Review of Programmed Cell Death. *Toxicologic Pathology*, *35*(4), 495-516. https://doi.org/10.1080/01926230701320337
Federation of Norwegian Industries. *Roadmap for the Aquaculture Industry*. https://www.norskindustri.no/siteassets/dokumenter/rapporter-og-brosjyrer/veikart-for-havbruksnaringen---kortversjon_eng.pdf#:~:text=Aquaculture%20is%20one%20of%20Norway%E2%80%99s%20most%20import-%20ant,the%20world%20in%20terms%20of%20total%20aquaculture%20production.
Felix, L. C., Ortega, V. A., & Goss, G. G. (2017). Cellular uptake and intracellular localization of poly (acrylic acid) nanoparticles in a rainbow trout (Oncorhynchus mykiss) gill epithelial cell line, RTgill-W1. *Aquatic Toxicology*, *192*, 58-68. https://doi.org/10.1016/j.aquatox.2017.09.008
Feng, X., Yang, X., Li, M., Qin, Y., Li, H., & Xie, Y. (2021). Production and method optimization of fluorescent polystyrene. *Journal of Molecular Structure*, *1243*, 130746. https://doi.org/10.1016/j.molstruc.2021.130746

Florence, D. (1998). Evaluation of nano- and microparticle uptake by the gastrointestinal tract. *Advanced Drug Delivery Reviews*, *34*(2), 221-233. https://doi.org/https://doi.org/10.1016/S0169-409X(98)00041-6

Food and Agriculture Organization of the United Nations. (2022). *The State of World Fisheries and Aquaculture*. https://www.fao.org/3/cc0461en/online/sofia/2022/world-fisheries-aquaculture-production.html

Gagnon, E., Duclos, D., Rondeau, C., Chevet, E., Cameron, P. H., Steele-Mortimer, O., Paiement, J., Bergeron, J. J. M., & Desjardins, M. (2002). Endoplasmic Reticulum-Mediated Phagocytosis Is a Mechanism of Entry into Macrophages. *Cell*, *110*(1), 119-131. https://doi.org/https://doi.org/10.1016/S0092-8674(02)00797-3

Gaiser, B. K., Fernandes, T. F., Jepson, M. A., Lead, J. R., Tyler, C. R., Baalousha, M., Biswas, A., Britton, G. J., Cole, P. A., Johnston, B. D., Ju-Nam, Y., Rosenkranz, P., Scown, T. M., & Stone, V. (2011). Interspecies comparisons on the uptake and toxicity of silver and cerium dioxide nanoparticles. *Ennvironmental Toxicology and Chemistry*, *31*(1), 144-154. https://doi.org/https://doi.org/10.1002/etc.703

GE, & Healthcare. (2014). *DeltaVision™ Elite Cell Imaging System*. www.gelifesciences.com/deltavision

Geven, E. J. W., & Klaren, P. H. M. (2017). The teleost head kidney: Integrating thyroid and immune signalling. *Dev Comp Immunol*, *66*, 73-83. https://doi.org/10.1016/j.dci.2016.06.025

Gibson, U. E., Heid, C. A., & Williams, P. M. (1996). A novel method for real time quantitative RT-PCR. *Genome Research*, *33*(4), 995-1001. https://doi.org/10.1101/gr.6.10.995

Genome Res. 1996. 6: 995-100

Gopinath, P., Gogoi, S. K., Sanpui, P., Paul, A., Chattopadhyay, A., & Ghosh, S. S. (2010). Signaling gene cascade in silver nanoparticle induced apoptosis. *Colloids and Surfaces B: Biointerfaces*, *77*(2), 240-245. https://doi.org/https://doi.org/10.1016/j.colsurfb.2010.01.033

Greene, C. J., Nguyen, J. A., Cheung, S. M., Arnold, C. R., Balce, D. R., Wang, Y. T., Soderholm, A., McKenna, N., Aggarwal, D., Campden, R. I., Ewanchuk, B. W., Virgin, H. W., & Yates, R. M. (2022). Macrophages disseminate pathogen associated molecular patterns through the direct extracellular release of the soluble content of their phagolysosomes. *Nature Communications*, *13*(1), 3072. https://doi.org/10.1038/s41467-022-30654-4

Grefsrud, E. S., Glover, K., Grøsvik, B. E., Husa, V., Karlsen, Ø., Kristiansen, O., Mortensen, S., Samuelsen, O. B., Stien, L. H., & Svåsand, T. (2018). *Risikorapport norsk fiskeoppdrett 2018*.

Gutierrez, M. G., Mishra, B. B., Jordao, L., Elliott, E., Anes, E., & Griffiths, G. (2008). NF-κB Activation Controls Phagolysosome Fusion-Mediated Killing of Mycobacteria by Macrophages1. *The Journal of Immunology*, *181*(4), 2651-2663. https://doi.org/10.4049/jimmunol.181.4.2651

Harris, S. L., & Levine, A. J. (2005). The p53 pathway: positive and negative feedback loops. *Oncogene*, *24*(17), 2899-2908. https://doi.org/10.1038/sj.onc.1208615

Hartmann, S., Louch, R., Zeumer, R., Steinhoff, B., Mozhayeva, D., Engelhard, C., Schönherr, H., Schlechtriem, C., & Witte, K. (2019). Comparative multi-generation

study on long-term effects of pristine and wastewater-borne silver and titanium dioxide nanoparticles on key lifecycle parameters in Daphnia magna. *NanoImpact*, *14*, 100163. https://doi.org/10.1016/j.impact.2019.100163
Havforskningsinstituttet. (2019). Atlantisk laks.
Henson, P. M., & Hume, D. A. (2006). Apoptotic cell removal in development and tissue homeostasis. *Trends in Immunology*, *27*(5), 244-250. https://doi.org/10.1016/j.it.2006.03.005
Hira, J., Wolfson, D., Andersen, A. J. C., Haug, T., & Stensvåg, K. (2020). Autofluorescence mediated red spherulocyte sorting provides insights into the source of spinochromes in sea urchins. *Scientific Reports*, *10*(1), 1149. https://doi.org/10.1038/s41598-019-57387-7
Hognes, E. S., & Skaar, C. (2017). Avfallshåndtering fra sjøbasert havbruk. *SiNTEF Ocean*.
Hongmei, Z. (2012). Extrinsic and Intrinsic Apoptosis Signal Pathway Review.
Hua, X., & Wang, D. (2022). Cellular Uptake, Transport, and Organelle Response After Exposure to Microplastics and Nanoplastics: Current Knowledge and Perspectives for Environmental and Health Risks. *Reviews of Environmental Contamination and Toxicology*, *260*(1), 12. https://doi.org/10.1007/s44169-022-00013-x
Ingerslev, H.-C., Pettersen, E. F., Jakobsen, R. A., Petersen, C. B., & Wergeland, H. I. (2006). Expression profiling and validation of reference gene candidates in immune relevant tissues and cells from Atlantic salmon (Salmo salar L.). *Molecular Immunology*, *43*(8), 1194-1201. https://doi.org/10.1016/j.molimm.2005.07.009
International Union for Conservation of Nature. (2021). Marine Plastic Pollution. *IUCN: Issues Brief*.
Ivar do Sul, J. A., & Costa, M. F. (2014). The present and future of microplastic pollution in the marine environment. *Environmental Pollution*, *185*, 352-364. https://doi.org/10.1016/j.envpol.2013.10.036
Jakubczyk, K., Dec, K., Kałduńska, J., Kawczuga, D., Kochman, J., & Janda, K. (2020). Reactive oxygen species - sources, functions, oxidative damage. *Pol Merkur Lekarski*, *48*(284), 124-127.
Jalili, M., Gerdol, M., Greco, S., Pallavicini, A., Buonocore, F., Scapigliati, G., Picchietti, S., Esteban, M., Rye, M., & Bones, A. (2020). Differential Effects of Dietary Supplementation of Krill Meal, Soybean Meal, Butyrate, and Bactocell ® on the Gene Expression of Atlantic Salmon Head Kidney. *International Journal of Molecular Sciences*, *21*, 886. https://doi.org/10.3390/ijms21030886
Jarai, B. M., & Fromen, C. A. (2022). Nanoparticle Internalization Promotes the Survival of Primary Macrophages. *Advanced NanoBiomed Research*, *2*(5), 2100127. https://doi.org/10.1002/anbr.202100127
Jørgensen, S. M., Lyng-Syvertsen, B., Lukacs, M., Grimholt, U., & Gjøen, T. (2006). Expression of MHC class I pathway genes in response to infectious salmon anaemia virus in Atlantic salmon (Salmo salar L.) cells. *Fish & Shellfish Immunology*, *21*(5), 548-560. https://doi.org/10.1016/j.fsi.2006.03.004
Kaksonen, M., & Roux, A. (2018). Mechanisms of clathrin-mediated endocytosis. *Nature Reviews Molecular Cell Biology*, *19*(5), 313-326. https://doi.org/10.1038/nrm.2017.132
KEGG: Kyoto Encyclopedia of Genes and Genomes. KEGG Pathway maps. In: Kanehisa Laboratories.

Kershaw, P., & Rochman, C. (2015). Sources, fate and effects of microplastics in the marine environment: part 2 of a global assessment. *Reports and Studies-IMO/FAO/Unesco-IOC/WMO/IAEA/UN/UNEP Joint Group of Experts on the Scientific Aspects of Marine Environmental Protection (GESAMP) Eng No. 93*.

Kim, J.-H., Yu, Y.-B., & Choi, J.-H. (2021). Toxic effects on bioaccumulation, hematological parameters, oxidative stress, immune responses and neurotoxicity in fish exposed to microplastics: A review. *Journal of Hazardous Materials*, *413*, 125423. https://doi.org/10.1016/j.jhazmat.2021.125423

Kim, J., Kundu, M., Viollet, B., & Guan, K.-L. (2011). AMPK and mTOR regulate autophagy through direct phosphorylation of Ulk1. *Nature Cell Biology*, *13*(2), 132-141. https://doi.org/10.1038/ncb2152

Kjølstad, E. M., & Svartaas, K. H. (2020). *Keratocyttlignende celler fra hornhinne og hud hos atlantisk laks (Salmo salar L.)*

Krone, P. H., & Heikkila, J. J. (1988). Analysis of hsp 30, hsp 70 and ubiquitin gene expression in Xenopus laevis tadpoles. *Development*, *103*(1), 59-67. https://doi.org/10.1242/dev.103.1.59

Krossøy, B., Hordvik, I., Nilsen, F., Nylund, A., & Endresen, C. (1999). The Putative Polymerase Sequence of Infectious Salmon Anemia Virus Suggests a New Genus within theOrthomyxoviridae. *Journal of Virology*, *73*(3), 2136-2142. https://doi.org/JVI.73.3.2136-2142.1999

Lakowicz, J. R. (1999). Introduction to Fluorescence. In J. R. Lakowicz (Ed.), *Principles of Fluorescence Spectroscopy* (pp. 1-23). Springer US. https://doi.org/10.1007/978-1-4757-3061-6_1

Levicán-Asenjo, J., Soto-Rifo, R., Aguayo, F., Gaggero, A., & Leon, O. (2019). Salmon cells SHK-1 internalize infectious pancreatic necrosis virus by macropinocytosis. *J Fish Dis*, *42*(7), 1035-1046. https://doi.org/10.1111/jfd.13009

Levican, J., Miranda-Cárdenas, C., Soto-Rifo, R., Aguayo, F., Gaggero, A., & León, O. (2017). Infectious pancreatic necrosis virus enters CHSE-214 cells via macropinocytosis. *Sci Rep*, *7*(1), 3068. https://doi.org/10.1038/s41598-017-03036-w

Li, N., Xia, T., & Nel, A. E. (2008). The role of oxidative stress in ambient particulate matter-induced lung diseases and its implications in the toxicity of engineered nanoparticles. *Free Radical Biology and Medicine*, *44*(9), 1689-1699. https://doi.org/10.1016/j.freeradbiomed.2008.01.028

Liang, Y., Chen, S.-Y., & Liu, G.-S. (2011). [Application of next generation sequencing techniques in plant transcriptome]. *Yi chuan = Hereditas*, *33*(12), 1317-1326. https://doi.org/10.3724/sp.j.1005.2011.01317

Lien, S., Koop, B. F., Sandve, S. R., Miller, J. R., Kent, M. P., Nome, T., Hvidsten, T. R., Leong, J. S., Minkley, D. R., Zimin, A., Grammes, F., Grove, H., Gjuvsland, A., Walenz, B., Hermansen, R. A., von Schalburg, K., Rondeau, E. B., Di Genova, A., Samy, J. K. A., . . . Davidson, W. S. (2016). The Atlantic salmon genome provides insights into rediploidization. *Nature*, *533*(7602), 200-205. https://doi.org/10.1038/nature17164

Lindemann, C., Thomanek, N., Hundt, F., Lerari, T., Meyer, H. E., Wolters, D., & Marcus, K. (2017). Strategies in relative and absolute quantitative mass spectrometry based proteomics. *Biological Chemistry*, *398*(5-6), 687-699. https://doi.org/10.1515/hsz-2017-0104

Linse, S., Cabaleiro-Lago, C., Xue, W.-F., Lynch, I., Lindman, S., Thulin, E., Radford, S. E., & Dawson, K. A. (2007). Nucleation of protein fibrillation by nanoparticles. *Proceedings of the National Academy of Sciences*, *104*(21), 8691-8696. https://doi.org/10.1073/pnas.0701250104

Liu, Z., Yu, P., Cai, M., Wu, D., Zhang, M., Huang, Y., & Zhao, Y. (2019). Polystyrene nanoplastic exposure induces immobilization, reproduction, and stress defense in the freshwater cladoceran Daphnia pulex. *Chemosphere*, *215*, 74-81. https://doi.org/https://doi.org/10.1016/j.chemosphere.2018.09.176

Lusher, A. L., Hollman, P. C., & Mendoza-Hill, J. (2017). Microplastics in fisheries and aquaculture.

McNally, J. G., Karpova, T., Cooper, J., & Conchello, J. A. (1999). Three-Dimensional Imaging by Deconvolution Microscopy. *Methods*, *19*(3), 373-385. https://doi.org/https://doi.org/10.1006/meth.1999.0873

Mehta, S., Easterly, C. W., Sajulga, R., Millikin, R. J., Argentini, A., Eguinoa, I., Martens, L., Shortreed, M. R., Smith, L. M., McGowan, T., Kumar, P., Johnson, J. E., Griffin, T. J., & Jagtap, P. D. (2020). Precursor Intensity-Based Label-Free Quantification Software Tools for Proteomic and Multi-Omic Analysis within the Galaxy Platform. *Proteomes*, *8*(3). https://doi.org/10.3390/proteomes8030015

Misund, B. (2023). *Fiskeoppdrett*. https://snl.no/fiskeoppdrett

Mizushima, N. (2007). Autophagy: process and function. *Genes Dev*, *21*(22), 2861-2873. https://doi.org/10.1101/gad.1599207

Monici, M. (2005). Cell and tissue autofluorescence research and diagnostic applications. *Biotechnol Annu Rev*, *11*, 227-256. https://doi.org/10.1016/s1387-2656(05)11007-2

Monjo, A. L., Poynter, S. J., & DeWitte-Orr, S. J. (2017). CHSE-214: A model for studying extracellular dsRNA sensing in vitro. *Fish & Shellfish Immunology*, *68*, 266-271. https://doi.org/10.1016/j.fsi.2017.07.025

Murray, A. G., & Peeler, E. J. (2005). A framework for understanding the potential for emerging diseases in aquaculture. *Preventive Veterinary Medicine*, *67*(2), 223-235. https://doi.org/10.1016/j.prevetmed.2004.10.012

Nabi , I. R., & Le , P. U. (2003). Caveolae/raft-dependent endocytosis. *Journal of Cell Biology*, *161*(4), 673-677. https://doi.org/10.1083/jcb.200302028

Natarajan, K., Li, H., Mariuzza, R. A., & Margulies, D. H. (1999). MHC class I molecules, structure and function. *Rev Immunogenet*, *1*(1), 32-46.

National Library of Medicine. (2015). *Salmo salar (Atlantic salmon)* https://www.ncbi.nlm.nih.gov/assembly/GCF_000233375.1/

Nel, A., Xia, T., Mädler, L., & Li, N. (2006). Toxic Potential of Materials at the Nanolevel. *Science*, *311*(5761), 622-627. https://doi.org/10.1126/science.1114397

Nobeli, I., Favia, A. D., & Thornton, J. M. (2009). Protein promiscuity and its implications for biotechnology. *Nature Biotechnology*, *27*(2), 157-167. https://doi.org/10.1038/nbt1519

Nogueria, L. A., Vangelsten, B. V., Bay-Larsen, I., Pedersen, V., & Johanessen, E. R. (2019). *Delrapport HAVPLAST - Marint avfall fra havbruksnæringen*.

Norwegian Seafood Council. (2022). *Record high Norwegian seafood exports in 2021*. https://en.seafood.no/news-and-media/news-archive/record-high-norwegian-seafood-exports-in-2021/

Novagen®. BCA Protein Assay Kit (71285-3). In M. Millipore (Ed.): Merck Millipore.

NOAA. (2023). *Chinook Salmon*. https://www.fisheries.noaa.gov/species/chinook-salmon
Olsvik, P. A., Kristensen, T., Waagbø, R., Rosseland, B. O., Tollefsen, K. E., Baeverfjord, G., & Berntssen, M. H. G. (2005). mRNA expression of antioxidant enzymes (SOD, CAT and GSH-Px) and lipid peroxidative stress in liver of Atlantic salmon (Salmo salar) exposed to hyperoxic water during smoltification. *Comparative Biochemistry and Physiology Part C: Toxicology & Pharmacology*, *141*(3), 314-323. https://doi.org/10.1016/j.cbpc.2005.07.009
Oswald, N. (2020). *What is a Cq (Ct) value?*
Papaliagkas, V., Anogianaki, A., Anogianakis, G., & Ilonidis, G. (2007). The proteins and the mechanisms of apoptosis: a mini-review of the fundamentals. *Hippokratia*, *11*(3), 108-113.
Patil, A., Kinoshita, K., & Nakamura, H. (2010). Hub Promiscuity in Protein-Protein Interaction Networks. *International Journal of Molecular Sciences*, *11*(4), 1930-1943. https://www.mdpi.com/1422-0067/11/4/1930
Perry, S. W., Norman, J. P., Barbieri, J., Brown, E. B., & Gelbard, H. A. (2011). Mitochondrial membrane potential probes and the proton gradient: a practical usage guide. *BioTechniques*, *50*(2), 98-115. https://doi.org/10.2144/000113610
Pfaffl, M. W. (2001). A new mathematical model for relative quantification in real-time RT–PCR. *Nucleic Acids Research*, *29*(9), e45-e45. https://doi.org/10.1093/nar/29.9.e45
Piazzon, M. C., Galindo-Villegas, J., Pereiro, P., Estensoro, I., Calduch-Giner, J. A., Gómez-Casado, E., Novoa, B., Mulero, V., Sitjà-Bobadilla, A., & Pérez-Sánchez, J. (2016). Differential Modulation of IgT and IgM upon Parasitic, Bacterial, Viral, and Dietary Challenges in a Perciform Fish [Original Research]. *Frontiers in Immunology*, *7*. https://doi.org/10.3389/fimmu.2016.00637
Picchietti, S., Bernini, C., Stocchi, V., Taddei, A. R., Meschini, R., Fausto, A. M., Rocco, L., Buonocore, F., Cervia, D., & Scapigliati, G. (2017). Engineered nanoparticles of titanium dioxide (TIO2): Uptake and biological effects in a sea bass cell line. *Fish & Shellfish Immunology*, *63*, 53-67. https://doi.org/https://doi.org/10.1016/j.fsi.2017.01.044
Poteryaev, D., Datta, S., Ackema, K., Zerial, M., & Spang, A. (2010). Identification of the Switch in Early-to-Late Endosome Transition. *Cell*, *141*(3), 497-508. https://doi.org/10.1016/j.cell.2010.03.011
Quecholac-Piña, X., García-Rivera, M. A., Espinosa-Valdemar, R. M., Vázquez-Morillas, A., Beltrán-Villavicencio, M., & Cisneros-Ramos, A. d. l. L. (2017). Biodegradation of compostable and oxodegradable plastic films by backyard composting and bioaugmentation. *Environmental Science and Pollution Research*, *24*(33), 25725-25730. https://doi.org/10.1007/s11356-016-6553-0
Quevedo, A. C., Ellis, L.-J. A., Lynch, I., & Valsami-Jones, E. (2021). Mechanisms of Silver Nanoparticle Uptake by Embryonic Zebrafish Cells. *Nanomaterials*, *11*(10), 2699. https://www.mdpi.com/2079-4991/11/10/2699
Rodig, S. J. (2022). Cell Staining. *Cold Spring Harb Protoc*, *2022*(6), Pdb.top099606. https://doi.org/10.1101/pdb.top099606
Rosales, C., & Uribe-Querol, E. (2017). Phagocytosis: A Fundamental Process in Immunity. *BioMed Research International*, *2017*, 9042851. https://doi.org/10.1155/2017/9042851

Ryo, S., Wijdeven, R. H., Tyagi, A., Hermsen, T., Kono, T., Karunasagar, I., Rombout, J. H., Sakai, M., Verburg-van Kemenade, B. M., & Savan, R. (2010). Common carp have two subclasses of bonyfish specific antibody IgZ showing differential expression in response to infection. *Dev Comp Immunol*, *34*(11), 1183-1190. https://doi.org/10.1016/j.dci.2010.06.012

Savoca, M. S., McInturf, A. G., & Hazen, E. L. (2021). Plastic ingestion by marine fish is widespread and increasing. *Global Change Biology*, *27*(10), 2188-2199. https://doi.org/10.1111/gcb.15533

Schiøtz, B. L., Roos, N., Rishovd, A. L., & Gjøen, T. (2010). Formation of autophagosomes and redistribution of LC3 upon in vitro infection with infectious salmon anemia virus. *Virus Res*, *151*(1), 104-107. https://doi.org/10.1016/j.virusres.2010.03.013

Schütz, I., Lopez-Hernandez, T., Gao, Q., Puchkov, D., Jabs, S., Nordmeyer, D., Schmudde, M., Rühl, E., Graf, C. M., & Haucke, V. (2016). Lysosomal Dysfunction Caused by Cellular Accumulation of Silica Nanoparticles *. *Journal of Biological Chemistry*, *291*(27), 14170-14184. https://doi.org/10.1074/jbc.M115.710947

Sendra, M., Pereiro, P., Yeste, M. P., Mercado, L., Figueras, A., & Novoa, B. (2021). Size matters: Zebrafish (Danio rerio) as a model to study toxicity of nanoplastics from cells to the whole organism. *Environmental Pollution*, *268*, 115769. https://doi.org/10.1016/j.envpol.2020.115769

Shoiynbayeva, G. T., Shokanov, A. K., Sydykova, Z. K., Sugirbekova, A. K., & Kurbanbekov, B. A. (2021). RETRACTED: Methodological foundations of teaching nanotechnology when training future physics teachers. *Thinking Skills and Creativity*, *42*, 100970. https://doi.org/https://doi.org/10.1016/j.tsc.2021.100970

Sigma Aldrich. (2023). CHSE-214 Cell Line from salmon. In S. Aldrich (Ed.). Merck: Merck.

Singh, M., Chakrapani, A., & O'Hagan, D. (2007). Nanoparticles and microparticles as vaccine-delivery systems. *Expert Review of Vaccines*, *6*(5), 797-808. https://doi.org/10.1586/14760584.6.5.797

SinoBiological. *Fluorescence-activated Cell Sorting (FACS)*. https://www.sinobiological.com/category/fcm-facs-facs

Skåre, J. U., Alexander, J., Haave, M., Jakubowicz, I., Knutsen, H. K., Lusher, A., Ogonowski, M., Rakkestad, K. E., Skaar, I., & Sverdrup, L. E. (2019). Microplastics; occurrence, levels and implications for environment and human health related to food. Scientific opinion of the Scientific Steering Committee of the Norwegian Scientific Committee for Food and Environment. *VKM report*.

Solomando, A., Capó, X., Alomar, C., Álvarez, E., Compa, M., Valencia, J. M., Pinya, S., Deudero, S., & Sureda, A. (2020). Long-term exposure to microplastics induces oxidative stress and a pro-inflammatory response in the gut of Sparus aurata Linnaeus, 1758. *Environmental Pollution*, *266*, 115295. https://doi.org/10.1016/j.envpol.2020.115295

Stern, S. T., Adiseshaiah, P. P., & Crist, R. M. (2012). Autophagy and lysosomal dysfunction as emerging mechanisms of nanomaterial toxicity. *Particle and Fibre Toxicology*, *9*(1), 20. https://doi.org/10.1186/1743-8977-9-20

Stette, M. H. S. (2022). *Nano- and microparticle interaction with corneal and epidermal keratocyte-like cells of Atlantic salmon (Salmo salar L.): High-resolution imaging using holotomographic microscopy* UiT: The Arctic University of Norway]. munin.uit.no.

Strømsnes, T. A. H., Schmidke, S. E., Azad, M., Singstad, Ø., Grønsberg, I. M., Dalmo, R. A., & Okoli, A. S. (2022). CRISPR/Cas9-Mediated Gene Editing in Salmonids Cells and Efficient Establishment of Edited Clonal Cell Lines. *International Journal of Molecular Sciences*, *23*(24), 16218. https://www.mdpi.com/1422-0067/23/24/16218

Teles, M., Soares, A. M. V. M., Tort, L., Guimarães, L., & Oliveira, M. (2017). Linking cortisol response with gene expression in fish exposed to gold nanoparticles. *Science of The Total Environment*, *584-585*, 1004-1011. https://doi.org/10.1016/j.scitotenv.2017.01.153

The National Wildlife Federation. Chinook Salmon. *nwf.org*.

ThermoFisher Scientific. *LysoTracker™ Deep Red*. Invitrogen™. https://www.thermofisher.com/order/catalog/product/L12492

ThermoFisher Scientific. *Orbitrap Exploris Mass Spectrometers*. ThermoFisher Scientific. https://www.thermofisher.com/no/en/home/industrial/mass-spectrometry/liquid-chromatography-mass-spectrometry-lc-ms/lc-ms-systems/orbitrap-lc-ms/orbitrap-exploris-mass-spectrometers.html

ThermoFisher Scientific. (2020). *SYBR™ Green PCR Master Mix*. Applied Biosystems™. https://www.thermofisher.com/order/catalog/product/4309155

Tung, J. W., Parks, D. R., Moore, W. A., Herzenberg, L. A., & Herzenberg, L. A. (2004). New approaches to fluorescence compensation and visualization of FACS data. *Clinical Immunology*, *110*(3), 277-283. https://doi.org/https://doi.org/10.1016/j.clim.2003.11.016

Wang, H., Guo, M., Wei, H., & Chen, Y. (2023). Targeting p53 pathways: mechanisms, structures, and advances in therapy. *Signal Transduction and Targeted Therapy*, *8*(1), 92. https://doi.org/10.1038/s41392-023-01347-1

Webb, J., Verspoor, E., Aubin-Horth, N., Romakkaniemi, A., & Amiro, P. (2007). The Atlantic Salmon. In *The Atlantic Salmon* (pp. 17-56). https://doi.org/10.1002/9780470995846.ch2

Wright, S. L., Ulke, J., Font, A., Chan, K. L. A., & Kelly, F. J. (2020). Atmospheric microplastic deposition in an urban environment and an evaluation of transport. *Environment International*, *136*, 105411. https://doi.org/10.1016/j.envint.2019.105411

Xie, Y., Song, L., Weng, Z., Liu, S., & Liu, Z. (2015). Hsp90, Hsp60 and sHsp families of heat shock protein genes in channel catfish and their expression after bacterial infections. *Fish Shellfish Immunol*, *44*(2), 642-651. https://doi.org/10.1016/j.fsi.2015.03.027

Yamaguchi, T., & Dijkstra, J. M. (2019). Major Histocompatibility Complex (MHC) Genes and Disease Resistance in Fish. *Cells*, *8*(4), 378. https://www.mdpi.com/2073-4409/8/4/378

Yang, Y., Wang, J., & Xia, M. (2020). Biodegradation and mineralization of polystyrene by plastic-eating superworms Zophobas atratus. *Sci Total Environ*, *708*, 135233. https://doi.org/10.1016/j.scitotenv.2019.135233

Yue, Y., Behra, R., Sigg, L., Suter, M. J. F., Pillai, S., & Schirmer, K. (2016). Silver nanoparticle–protein interactions in intact rainbow trout gill cells [10.1039/C6EN00119J]. *Environmental Science: Nano*, *3*(5), 1174-1185. https://doi.org/10.1039/C6EN00119J

Zhang, L., & Elias, J. E. (2017). Relative Protein Quantification Using Tandem Mass Tag Mass Spectrometry. In L. Comai, J. E. Katz, & P. Mallick (Eds.), *Proteomics:*

Methods and Protocols (pp. 185-198). Springer New York. https://doi.org/10.1007/978-1-4939-6747-6_14

Zimmermann, K. C., & Green, D. R. (2001). How cells die: Apoptosis pathways. *Journal of Allergy and Clinical Immunology*, *108*(4), S99-S103. https://doi.org/10.1067/mai.2001.117819

Aandahl, P. T., & Brækkan, E. H. (2023). Norge eksporterte sjømat for 151,4 milliarder kroner i 2022. *Norges Sjømatråd*. https://www.mynewsdesk.com/no/seafood/pressreleases/norge-eksporterte-sjoemat-for-1514-milliarder-kroner-i-2022-3226081

Åsbakk, K., & Dalmo, R. (1998). Atlantic salmon (Salmo salar L.) epidermal Malpighian cells—motile cells clearing away latex beads in vitro. *Journal of Marine Biotechnology*, *6*, 30-34.

7 Appendix

Appendix – A

Protein concentration assay – BCA assay

Table 15: Guidelines on how to prepare the BSA standard dilutions according to the BCA Protein Assay protocol compiled by Novagen (Novagen®)(Novagen). Milli-Q water was used as diluent for BSA standards.

Dilutions for Protein samples			
Tube	Volume of protein sample	Volume of diluent	Dilution relation
a	20 µl from original sample	20 µl	1:2
b	20 µl from original sample	80 µl	1:5
c	50 µl from tube B	50 µl	1:10

Table 16: Dilution setup for unknown protein samples. Milli-Q water was used as diluent for protein samples. All samples were mixed thoroughly in between dilutions. The BCA working reagent was prepared by mixing 200 µl of BCA solution with 4 µl of 4% Cupric Sulfate for every well in the microplate. A total volume of ~ 7 ml of the working reagent was prepared.

	1	2	3	4	5	6	7	8	9	10	11	12
A	ST-1	ST-1	ST-1	PS-A	PS-A	PS-A	BLANK					
B	ST-2	ST-2	ST-2	PS-B	PS-B	PS-B	BLANK					
C	ST-3	ST-3	ST-3	PS-C	PS-C	PS-C	BLANK					
D	ST-4	ST-4	ST-4				BLANK					
E	ST-5	ST-5	ST-5				BLANK					
F	ST-6	ST-6	ST-6				BLANK					
G												
H												

Table 17: Dilutions of standards for enhanced BCA Protein assay.

Dilutions for enhanced BCA Protein Assay			
Tube	Volume of BSA	Volume of diluent	Final BSA concentration
1	100 µl from 2 mg/ml solution	700 µl	250 µg/ml
2	400 µl from tube 1	400 µl	125 µg/ml
3	300 µl from tube 2	450 µl	50 µg/ml
4	200 µl from tube 3	200 µl	25 µg/ml
5	100 µl from tube 4	400 µl	5 µg/ml
6	0	400 µl	0

Table 18: Concentration of proteins from BCA assay, including calculated protein weight.

Sample	Volume (ul)	Concentration (ug/ml)	Protein (ug)
1	50	2091,14	104,56
2	50	1951,43	97,57
3	50	2231,43	111,57

Table 19: Measured absorbance for all samples and standards used in BCA protein assay.

	1	2	3	4	5	6	7	8	9	10	11	12
A	0.176	0.166	0.155	0.79	0.744	0.649	BLANK					
B	0.08	0.074	0.064	0.276	0.28	0.351	BLANK					
C	0.018	0.032	0.025	0.15	0.154	0.152	BLANK					
D	0.015	0.013	0.005				BLANK					
E	0.012	-0.001	-0.003				BLANK					
F	0.002	0.001	-0.004				BLANK					
G												
H												

Appendix – B

Mass spectrometry results – Upregulated proteins

Table 20: Significantly upregulated proteins from the MS analysis of ASK-1 cells exposed to NPs. Data derived for Proteome Discoverer™ software which also set a p-value at 0.05 and filtered out all proteins not significantly upregulated. Accession number, a short description of the protein, number of peptides found, number of peptide spectral matches (PSMs) found, number of unique peptides found, associated biological process, genetic symbol, and abundance ratio (NP/C), derived from the PD software are all included.

Accession	Description	# Peptides	# PSMs	# Unique Peptides	Biological Process	Gene Symbol	Abundance Ratios
A0A1S3S9X7	heme-binding protein 2-like OS=Salmo salar OX=8030 GN=LOC106608028 PE=3 SV=1	6	20	6		*LOC106608028*	46
A0A1S3KSB8	cytoskeleton-associated protein 5-like isoform X1 OS=Salmo salar OX=8030 GN=LOC106561606 PE=3 SV=1	38	231	3	cell cycle, cell proliferation, cell organization and biogenesis, other biological processes	*LOC106561606*	24
B5X1Q2	ATP-dependent DNA helicase 2 subunit 1 OS=Salmo salar OX=8030 GN=KU70 PE=2 SV=1	9	45	9	cell organization and biogenesis, DNA metabolism, other metabolic processes, stress response	*KU70*	8.73
B5X6Y7	ATP synthase F1 subunit epsilon OS=Salmo salar OX=8030 GN=ATIF1 PE=2 SV=1	3	66	3	other biological processes	*ATIF1*	6.61
A0A1S3PYA2	vacuolar protein sorting-associated protein 45-like OS=Salmo salar OX=8030 GN=LOC106588336 PE=3 SV=1	21	187	4	transport	*LOC106588336*	5.38

A0A1S3PCV9	BET1-like protein isoform X1 OS=Salmo salar OX=8030 GN=bet1l PE=4 SV=1	4	26	4	transport	*bet1l*	4.49
A0A1S3Q525	sn-1-specific diacylglycerol lipase OS=Salmo salar OX=8030 GN=LOC100286527 PE=4 SV=1	4	24	4	other metabolic processes	*LOC100286527*	4.33
Q7ZTG9	Aryl hydrocarbon receptor 2 delta OS=Salmo salar OX=8030 GN=AhR2d PE=2 SV=1	4	20	4	other biological processes	*AhR2d*	3.93
A0A1S3KLC2	MIP18 family protein FAM96A OS=Salmo salar OX=8030 GN=fam96a PE=3 SV=1	3	14	3	cell cycle, cell proliferation, protein metabolism, other metabolic processes	*fam96a*	3.8
A0A1S3N526	uncharacterized protein LOC106577146 isoform X1 OS=Salmo salar OX=8030 GN=LOC106577146 PE=4 SV=1	4	32	4		*LOC106577146*	3.56
A0A1S3R294	desmocollin-2-like isoform X1 OS=Salmo salar OX=8030 GN=LOC106599708 PE=4 SV=1	9	34	9	cell adhesion	*LOC106599708*	3.44
A0A1S3N6K9	mitotic spindle assembly checkpoint protein MAD2A-like OS=Salmo salar OX=8030 GN=LOC106577502 PE=4 SV=1	4	16	4		*LOC106577502*	3.4
A0A1S3RVD9	uncharacterized protein LOC106605302 OS=Salmo salar OX=8030 GN=LOC106605302 PE=4 SV=1	10	88	5		*LOC106605302*	3.23

A0A1S3LEL7	diphosphoinositol polyphosphate phosphohydrolase 1-like OS=Salmo salar OX=8030 GN=LOC106566013 PE=4 SV=1	5	39	4		*LOC106566013*	3.23
A0A1S3PAS6	CTP synthase OS=Salmo salar OX=8030 GN=LOC106584221 PE=3 SV=1	9	58	3	other metabolic processes	*LOC106584221*	2.91
A0A1S3NBF2	Palmitoyltransferase OS=Salmo salar OX=8030 GN=LOC106578454 PE=3 SV=1	3	23	3		*LOC106578454*	2.58
B5X1U5	Tropomyosin-1 alpha chain OS=Salmo salar OX=8030 GN=TPM1 PE=2 SV=1	12	336	4		*TPM1*	2.53
B5X3P6	Signal peptide peptidase-like 2B OS=Salmo salar OX=8030 GN=PSL1 PE=2 SV=1	3	11	3		*PSL1*	2.48
A0A1S3SX58	rho GTPase-activating protein 35-like OS=Salmo salar OX=8030 GN=LOC106612372 PE=4 SV=1	10	41	6	signal transduction	*LOC106612372*	2.43
A0A1S3MEZ9	cytosolic acyl coenzyme A thioester hydrolase OS=Salmo salar OX=8030 GN=acot7 PE=4 SV=1	3	21	3		*acot7*	2.35
A0A1S3QKR3	melanoma-associated antigen G1-like isoform X1 OS=Salmo salar OX=8030 GN=LOC106593143 PE=4 SV=1	3	22	3		*LOC106593143*	2.33
A0A1S3RAD0	protein-tyrosine-phosphatase OS=Salmo salar OX=8030 GN=LOC106601406 PE=3 SV=1	3	10	3	protein metabolism, other metabolic processes	*LOC106601406*	2.28

A0A1S3SMB9	kanadaptin OS=Salmo salar OX=8030 GN=slc4a1ap PE=4 SV=1	8	30	8		*slc4a1ap*	2.26
A0A1S3NXZ1	Importin subunit alpha OS=Salmo salar OX=8030 GN=LOC106582012 PE=3 SV=1	13	135	4	transport	*LOC106582012*	2.25
A0A1S3R4V2	Peroxisomal biogenesis factor 19 OS=Salmo salar OX=8030 GN=LOC106600385 PE=3 SV=1	6	36	6	cell organization and biogenesis	*LOC106600385*	2.2
A0A1S3ME36	Cytochrome c oxidase subunit 4 OS=Salmo salar OX=8030 GN=LOC106572114 PE=3 SV=1	4	42	4	other metabolic processes	*LOC106572114*	2.2
A0A1S3MIV0	leucine-rich repeat-containing protein 16A-like OS=Salmo salar OX=8030 GN=LOC106572945 PE=4 SV=1	7	13	6		*LOC106572945*	2.17
A0A1S3RGZ5	tripartite motif-containing protein 2 isoform X1 OS=Salmo salar OX=8030 GN=LOC106602744 PE=3 SV=1	5	33	4		*LOC106602744*	2.14
A0A1S3L5A6	serine hydrolase-like protein OS=Salmo salar OX=8030 GN=LOC106564548 PE=4 SV=1	5	30	5		*LOC106564548*	2.1
A0A1S3QFV0	WD repeat domain phosphoinositide-interacting protein 2 OS=Salmo salar OX=8030 GN=LOC106592102 PE=3 SV=1	4	22	4		*LOC106592102*	2.09
B5X4U9	ER membrane protein complex subunit 6 OS=Salmo salar OX=8030 GN=TMM93 PE=2 SV=1	3	21	3		*TMM93*	2.09

A0A1S3LYW5	RING-type E3 ubiquitin transferase OS=Salmo salar OX=8030 GN=LOC106569317 PE=4 SV=1	6	11	6	protein metabolism, other metabolic processes, signal transduction	*LOC106569317*	2.08
B9EP31	Eukaryotic Translation initiation factor 4E-1A OS=Salmo salar OX=8030 GN=IF4EA PE=2 SV=1	5	43	3	protein metabolism, other metabolic processes	*IF4EA*	2.03
A0A1S3RZY9	39S ribosomal protein L13, mitochondrial-like OS=Salmo salar OX=8030 GN=LOC106606163 PE=3 SV=1	4	30	4	protein metabolism, other metabolic processes	*LOC106606163*	2.03

Mass spectrometry results – Downregulated proteins

Table 21: Significantly downregulated proteins from the MS analysis of ASK-1 cells exposed to NPs. Data derived for Proteome Discoverer™ software which also set a p-value at 0.05 and filtered out all proteins not significantly upregulated. Accession number, a short description of the protein, number of peptides found, number of peptide spectral matches (PSMs) found, number of unique peptides found, associated biological process, genetic symbol, and abundance ratio (NP/C), derived from the PD software are all included.

Accession	Description	# Peptides	# PSMs	# Unique Peptides	Biological Process	Gene Symbol	Abundance Ratios
A0A1S3KQQ5	Fatty acyl-CoA reductase OS=Salmo salar OX=8030 GN=LOC106561480 PE=3 SV=1	7	13	7	other metabolic processes	*LOC106561480*	0.01
A0A1S3P5U7	Peroxisomal targeting signal 1 receptor OS=Salmo salar OX=8030 GN=LOC106583355 PE=3 SV=1	7	36	7		*LOC106583355*	0.01
A0A1S3PX29	cell surface glycoprotein 1-like OS=Salmo salar OX=8030 GN=LOC106587688 PE=4 SV=1	4	19	4		*LOC106587688*	0.01
A0A1S3PDN7	Eukaryotic translation initiation factor 3 subunit J OS=Salmo salar OX=8030 GN=LOC106584719 PE=3 SV=1	5	18	4	cell organization and biogenesis, protein metabolism, other metabolic processes	*LOC106584719*	0.01
A0A1S3SEM6	Kinesin light chain OS=Salmo salar OX=8030 GN=LOC106608996 PE=3 SV=1	17	190	4		*LOC106608996*	0.01
A0A1S3M4U1	protein zer-1 homolog OS=Salmo salar OX=8030 GN=LOC106570444 PE=3 SV=1	3	7	3		*LOC106570444*	0.01

B5X4U8	Cleavage and polyadenylation specificity factor subunit 2 OS=Salmo salar OX=8030 GN=CPSF2 PE=2 SV=1	7	32	7	RNA metabolism, transcription, other metabolic processes	*CPSF2*	0.01
A0A1S3MWN8	metalloreductase STEAP3 isoform X1 OS=Salmo salar OX=8030 GN=steap3 PE=3 SV=1	6	31	3	other biological processes	*steap3*	0.01
A0A1S3R6J4	COMM domain-containing protein 8-like isoform X1 OS=Salmo salar OX=8030 GN=LOC106600549 PE=4 SV=1	4	19	4		*LOC106600549*	0.01
A0A1S3N0I8	golgin subfamily B member 1-like isoform X1 OS=Salmo salar OX=8030 GN=LOC106576351 PE=4 SV=1	39	162	13		*LOC106576351*	0.01
A0A1S3NW90	uncharacterized protein C7orf57 homolog isoform X1 OS=Salmo salar OX=8030 GN=LOC106581816 PE=4 SV=1	6	42	3		*LOC106581816*	0.01
A0A1S3QW59	nucleolar transcription factor 1 isoform X1 OS=Salmo salar OX=8030 GN=ubf1 PE=4 SV=1	4	26	4		*ubf1*	0.01
A0A1S3Q1G4	non-syndromic hearing impairment protein 5-like isoform X1 OS=Salmo salar OX=8030 GN=LOC106588856 PE=3 SV=1	13	74	13	other biological processes	*LOC106588856*	0.01
A0A1S3R8I8	KN motif and ankyrin repeat domain-containing protein 2-like OS=Salmo salar OX=8030 GN=LOC106601060 PE=4 SV=1	23	204	3		*LOC106601060*	0.01

A0A1S3RLW4	Bifunctional lysine-specific demethylase and histidyl-hydroxylase OS=Salmo salar OX=8030 GN=mina PE=3 SV=1	5	22	5		*mina*	0.01
A0A1S3MM29	transcriptional repressor p66-alpha-like isoform X1 OS=Salmo salar OX=8030 GN=LOC106573594 PE=4 SV=1	4	21	3	other biological processes	*LOC106573594*	0.01
A0A1S3NPH6	Serine/threonine-protein phosphatase OS=Salmo salar OX=8030 GN=LOC106580517 PE=3 SV=1	9	109	4	signal transduction	*LOC106580517*	0.01
A0A1S3KVB2	Serine/threonine-protein kinase ULK3 OS=Salmo salar OX=8030 GN=LOC106562348 PE=3 SV=1	3	7	3	protein metabolism, other metabolic processes	*LOC106562348*	0.01
A0A1S3QVS4	E3 ubiquitin-protein ligase RNF213 isoform X1 OS=Salmo salar OX=8030 GN=LOC100380659 PE=4 SV=1	11	43	6	protein metabolism, other metabolic processes	*LOC100380659*	0.01
A0A1S3P9G1	Protein O-linked-mannose beta-1,2-N-acetylglucosaminyltransferase OS=Salmo salar OX=8030 GN=pomgnt1 PE=3 SV=1	3	5	3	protein metabolism, other metabolic processes	*pomgnt1*	0.01
A0A1S3SZH6	protein KIAA0100 homolog isoform X1 OS=Salmo salar OX=8030 GN=kiaa0100 PE=4 SV=1	8	26	8		*kiaa0100*	0.01
A0A1S3QN23	uncharacterized protein LOC106593927 OS=Salmo salar OX=8030 GN=LOC106593927 PE=4 SV=1	3	8	3		*LOC106593927*	0.01
A0A1S3PVG9	transcription factor 25-like OS=Salmo salar OX=8030 GN=LOC106587382 PE=3 SV=1	6	22	6		*LOC106587382*	0.01

A0A1S3P550	tRNA (guanine-N(7)-)-methyltransferase OS=Salmo salar OX=8030 GN=mettl1 PE=3 SV=1	3	11	3	RNA metabolism, transcription, other metabolic processes	*mettl1*	0.01
A0A1S3MJ56	adenosine deaminase-like protein isoform X1 OS=Salmo salar OX=8030 GN=adal PE=4 SV=1	5	16	5		*adal*	0.01
A0A1S3RGP0	WD repeat and HMG-box DNA-binding protein 1 isoform X1 OS=Salmo salar OX=8030 GN=wdhd1 PE=4 SV=1	7	29	7		*wdhd1*	0.038
A0A1S3S944	CSC1-like protein 1 OS=Salmo salar OX=8030 GN=LOC106607901 PE=3 SV=1	3	13	3	transport	*LOC106607901*	0.046
A0A1S3PA40	WD repeat-containing protein 26-like isoform X1 OS=Salmo salar OX=8030 GN=LOC106584119 PE=4 SV=1	14	63	5		*LOC106584119*	0.059
A0A1S3KNY7	choline/ethanolamine kinase OS=Salmo salar OX=8030 GN=chkb PE=4 SV=1	9	55	9	other metabolic processes	*chkb*	0.07
A0A1S3N0B8	propionate--CoA ligase OS=Salmo salar OX=8030 GN=acss3 PE=3 SV=1	7	27	7	other metabolic processes	*acss3*	0.082
A0A1S3R9Z4	cTAGE family member 5-like isoform X1 OS=Salmo salar OX=8030 GN=LOC106601134 PE=4 SV=1	6	18	3		*LOC106601134*	0.089
A0A1S3LEN4	Ubiquinone biosynthesis protein COQ4 homolog, mitochondrial OS=Salmo salar OX=8030 GN=coq4 PE=3 SV=1	4	21	4	other metabolic processes	*coq4*	0.09

A0A1S3LUD5	zinc finger protein 622 isoform X1 OS=Salmo salar OX=8030 GN=znf622 PE=3 SV=1	6	42	6	other biological processes	*znf622*	0.107
A0A1S3PL08	N-acetylserotonin O-methyltransferase-like protein isoform X1 OS=Salmo salar OX=8030 GN=asmtl PE=3 SV=1	7	25	7	other metabolic processes	*asmtl*	0.165
A0A1S3T1E7	solute carrier family 12 member 9-like OS=Salmo salar OX=8030 GN=LOC106613052 PE=3 SV=1	9	49	9	transport	*LOC106613052*	0.172
A0A1S3Q165	Septin OS=Salmo salar OX=8030 GN=LOC106588576 PE=3 SV=1	6	64	3		*LOC106588576*	0.182
A0A1S3Q392	calcium-binding and coiled-coil domain-containing protein 2 isoform X1 OS=Salmo salar OX=8030 GN=calcoco2 PE=4 SV=1	7	29	3		*calcoco2*	0.183
A0A1S3LGS1	1-phosphatidylinositol 4,5-bisphosphate phosphodiesterase gamma OS=Salmo salar OX=8030 GN=plcg1 PE=4 SV=1	4	13	4	other metabolic processes, signal transduction	*plcg1*	0.2
A0A1S3QA10	structural maintenance of chromosomes flexible hinge domain-containing protein 1 isoform X1 OS=Salmo salar OX=8030 GN=smchd1 PE=4 SV=1	8	27	8	Cell organization and biogenesis, DNA metabolism, other metabolic processes, stress response	*smchd1*	0.202
A0A1S3QFS8	RNA-binding protein 26 OS=Salmo salar OX=8030 GN=rbm26 PE=4 SV=1	3	4	3	RNA metabolism, transcription, other metabolic processes	*rbm26*	0.232
A0A1S3QFW0	CWF19-like protein 1 OS=Salmo salar OX=8030 GN=cwf19l1 PE=3 SV=1	5	37	5		*cwf19l1*	0.246

A0A1S3SJD6	protocadherin Fat 1-like isoform X1 OS=Salmo salar OX=8030 GN=LOC106609939 PE=4 SV=1	10	28	3	cell adhesion	*LOC106609939*	0.258
A0A1S3QNW2	TBC1 domain family member 15-like OS=Salmo salar OX=8030 GN=LOC106594572 PE=4 SV=1	6	28	5		*LOC106594572*	0.271
A0A1S3P1G5	Eukaryotic translation initiation factor 6 OS=Salmo salar OX=8030 GN=eif6 PE=3 SV=1	7	127	3	Cell organization and biogenesis, protein metabolism, other metabolic processes, other biological processes	*eif6*	0.278
A0A1S3MP38	DNA methyltransferase 1-associated protein 1 isoform X1 OS=Salmo salar OX=8030 GN=dmap1 PE=4 SV=1	4	21	4	cell organization and biogenesis, protein metabolism, DNA metabolism, other metabolic processes, stress response, other biological processes	*dmap1*	0.282
C0H9M9	Serine/threonine-protein kinase 38 OS=Salmo salar OX=8030 GN=STK38 PE=2 SV=1	13	141	4	protein metabolism, other metabolic processes	*STK38*	0.283
A0A1S3PXY0	E2/E3 hybrid ubiquitin-protein ligase UBE2O-like isoform X1 OS=Salmo salar OX=8030 GN=LOC106588250 PE=4 SV=1	8	24	8		*LOC106588250*	0.294
A0A1S3MED7	bcl-2-like protein 1 OS=Salmo salar OX=8030 GN=LOC106572112 PE=3 SV=1	5	32	4	other biological processes	*LOC106572112*	0.303
A0A1S3SXH2	high mobility group-T protein-like isoform X1 OS=Salmo salar OX=8030 GN=LOC106612439 PE=4 SV=1	6	51	4		*LOC106612439*	0.314

A0A1S3T3T5	26S proteasome non-ATPase regulatory subunit 1 OS=Salmo salar OX=8030 GN=LOC106613492 PE=3 SV=1	37	743	3	other biological processes	*LOC106613492*	0.316
A0A1S3PU01	retinal dehydrogenase 2-like OS=Salmo salar OX=8030 GN=LOC106587345 PE=3 SV=1	8	84	7		*LOC106587345*	0.318
A0A1S3PM31	lupus La protein homolog B-like OS=Salmo salar OX=8030 GN=LOC106586213 PE=4 SV=1	14	156	8	RNA metabolism, transcription, other metabolic processes	*LOC106586213*	0.318
A0A1S3R303	catenin alpha-1-like OS=Salmo salar OX=8030 GN=LOC106599912 PE=3 SV=1	3	41	3	cell adhesion	*LOC106599912*	0.318
A0A1S3RQI1	Copper homeostasis protein cutC homolog OS=Salmo salar OX=8030 GN=cutc PE=3 SV=1	3	18	3		*cutc*	0.328
A0A1S3SR62	ribose-5-phosphate isomerase OS=Salmo salar OX=8030 GN=LOC106611309 PE=3 SV=1	11	177	3	other metabolic processes	*LOC106611309*	0.335
A0A1S3R6X4	Cathepsin D OS=Salmo salar OX=8030 GN=LOC106600890 PE=3 SV=1	9	85	5	protein metabolism	*LOC106600890*	0.336
A0A1S3KKL3	ras-related protein Rab-6B isoform X1 OS=Salmo salar OX=8030 GN=LOC106560618 PE=4 SV=1	6	120	3		*LOC106560618*	0.341
A0A1S3QD93	lysine-specific demethylase PHF2 OS=Salmo salar OX=8030 GN=phf2 PE=3 SV=1	4	19	3	cell organization and biogenesis	*phf2*	0.343

A0A1S3RH76	protein NipSnap homolog 2-like OS=Salmo salar OX=8030 GN=LOC106602830 PE=3 SV=1	4	29	3		*LOC106602830*	0.356
A0A1S3RLR1	protein FAM114A2-like isoform X1 OS=Salmo salar OX=8030 GN=LOC106603491 PE=3 SV=1	6	32	5		*LOC106603491*	0.359
A0A1S3L6R8	hexokinase OS=Salmo salar OX=8030 GN=LOC106564733 PE=3 SV=1	16	360	4	other metabolic processes, other biological processes	*LOC106564733*	0.36
A0A1S3Q637	TATA-box-binding protein-like OS=Salmo salar OX=8030 GN=LOC106589653 PE=3 SV=1	3	8	3	RNA metabolism, transcription, other metabolic processes	*LOC106589653*	0.363
A0A1S3LME3	Tyrosine-protein phosphatase non-receptor type OS=Salmo salar OX=8030 GN=LOC106567201 PE=3 SV=1	7	69	4	protein metabolism, other metabolic processes	*LOC106567201*	0.366
B5X3C9	Bromodomain-containing protein 7 OS=Salmo salar OX=8030 GN=BRD7 PE=2 SV=1	3	5	3		*BRD7*	0.381
B9ELF3	COMM domain-containing protein 10 OS=Salmo salar OX=8030 GN=COMDA PE=2 SV=1	3	22	3		*COMDA*	0.386
C0HB56	small monomeric GTPase OS=Salmo salar OX=8030 GN=RAP2C PE=2 SV=1	7	77	3	signal transduction	*RAP2C*	0.387
A0A1S3NXI3	filamin A-interacting protein 1-like OS=Salmo salar OX=8030 GN=LOC106582008 PE=4 SV=1	6	16	6		*LOC106582008*	0.402

A0A1S3L7Y6	RNA-binding protein 12-like isoform X1 OS=Salmo salar OX=8030 GN=LOC106565030 PE=4 SV=1	14	107	12		*LOC106565030*	0.403
A0A1S3NG98	protein kinase C and casein kinase substrate in neurons protein 3-like isoform X1 OS=Salmo salar OX=8030 GN=LOC106579238 PE=4 SV=1	6	24	6	other metabolic processes	*LOC106579238*	0.41
A0A1S3P976	Zinc finger Ran-binding domain-containing protein 2 OS=Salmo salar OX=8030 GN=zranb2 PE=3 SV=1	3	12	3	RNA metabolism, transcription, other metabolic processes	*zranb2*	0.412
A0A1S3RQ45	Probable RNA-binding protein EIF1AD OS=Salmo salar OX=8030 GN=eif1ad PE=3 SV=1	4	30	4	protein metabolism, other metabolic processes	*eif1ad*	0.433
A0A1S3NV26	ceroid-lipofuscinosis neuronal protein 5 OS=Salmo salar OX=8030 GN=cln5 PE=3 SV=1	4	23	4		*cln5*	0.437
A0A1S3MK28	protein C12orf4 homolog OS=Salmo salar OX=8030 GN=LOC106573194 PE=4 SV=1	6	26	6		*LOC106573194*	0.442
A0A1S3P6X2	protein polybromo-1-like isoform X1 OS=Salmo salar OX=8030 GN=LOC106583529 PE=4 SV=1	11	45	11	cell organization and biogenesis	*LOC106583529*	0.453
A0A1S3N8P4	Metallo-beta-lactamase domain-containing protein 1 OS=Salmo salar OX=8030 GN=mblac1 PE=3 SV=1	3	10	3		*mblac1*	0.458
Q3ZBS7	TREMBL:Q3ZBS7 (Bos taurus) Vitronectin	11	268	11			0.459

A0A1S3MLQ3	Lipoprotein lipase OS=Salmo salar OX=8030 GN=LOC106573546 PE=3 SV=1	6	26	6	other metabolic processes	*LOC106573546*	0.464
A0A1S3SIW4	nuclear respiratory factor 1 isoform X5 OS=Salmo salar OX=8030 GN=nrf1 PE=3 SV=1	3	17	3	RNA metabolism, transcription, other biological processes	*nrf1*	0.477
A0A1S3P6B7	protein bicaudal D homolog 2-like isoform X1 OS=Salmo salar OX=8030 GN=LOC106583446 PE=3 SV=1	11	56	4		*LOC106583446*	0.48
A0A1S3RFV6	protein PAT1 homolog 1-like OS=Salmo salar OX=8030 GN=LOC106602767 PE=3 SV=1	5	18	5	RNA metabolism, transcription, other metabolic processes	*LOC106602767*	0.481
A0A1S3SA21	kelch-like protein 29 isoform X1 OS=Salmo salar OX=8030 GN=klhl29 PE=4 SV=1	3	13	3		*klhl29*	0.484
Q28194	TREMBL:Q28194 (Bos taurus) Thrombospondin-1	6	48	5	cell adhesion	*THBS1*	0.492
B9EMX9	Ketimine reductase mu-crystallin OS=Salmo salar OX=8030 GN=CRYM PE=2 SV=1	6	10	6		*CRYM*	0.498

Appendix – C

qPCR details

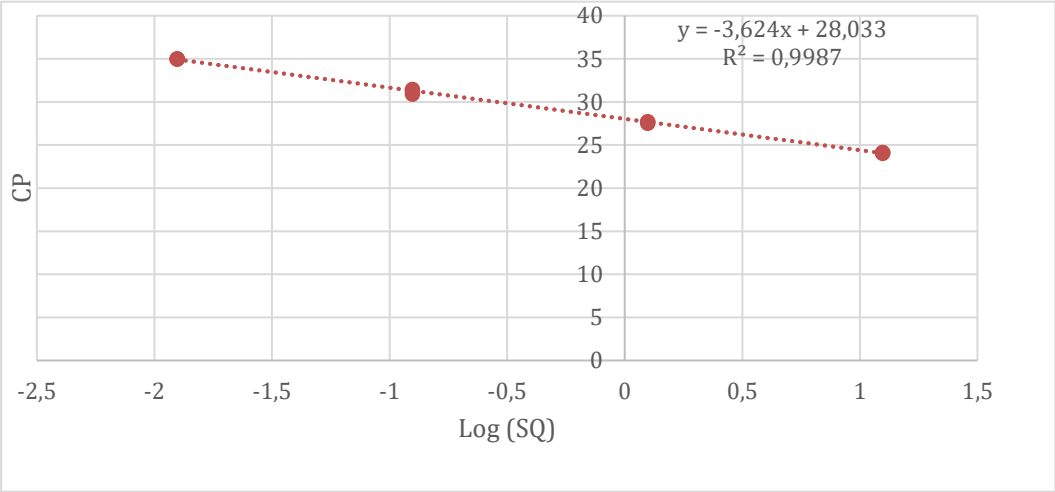

Figure 37: Standard curve for the gene Hsp90. X-axis showed the logarithmic scale of the starting concentrations used to generate the curve. The concentrations ranged from 0,0125 ng/µl to 12,5 ng/µl. The y-axis gives the cp-values for the standard curve generated through the LightCycler® software. The final equation for the slope of the standard curve, as well as the R-value, is given in the diagram.

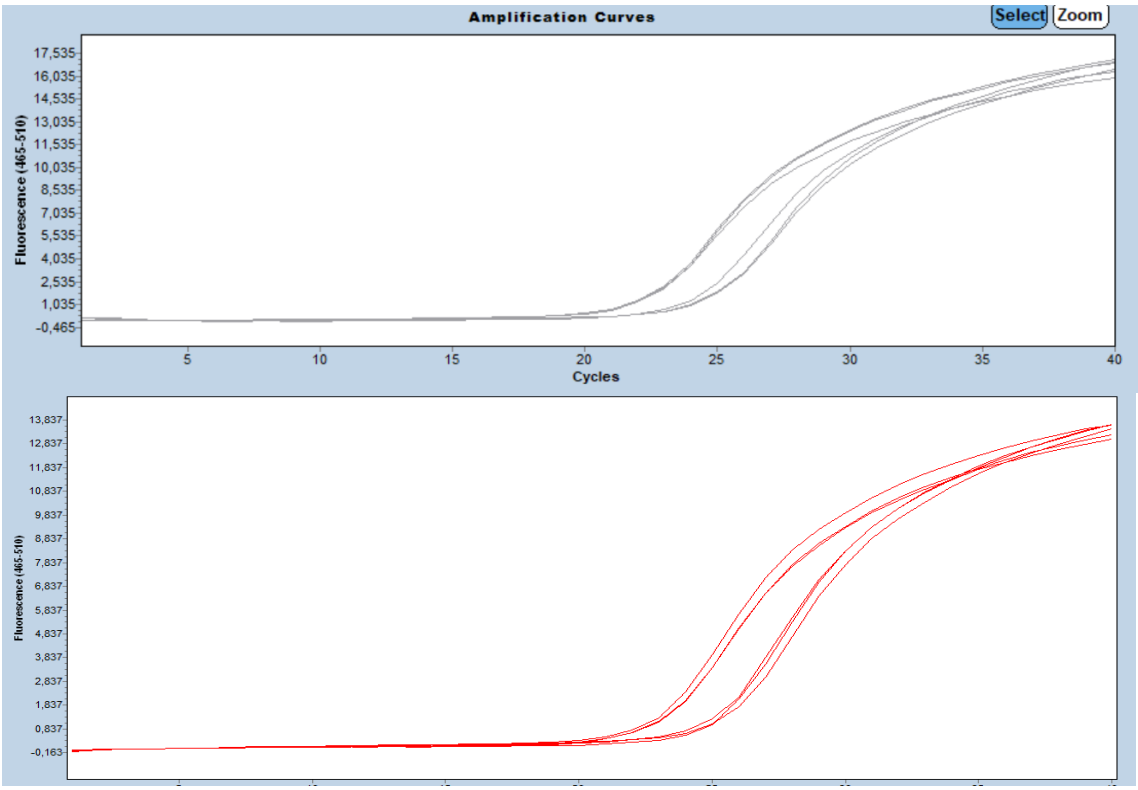

Figure 36: Amplification curve of ASK-1 cells exposed to polystyrene particles and control cells not exposed to particles. The curves with the lowest Cp-value, and correspondingly the highest measured fluorescence in qPCR is from cells exposed to polystyrene. This curve is based on the expression of the stress related gene Hsp90*. Top curve is created from the first qPCR run and the bottom curve is from the second run. Although different cp-values, the trends of the curves were similar for both runs.*

Table 22: Estimated relative expression of the hsp90 target gene with associated cDNA input levels, PCR efficiency and the difference in Cp-values between reference and target gene. For sample 4, the control from sample 3 has been used to calculate relative expression.

	Hsp90 – sample 1	Hsp90 – sample 2	Hsp90 – sample 3	Hsp90 – sample 4
cDNA input level	5 ng	5 ng	5 ng	5 ng
PCR efficiency (E)	1,88	1,88	1,98	1,98
ΔCP_{target}	2,19	-0,02	0,083	2,19
Relative expression ratio (R)	4,022	0,987	1,059	4,467